2017-05-09

The Mathematical Modelling of Spatial Structure of Ecological System in Heterogeneous Environment

Bo Zhang
University of Miami, bo@bio.miami.edu

UNIVERSITY OF MIAMI

THE MATHEMATICAL MODELLING OF SPATIAL STRUCTURE OF ECOLOGICAL SYSTEM IN HETEROGENEOUS ENVIRONMENT

By

Bo Zhang

A DISSERTATION

Submitted to the Faculty
of the University of Miami
in partial fulfillment of the requirements for
the degree of Doctor of Philosophy

Coral Gables, Florida

May 2017

UNIVERSITY OF MIAMI

A dissertation submitted in partial fulfillment of
the requirements for the degree of
Doctor of Philosophy

THE MATHEMATICAL MODELLING OF SPATIAL STRUCTURE OF ECOLOGICAL SYSTEM IN HETEROGENEOUS ENVIRONMENT

Bo Zhang

Approved:

_____
Donald L. DeAngelis, Ph.D.
Professor of Biology

_____
Carol C. Horvitz, Ph.D.
Professor of Biology

_____
Leonel Sternberg, Ph.D.
Professor of Biology

_____
Chris Cosner, Ph.D.
Professor of Mathematics

_____
Daniel B. Botkin, Ph.D.
Professor of Biology
UC Santa Barbara

_____
Guillermo Prado, Ph.D.
Dean of the Graduate School

_____
Wei-Ming Ni, Ph.D.
Professor of Mathematics
University of Minnesota

ZHANG, BO (Ph.D., Biology)

The Mathematical Modelling Of Spatial Structure Of Ecological System In Heterogeneous Environment. (May 2017)

Abstract of a dissertation at the University of Miami.

Dissertation supervised by Professor Donald DeAngelis.
No. of pages in text. (161)

As a daughter of a forest ecologist, I have always been fascinated by the beauty and mystery of our ecosystem. After finishing my B.S in forestry, I continued Ph.D. in University of Miami. In the beginning, I participated a wonderful work-shop: "Everything Disperses to Miami" and I realized pure mathematics is just as complex as ecosystem ecology, but it has a significant role on helping to understand ecosystem ecology. In this dissertation work, I applied mathematical modeling to bridge pure mathematic theory with real ecology problems into two sections: (1) testing and understanding the impact of dispersal on total population size in a heterogeneous environment; (2) understanding and simulating the impact of biological control on an invasive plant and the long term dynamic change of the ecosystem in south Florida.

Motivated by the work-shop, I started my first chapter as combining a greenhouse experiment and mathematical modelling to test an intriguing recent result from mathematics that a population diffusing at an intermediate rate in an environment in which resources vary spatially will reach a higher total equilibrium biomass than the population in an environment in which the same total resources are distributed homogeneously. With the guidance of my advisor, we extended the current mathematical theory to apply to logistic growth and also showed that the result applies to patchy

systems with dispersal among patches, both for continuous and discrete time. This allowed us to make specific predictions, through simulations, concerning the biomass dynamics, which were verified by a laboratory experiment. The experiment was a study of biomass growth of duckweed (*Lemna minor* Linn), where the resources (nutrients added to water) were distributed homogeneously among a discrete series of water-filled containers in one treatment, and distributed heterogeneously in another treatment. The experimental results showed that total biomass peaked at an intermediate, relatively low, diffusion rate, higher than the total carrying capacity of the system in the absence of diffusion and agreeing with the simulation model.

Later on, with the guidance of my advisor, we extended the previous theory to include exploitable resources, proving qualitatively novel results, which I tested experimentally using spatially diffusing laboratory populations of yeast. Consistent with previous theory, I predicted and experimentally observed that spatial diffusion increased total carrying capacity in heterogeneous environments, with the effect size depending on the relationship between r and K. However, consistent with newer theory, I discovered that homogeneously distributed resources support higher total carrying capacity than heterogeneously distributed resources, even with species diffusion. My results provide rigorous experimental tests of new and old theory, demonstrating how carrying capacity in spatially distributed species depends on the interplay between growth parameters, population diffusion and resource distribution.

Collaborating with empirical ecologists on invasive plant management my dissertation to another direction, in which I projected likely future changes in plant communities using the individual based modeling platform, JABOWA-II, by simulating

successional processes occurring in two types of southern Florida habitat, cypress swamp and bay swamp, occupied by native species and melaleuca, with the impact of insect herbivores. Computer simulations show melaleuca invasion leads to decreases in density and basal area of native species, but high levels of introduced insects would effectively control melaleuca to low levels, resulting in a recovery of native species. When herbivory was modeled on pure melaleuca stands, it was more effective in stands with initially larger-sized melaleuca. Although the simulated herbivory did not eliminate melaleuca, it decreased its presence dramatically in all cases, supporting the long-term effectiveness of herbivory in controlling melaleuca invasion.

Furthermore, I used a modeling approach to estimate the effect of different levels of herbivory on foliage by biocontrol agents on melaleuca in which the tree could change its carbon and nutrient allocation strategies in order to mitigate effects of increasing herbivory, to deeply understand how biological control works on control melaleuca's growth and spread. The model predicted that melaleuca should reallocate more resources to production and maintenance of photosynthetic tissues, at the expense of roots, to compensate and tolerate a certain level of herbivory. This compensation buffered the severity of the defoliation effect, but there was a limit of the maximum herbivory level melaleuca could survive. The model also showed that the level of available soil nutrient plays an important role in a tree's ability to compensate for herbivory. However, counterintuitively, under some circumstances in which nutrient is more limiting than carbon, it may be more favorable for the plant to increase the fraction of carbon going to roots if there is an increase in nutrient availability for a given level of herbivory.

Acknowledgements

First and foremost, I would like to thank my advisor, Donald L. DeAngelis, as knowing him for almost 10 years, he has given me support and help to more than just my dissertation. He is an amazing role model as a great scientist, mentor and friend. I truly appreciate he accepted me as his student in the beginning and he has always encouraged me to try new idea, supported and helped me to improve my research. I also wish to thank the remainder of my committee: Carol C. Horvitz, Leonel Sternberg, Chris Cosner, Daniel B. Botkin and Wei-Ming Ni, for guidance, advice and support since the beginning.

Thank you to J. David Van Dyken, who offered me such a great opportunity to apply my research knowledge and expand that knowledge to microbial ecosystem dynamics, and always encourage me to go one step beyond what I thought I can. Additional thanks to Min B. Rayamajhi to give me a lot of suggestions and help on finishing the work presented in Chapter 4, 5. Thanks as well to Jiang Jiang, who gave me so much advice on Matlab, data analysis and paper writing. Thanks as well to Xin Liu, Alex Kula, Justin Kallman, Arrix L. Ryce who provided great help on finishing Chapter 2,3.

I wish to thank the Department of Biology, University of Miami for providing funds for me to attend workshop and conferences. Also, thanks to USGS' Greater Everglades Priority Ecosystem Science funding, for supporting me for three years.

Sincere thanks to my parents for loving and supporting me; to my husband, Lu Zhai, also my lifelong collaborator, for sharing this journey with me for 10 years. I also want to thank all support I got from Geoff Wang, Fangliang He. Last but not least, thank

you to all my great friends, especially Andrea Westerband, Jian Gou for all the wonderful memories we shared together and all the support we gave to each other.

TABLE OF CONTENTS

LIST OF FIGURES

Chapter 2 **Page**

Chapter 3

Chapter 4

Chapter 5

LIST OF TABLES

Chapter One

Introduction

Why do we need mathematical modeling

Ecological modelling yields more general understanding and theory and provides testable and robust predictions. In particular, it is currently reaching the "next level" towards predictive and re-usable theory that can support environmental decision-making (Evans et al. 2013b). Therefore, in this dissertation work, I applied mathematical modeling to bridge pure mathematic theory with real ecology problems into two sections: (1) testing and understanding the impact of dispersal on total population size in a heterogeneous environment; (2) understanding and simulating the impact of biological control on an invasive plant and the long term dynamic change of the ecosystem in southern Florida.

Could we have larger total population than total carrying capacity in a heterogeneous environment?

Carrying capacity is a fundamental concept in ecology. An assumption in most non-spatial population models is that there is an upper limit on the size of the population, its carrying capacity, which is governed by the limiting resource. For example, for a plant population, this is typically space, light, or a nutrient. When the concept of carrying capacity is extended to an environment of spatially heterogeneous resources, the usual approach is to assume that the summation over the local carrying capacities yields the total carrying capacity of the whole domain.

However, when the population disperses randomly in this domain, mathematical models predict that the upper limit on population size is no longer the summation over

local carrying capacities. In studying a population in a two-patch system with logistic growth on each patch, where the per capita growth rates when the population is close to zero, r, and carrying capacities, K, differ on the two patches. When the two patches are connected by rapid diffusion and there is a relationship $r_1/K_1 > r_2/K_2$ for $K_1 > K_2$ between K and r of the two patches, the total population can reach a higher total steady state, or equilibrium, size than the sum of the subpopulations on the two patches without any connection. A mathematical derivation of a similar result was made, that considered a population of consumers in a continuous environment described by a reaction-diffusion equation with spatially varying carrying capacity (identical to the maximum growth rate), and showed that the total steady state size of a dispersed population exceeded the summation over all local carrying capacities for all diffusion rates. Further studies extended these results for both continuous spatial and multi-patch systems for populations with logistic growth in which parameters governing growth rate and carrying capacity could vary independently spatially, showing that the results held for small diffusion rates when a positive relationship existed between r and K, and for all diffusion rates when r is an accelerating convex function of K.

Still, rigorous empirical validation of this ‘paradox’ is generally lacking, so it is not known whether these results apply to real populations. Testing these results in the field or experimentally is further complicated by the fact that real populations are usually limited by exploitable resources, whereas the resources in previous models are assumed non-exploitable and not influenced by feedback from the consumer. Thus, it is not known how this more complex situation would change the results and other mathematical models.

What is the long-term impact of biological control on an invasive species and our natural ecosystem?

Melaleuca quinquenervia (Cav.) Blake (common names: melaleuca, paper bark, punk tree; Family, Myrtaceae, referred to as melaleuca thereafter) is a large (25-30m tall) native Australian tree introduced into the Florida landscape during the late 19th century for pulp production and ornamental purposes. It has strong invasive attributes, such as ecological fire adaptation and high reproductive potential. A single 10-m tall open-grown tree can store over 20 million seeds in its capsules at any given time. By the end of the 1900s melaleuca had spread over 200,000 ha of ecologically sensitive freshwater ecosystems of southern Florida displacing native vegetation such as slash pine (*Pinus elliottii* Engelm.) and pond cypress (*Taxodium ascendens* Brong.), threatening native biodiversity. Melaleuca invasion has caused adverse economic and environmental impacts to southern Florida, with the loss valued, 16 years ago, at nearly $30 million per year.

Predicting the effects of invading species such as melaleuca is of current general interest because of the ecological and environmental damage of many invading species. The difficulty of making predictions of the establishment and spread has been pointed out. Modeling has been applied to make predictions of future spread in many cases, including both niche modeling and mechanistic models. Various control methods have been applied in many cases, including the use of biocontrol agents that are natural enemies of the pest species. Because use of both biocontrol and other methods of control is costly, prediction of the efficacy of control is equally urgent. The long-term success of biocontrol is still

uncertain, so modeling has been used in a number of cases of invasive species, including plant species.

Research objectives

The main objective of my dissertation research is to contribute to addressing these two questions as follows:

In Chapter 2, I first aimed to determine if the mathematical result and others has relevance to empirical systems. That is, will a diffusing population in an environment with spatially varying resources reach a higher total equilibrium biomass than the population in the same environment without diffusion? The second objective is to test the mathematical result that a hump-shaped pattern appears when the equilibrium biomass is plotted as a function of the rate of diffusion.

In Chapter 3, I tested three hypotheses suggested by the earlier mathematical results. Hypothesis 1: when a consumer exists in a domain with a heterogeneously distributed input of exploitable limiting resource, the steady state population can reach a greater size when it disperses than when it does not. Hypothesis 2: the higher population in a heterogeneous environment with diffusion is concomitant with a positive relationship of growth rate and carrying capacity. Hypothesis 3: a consumer population diffusing randomly in a domain with a heterogeneously distributed input of exploitable limiting resource can reach a greater steady state size than a population diffusing (or not) in a domain with the same total input of resources spread homogeneously in the domain. We utilized a budding yeast population to test these hypotheses experimentally, and, thereafter, used mathematical analysis to extend previous mathematical models to this case of exploitable resources.

In Chapter 4, the objective is to improve understanding of the possible effects of herbivory on the landscape dynamics of melaleuca in native southern Florida plant communities. To do that, I projected likely future changes in plant communities using the individual based modeling platform, JABOWA-II, by simulating successional processes occurring in two types of southern Florida habitat, cypress swamp and bay swamp, occupied by native species and melaleuca, with the impact of insect herbivores.

In Chapter 5, my goal is to estimate the rate of defoliation needed to achieve a specified reduction in the growth rate under various conditions of nutrient availability to the tree and how it might change its allocations to foliage and roots in an optimal way.

Chapter Two

Effects of dispersal on total biomass in a patchy, heterogeneous system: Analysis and experiment

Summary

An intriguing recent result from mathematics is that a population diffusing at an intermediate rate in an environment in which resources vary spatially will reach a higher total equilibrium biomass than the population in an environment in which the same total resources are distributed homogeneously. We extended the current mathematical theory to apply to logistic growth and also showed that the result applies to patchy systems with dispersal among patches, both for continuous and discrete time. This allowed us to make specific predictions, through simulations, concerning the biomass dynamics, which were verified by a laboratory experiment. The experiment was a study of biomass growth of duckweed (*Lemna minor* Linn), where the resources (nutrients added to water) were distributed homogeneously among a discrete series of water-filled containers in one treatment, and distributed heterogeneously in another treatment. The experimental results showed that total biomass peaked at an intermediate, relatively low, diffusion rate, higher than the total carrying capacity of the system and agreeing with the simulation model. The implications of the experiment to dynamics of source, sink, and pseudo-sink dynamics are discussed.

1. Background

The effects of spatial heterogeneity and dispersal on populations and on ecosystem properties such as productivity are key issues in ecology. An interesting recent result from mathematics is that a population in an environment in which resources vary spatially will reach a higher total equilibrium biomass with diffusion than without diffusion in heterogeneous environment (Lou 2006; He and Ni 2013), which they referred to as 'a curious fact indeed'. The mathematical result depends on the population being able to diffuse in space. This result from mathematical theory have implications for ecology. Ecologists attempt to understand the factors regulating populations in spatially structured habitats with regional factors such as spatially distributed environmental heterogeneity and dispersal (Matthiessen and Mielke 2010). A number of ecological investigations carried out in recent years have established that spatial heterogeneity in the availability of soil-based resources can strongly influence the growth and patterns of biomass allocation of single plants (Hutchings et al. 2003). However, these studies did not involve spatial diffusion, so results for the two factors of spatial heterogeneity and diffusion together have, to our knowledge, rarely been tested empirically, despite the relevance of dispersal to key ecological issues.

Lou considered a population in an inhomogeneous environment; i.e., where the population growth rate as a function of distance, s, along one dimension, and g(s) ≠ constant, and where the population can diffuse at some constant rate (D). He used an equation of the form

$$\frac{\partial X}{\partial t} = D\frac{\partial^2 X}{\partial s^2} + [g(s) - X]X, \tag{1.1}$$

with Neumann (no-flux) boundary conditions on *X*. Here 'resources', g(s), represent both growth rate and carrying capacity, and the resource level is assumed fixed externally. Lou noted that, at equilibrium, when both sides are divided by X and integration is performed over all space Ω, the following holds;

$$D\int_{\Omega}\frac{1}{X(s)^2}\left|\frac{\partial X(s)}{\partial s}\right|^2 > 0\,, \tag{1.2}$$

which implies

$$\int_{\Omega}[X(s)-g(s)]ds > 0\,; \tag{1.3}$$

The diffusion of individuals away from the areas of high productivity keeps the population levels in those areas below carrying capacity, so that high production continues. The diffusion allows higher population levels to be attained in the lower resource areas than the carrying capacity would predict. The result is that the total population over all space exceeds that which would occur in a homogeneous space with the same total resource production. In order to apply the above results to typical ecological models, it is necessary to extend (1.1) to a logistic equation

$$\frac{\partial X}{\partial t} = D\frac{\partial^2 X}{\partial s^2} + r(s)[1-\frac{X}{K(s)}]X\,, \tag{1.4}$$

where the maximum growth rate, *r(s)*, and carrying capacity, *K(s)*, are standard parameters in ecological models. It is useful at first to switch from continuous to discrete space (patches or compartments) to demonstrate in a simple manner how to make the extension. The discrete space model can then be used to simulate planned empirical experiments.

The first objective of this research is to determine if the mathematical result of Lou has relevance to empirical systems. This is, will a diffusing population in an environment with spatially varying resources reach a higher total equilibrium biomass than the population in an environment with the same total resources distributed homogeneously with diffusion? The second objective is to test the mathematical result that in a heterogeneous environment a hump-shaped pattern appears when the equilibrium biomass is plotted as a function of the rate of diffusion.

2. Methods

2.1 Discrete patch model

The discrete patch model analogous to (1.4) uses logistic growth equations in which carrying capacities can be specified for a one-dimensional series of compartments linked through population diffusion. Consider n compartments, which have biomasses represented by the variables *X1, X2, ..., Xn* (for example, grams dry weight biomass). Relevant equations for continuous diffusion among compartments are the following, in which there are fluxes between the two patches on either end as well (i.e., wraparound conditions);

$$\frac{dX_i}{dt} = r_i(1 - X_i / K_i)X_i - DX_i + \frac{1}{2}DX_{i-1} + \frac{1}{2}DX_{i+1} \qquad (i = 1, \ldots, n) \qquad (2.1)$$

where it is understood that $i\text{-}1 = n$ when $i = 1$ and $i+1 = 1$ when $i = n$.

The system is described by the parameters, r_i, K_i, and D. Here, r_i (for example, day-1) is the maximum growth rate in patch i, while K_i (for example, grams dry weight biomass) is the carrying capacity for patch i, with $r_i(1 - X_i/K_i)$ being the actual growth rate at any time. The parameter D (day^{-1}) is the diffusion coefficient.

Because of the use of two parameters, r and K, rather than the single parameter, g, the model 2. 1 differs from the mathematical model (1.1), but is more flexible in describing population growth. When r_i andK_i, take on independent values for each compartment i, it can be shown that there is no guarantee that diffusion in an heterogeneous environment leads to greater equilibrium biomass than in the absence of diffusion. Specifically, it can be shown that the inequality

$$\sum_{i=1,n} \frac{r_i}{K_i}\left(X_i - K_i\right) > 0 \tag{2.2}$$

holds for this system (see Appendix 1), but this does not necessarily imply that

$$\sum_{i=1,n}\left(X_i - K_i\right) > 0 \tag{2.3}$$

i.e., that total biomass is greater in a heterogeneous system with diffusion than without diffusion (analogous to 1.3). However, a criterion for (2.3) can be found (see Appendix 2); that is, the inequality

$$\sum_{i=1,n}\left(\frac{(r_i - r_{i-1})(K_i - K_{i-1})}{r_i r_{i-1}}\right) > 0 \tag{2.4}$$

guarantees that

$$X_{total} = \sum_{i=1,n} X_i$$

increases as D increases from zero for small values of D, so that (2.3) holds at least for small values of D. A sufficient condition for criterion (2.4) to be satisfied is that r_i and K_i both be increasing or both be decreasing together. We have used simulations to exhaustively test this result. A criterion parallel to (2.4) can be found for the spatially continuous form with $r(s)$ and $K(s)$; that is, for

$$\frac{\partial X}{\partial t} = D\frac{\partial^2 X}{\partial s^2} + r(s)\left[1 - \frac{X(s)}{K(s)}\right]X(s). \tag{2.5}$$

The criterion for $X_{total} = \int_{\Omega} X(s)$ to increase for small increases in D from zero is now,

$$\int_{\Omega} \frac{\partial K}{\partial s} \cdot \frac{\partial}{\partial s}\left(\frac{1}{r}\right) < 0. \tag{2.6}$$

The proof is outlined in Appendix 3. Both (2.4) and (2.6) are new mathematical results.

2.2 Discrete patch, discrete time model simulations

System (2.1), as written, represents a continuous-in-time but discrete-in-space diffusion. It was impractical to design an experiment in which diffusion occurred continuously in time. Instead, an artificial experiment was designed, in which diffusion was simulated by manual transfer of floating aquatic plants between containers (patches) with different nutrient levels. To represent this in a model, equations (2.1) were discretized in time and the number of compartments was set to n = 5. In the time-discretized version designed to represent the experiment, growth was assumed to occur according to the logistic equation over equal time periods (equation 2.7a), and then amounts of biomass were transferred among compartments at regular time intervals:

$$\frac{dX_i}{dt} = r_i(1 - X_i / K_i)X_i \qquad (t_{j(+)} \le t \le t_{j+1(-)}) \tag{2.7a}$$

$$X_i(t_{j(+)}) = X_i(t_{j(-)})(1 - M) + \frac{1}{2}MX_{i-1}(t_{j(-)}) + \frac{1}{2}MX_{i+1}(t_{j(-)}) \text{ for } t = t_j \tag{2.7b}$$

where compartment number $i + 1 = 1$ when $i = 5$ and $i - 1 = 5$ when $i = 1$, and where tj(-) means the value before biomass transfer (diffusion) and tj(+) means the value after transfer. The new parameter *M* represents the fraction moved between

compartments at discrete time intervals (every four days in the experiment), rather than a continuous rate of diffusion. Because it was not possible to control r_i andK_i independently in the experiment through different nutrient concentrations, the mathematical results above imply that success of the experiment in showing higher biomass at non-zero diffusion rates depend on r_i andK_i being positively correlated.

Simulations were performed to help design and interpret an experiment.

2.3 Experiment

The objective of the experiment was to determine whether there is a non-zero diffusion rate that maximizes total vegetation biomass in a region in which resources are distributed heterogeneously, and to estimate that diffusion rate and the maximum vegetation biomass. We used duckweed (*Lemna minor Linn*) in our experiment. Duckweed is an aquatic plant that floats on or just beneath the surface of still or slow-moving bodies of fresh water and wetlands. These plants are simple, lacking an obvious stem or leaves. Duckweed was convenient to use, because it is easy to maintain in laboratory containers, as well as to manipulate to simulate a specific type of movement, namely density-independent diffusion in this case. This was done through transfers between a row of five compartments (containers in which duckweed was grown) with different nutrient levels (Figure 2.1 shows a schematic of the experimental arrangement). Biomass could also easily be measured through time.

3. Results

3.1 Simulation model

A comparison of simulations of total biomass through time in the homogeneous and heterogeneous five-compartment systems, with diffusion in both cases, is shown in

Figure 2.2. Note that the solid wavy line in the heterogeneous system results from the biomass transfers every four days. The parameter values, r_i and K_i, were chosen to best fit the experiment. Higher overall biomass is clearly in the heterogeneous system with M = 0.20. However, in the absence of diffusion, the final total biomasses in the homogeneous and heterogeneous treatments were precisely the same (dashed line in Figure 2.2).

In order to compare the total biomasses resulting in a heterogeneous distribution of resources for different diffusion rates, a sequence of values of transfer from M = 0 to 0.25 was used. Because we did not know a priori the growth rates, r_i, and carrying capacities, K_i, of the individual containers, we examined results for a reasonable range of parameters. All simulations showed a peak in total biomass as a function of M, when the values of r_i and K_i obeyed criterion (2.4). The best fit to the total experimental population biomass (see below) as a function of diffusion rate, M, is shown in Figure 2.3 (values of r_i and K_i are in the caption), with a peak in total biomass at about $M = Mmax$ = 0.07. In addition, the biomass of each of the containers is plotted as a function of M (Figure 2.4). It is clear that the biomasses of the five compartments converge as a function of increasing M, as predicted from theory.

Sensitivity analysis of model simulation

The plots shown in Figures 3 and 4 represent parameter sets that best fit the experimental data below. These parameters showed a somewhat more non-linear gradient of values then we expected based on the nutrients added; i.e. the best set of values was r_1 = 0.0068, r_2 = 0.0204, r_3 = 0.0476, r_4 = 0.0680, r_5 = 0.1700 day^{-1}, K_1= 0.2, K_2 = 0.6, K_3 = 1.4, K_4= 2.0, K_5= 5.0 g dW. Note that we are assuming r_i / K_i = constant.

We explored the sensitivity of the simulation results to the mean values of the r_is (solid lines) and K_is (dotted lines), as well as to the mean gradients, S, of resources across the patches represented by the sets the r_is and K_is. Each of these was changed by +,- 10% and +,- 20% and the sensitivity to these of the peak biomass, the diffusion coefficient at which the peak in total biomass occurs, M_{max} , and the sharpness of the peak (ratio of peak biomass to biomass in the absence of diffusion) was calculated. In the case of the gradient, S, sensitivity to a +/- 10% change was created by, respectively increasing or decreasing r_1 and K_1 by 10%, r_2 and K_2 by 5%, and respectively decreasing or increasing r_5 and K_5 by 10% and r_4 and K_4 by 5%. It can be seen that all three, r, K, and S, have a positive effect on maximum total biomass (Figure 2.5a). Parameters K_i and S have a positive effect on M_{max}, but r_i has a negative effect (Figure 2.5b). Parameters K_i and S have a positive effect on sharpness of the peak, but r_i has no effect (Figure 2.5c). More generally, through exhaustive simulations, we confirmed that satisfaction of criterion (2.4) guarantees that (2.3) is true, at least for small values of diffusion. The condition that whenever $K_i > K_{i-1}$, it is also true that $r_i > r_{i-1}$, and vice versa is sufficient to guarantee that (2.4) holds, but is not a necessary condition.

3.2 Experiment

The central goal of the experiment was to determine which diffusion rate may lead to the peak biomass in the heterogeneous system. We found a significantly higher biomass in heterogeneous system than homogeneous system with 20% diffusion (Figure 2.6). We conducted further experiments to measure the total dry biomass with 0%, 6% and 10% diffusion rates. Although experiments 1 and 2 were carried out 20 days apart, biomass for the heterogeneous resource distribution and 0% diffusion did not differ between the two

experiments ($p = 0.194$). Thus we assumed that we could compare the total biomasses with four different diffusion rates, (M = 0%, 6%, 10% and 20%), under the heterogeneous conditions described in the Methods section. Therefore, we had a total of 4 treatments (0, 6, 10 and 20% diffusion rates) with 0% diffusion rate having 6 replicates and other treatment having 3 replicates. The diffusion rate significantly affected biomass, with non-zero values of the diffusion rate having significantly higher biomass than 0% diffusion. The highest biomass occurred at M = 6% (Figure 2.7), which is close to the peak of the simulation results (Figure 2.4a) which are also plotted in Figure 2.7.

4. Discussion

We set out to experimentally test the mathematical result of Lou of how a single plant population responds to spatial heterogeneity and dispersal through diffusion. We first extended Lou's results to a logistic growth model and to a discretized model. For the experimental test, we planted duckweed (*Lemna minor* Linn) in situations of both heterogeneously and homogeneously distributed resource. We manually controlled rates of diffusion; i.e., the percentage of duckweed transferred from each water container to adjacent ones. Based on this experimental design, a simulation model was developed to determine the range of results expected from the laboratory experiment.

The experiment, in which the diffusion was applied artificially every four days at levels of 6% and 10%, in addition to a 0% control, confirmed that a moderate level of diffusion increased total biomass above the level of the non-diffusing population in a heterogeneous environment. In particular, 6% diffusion produced a total biomass that appears to be close to a peak value. In the heterogeneous system, without diffusion, the biomass growth will follow the resource distribution, the total biomass increases to total

carrying capacity. But with a moderate level of diffusion, the biomass exported from the higher productivity region results in larger increases in standing stock biomass in lower resource areas than the decreases in biomass in higher resource areas. This can increase the total biomass level of the whole system to be greater than total carrying capacity. However, as diffusion is increased to high levels, biomass becomes homogeneous over the whole region and the total biomass again becomes equal to the total carrying capacity.

Modeling studies of this phenomenon are rare. But a somewhat analogous result to biomass maximization at intermediate diffusion rates was obtained by Pulliam and Danielson (Pulliam and Danielson 1991). They simulated different relative amounts of high- and poor-quality habitat, in which population movement from high- to low-quality habitat was more likely the lower the ratio of the former to the latter. However, in this study the trend of total population biomass was not monotonically decreasing with lower ratio of high-quality to low-quality habitat, and, in fact, there was a peak for an intermediate ratio. The reason seems to be related to our finding that intermediate diffusion levels maximize total biomass; that is, as long as the population levels in the high-quality sites are not too negatively affected by movement into low-quality sites, the enhancement of population at the low-quality sites causes the total population to be higher.

Our model simulation and experiment relate to an important concept of spatial ecology, the occurrence of sources and sinks on landscapes. Sources are areas in which surplus population is created (reproduction and growth exceed losses) and sinks are areas in which losses exceeds births and growth. This concept has implications for conservation ecology, because it is possible that individuals may be attracted to sink areas,

where they die or fail to reproduce, threatening the population (Pulliam 2004). That influential paper has been followed by many others, expanding on the idea (Howe and Davis 1991; Watkinson and Sutherland 1995; Brawn and Robinson 1996; Diaz 1996; Holt 1997; Loreau and DeAngelis 1997; Ritchie 1997; Amezcua and Holyoak 2000; Wilson 2001; Amarasekare 2004). The simple source and sink idea has been replaced by a more complex picture in which 'pseudo-sinks' are included (Watkinson and Sutherland 1995). Pseudo-sinks are areas into which net population fluxes may be observed at times. However, these areas are actually self-sustaining and the net flux occurs only because there are more productive sources nearby from which individuals migrate. Habitat patches that vary in quality can cause population dynamics to differ between patches. Populations in better quality patches are more productive and should produce more emigrants (Donahue et al. 2003).

Our experiment is relevant to the concept of pseudo-sinks, because none of the containers in the experiment was actually a sink. All the individual containers, in isolation, could maintain populations, though at different levels. Containers become pseudo-sinks in the context of receiving input from more productive containers. The model simulation and empirical experiments show how pseudo-sinks may provide a positive role in maintaining a population and also imply that, under certain conditions of resource heterogeneity, there is higher total vegetation biomass than under homogeneous conditions.

The experiments and model suggest that different rates of dispersal among sources and pseudo-sinks in nature can affect regional population size and there might be rates of diffusion that maximize the size of the total population in a heterogeneous region.

However, this would in general be difficult to test in the field, as dynamics of a population in nature are affected by a large number of factors that were eliminated in our experiment. This is especially true for animal populations, the individuals of which are unlikely to move by diffusion (i.e., randomly). They more often move within home ranges, with frequent returns to core areas, or show directed movements in response to environmental gradients. Nevertheless, dispersal of populations of both plants and animals over long time scales can often be represented as diffusive (e.g., Kareiva (1983)), and, in that case, steady state patterns of biomass density on landscapes may be influenced by the interactions of heterogeneity and diffusion. A part of the population will diffuse from the most productive areas, and that surplus population can enhance the populations of the less productive areas and increase the total population level of the whole system.

Manipulations of simple systems in nature that demonstrate such effects are possible. In an experiment described by Keddy (1981, 1982) and Watkinson (1995), densities of seeds of the plant *Cakile edentula* were manipulated along a sand dune gradient. The seaward or beach end of the gradient was a source, while the middle and landward sites were shown to be net sinks where mortality was higher than reproduction. Interestingly, in a model by Watkinson (1995), the plants were most abundant in the sink sites because of the high seed migration from the source. Watkinson's work suggests that in his system diffusion can cause the overall population in a heterogeneous environment to exceed that in a homogeneous environment.

The experiments of Keddy (1981, 1982) and the model of Pulliam and Danielson (1991), as well as our experiment and model, simplify the importance of spatial

configuration. Our experiment used a very specific one-dimensional spatial configuration of containers with a linear gradient of resources, the relative levels of which were at least roughly known. In nature, the configurations of sources, sinks, and pseudo-sinks may take highly complex forms in two dimensions (Shriver and Vickery 1999; Breininger and Carter 2003). In addition, carrying capacities of different natural habitats are difficult to estimate, as they depend on many factors that are difficult to measure. It is still possible, however, that more complex, but still quantifiable experiments in the field, could be carried out in the future.

Our experiment involved only biomass of a single population. Spatial heterogeneity and diffusion also have implications for species richness. The interaction of spatial movement and competition in shaping ecological communities has been the object of much study (Chesson 1985; Tilman 1994; Cantrell and Cosner 1998; Latore et al 1999; Muko and Iwasa 2000; Amarasekare and Nisbet 2001; Yu et al. 2001; Lutscher et al. 2007), with spatial heterogeneity playing an important role in the interaction (Amarasekare and Nisbet 2001; Snyder and Chesson 2003, 2004). A trade-off between competition and dispersal can lead to regional coexistence of competing species (Haegeman and Loreau 2014). Also, given enough heterogeneity in the resources over the area occupied by the community, many species could, in principle, coexist (Chesson 1985; Silvertown and Law 1987; Yu et al. 2001). Therefore, spatial heterogeneity is an important consideration of species coexistence (Hara 1993). The general relationship between richness and ecosystem functioning remains valid in open systems, but the maintenance of ecosystem processes significantly depends on the effects of dispersal on species richness and local interactions. Without dispersal, experimental systems lack a

key process counteracting competitive exclusion (Mattiessen and Hillebrand 2006). Moderate to intermediate dispersal rates between local communities can weaken local competitive exclusion either by a colonization–competition trade-off and/or by source–sink dynamics when resource availability is spatially distributed.

Our experiment had a number of limitations. Due to the uncertainties in the amount of light and nutrient level in each container during the course of the experiment, we can only estimate that light was approximately the same for all containers and the nutrient levels had a strong gradient across the containers. A larger amount of experimental replicates with different levels of heterogeneity and additional diffusion rates would have help to better confirm our results. But our experiments fit a model well and give reasonable support to our hypothesis that diffusion in a heterogeneous environment can increase biomass over an equivalent homogeneous environment or over a heterogeneous environment with no diffusion. The model simulation provides a perspective how population biomass is regulated by the interacting effects of spatial heterogeneity and diffusion in natural system. Our future plan is going to test our results in a natural system, and also possibly to test two-species competition for limited resource in heterogeneous conditions.

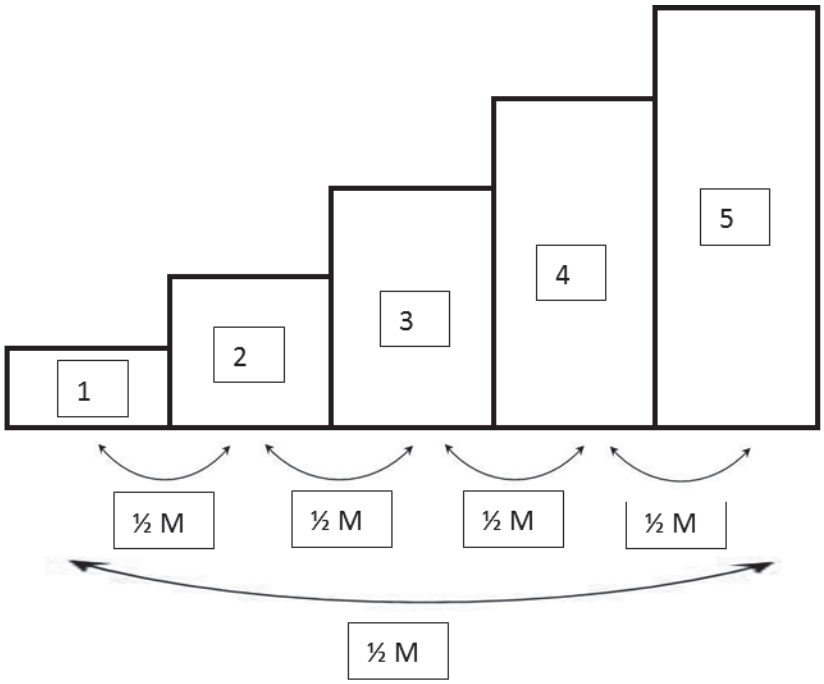

Figure 2.1. Model configuration, showing the five containers with gradient in nutrient supply (in the proportions 0:0.5:1:1.5:2, from compartment 1 to compartment 5) with rates of diffusion (*M*). Half of the biomass removed from each container was transferred to the container on the right and half to the container on the left (this included moving plant biomass between containers 1 and 5).

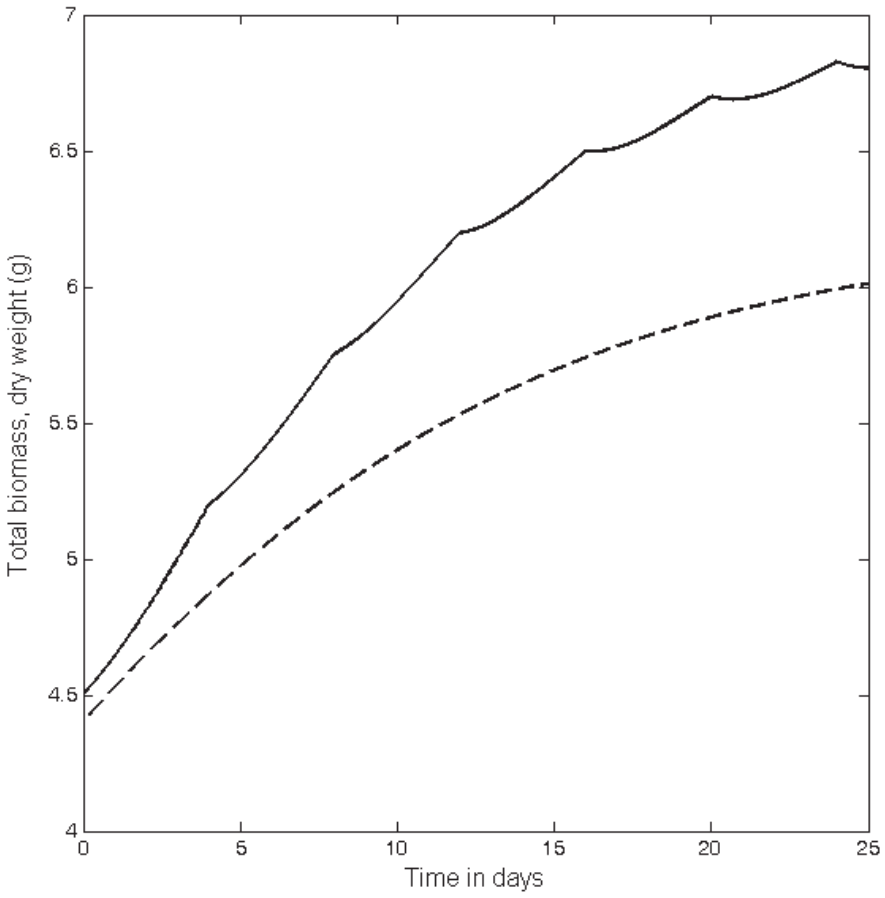

Figure 2.2: Simulations of total biomass as a function of time under heterogeneous conditions with 20% diffusion (solid curve). Homogeneous conditions with 20% diffusion and without diffusion, and heterogeneous condition without diffusion, all those three cases followed the same biomass growth (dashed curve). The diffusion, M, for each condition was 20% every four days. The result shows that there was a higher total biomass in the heterogeneous case. The parameter values for the heterogeneous case are $r_1 = 0.011$, $r_2 = 0.033$, $r_3 = 0.077$, $r_4 = 0.11$, $r_5 = 0.275$ day^{-1}, $K_1 = 0.135$, $K_2 = 0.405$, $K_3 = 0.945$, $K_4 = 1.35$, $K_5 = 3.37$ g dW. The parameter values of the homogeneous case are $r_i = 0.10$ and $K_i = 1.242$ for $i = 1, 2, .., 5$.

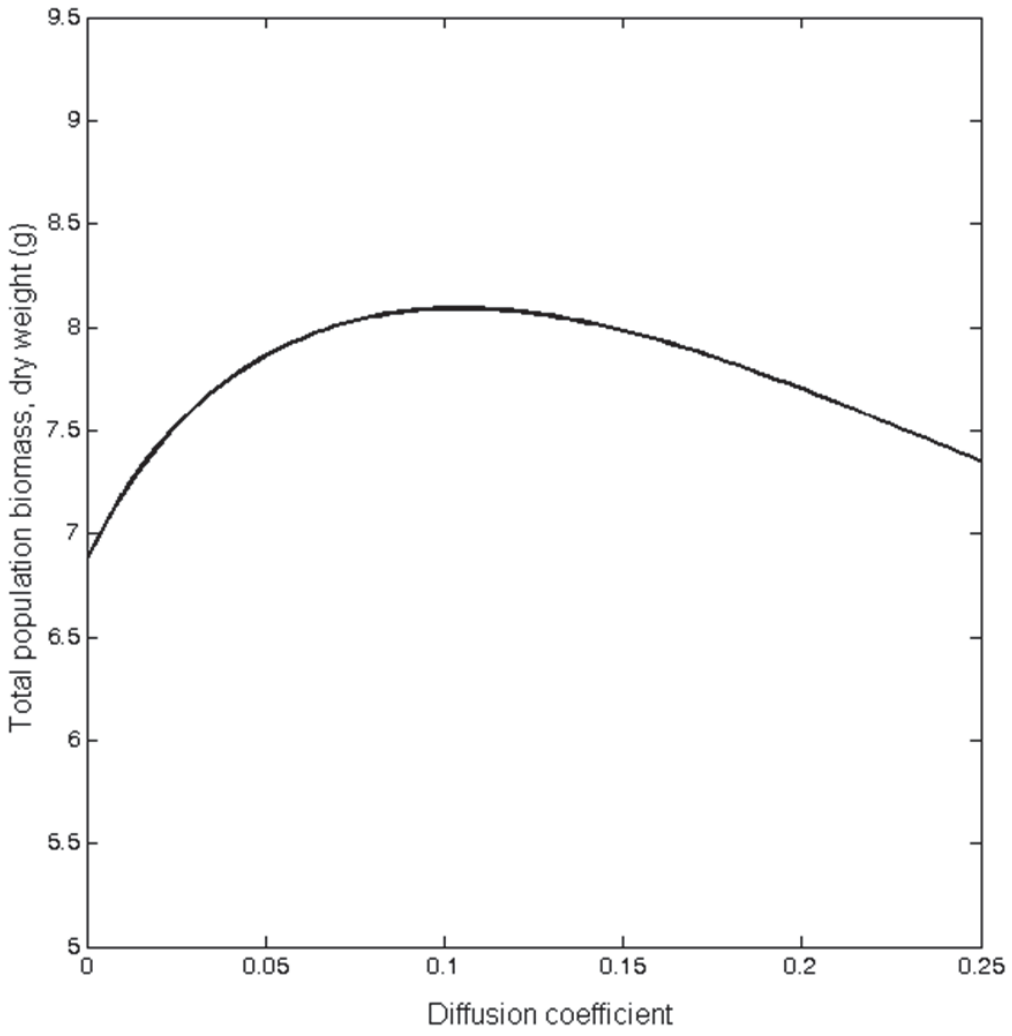

Figure 2.3. Total biomass versus diffusion rate in model simulations. Other parameters were chosen within reasonable ranges to fit the experimental data (see Figure 2.6). These are $r_1 = 0.0068$, $r_2 = 0.0204$, $r_3 = 0.0476$, $r_4 = 0.0680$, $r_5 = 0.1700$ day^{-1}, $K_1 = 0.2$, $K_2 = 0.6$, $K_3 = 1.4$, $K_4 = 2.0$, $K_5 = 5.0$ g dW.

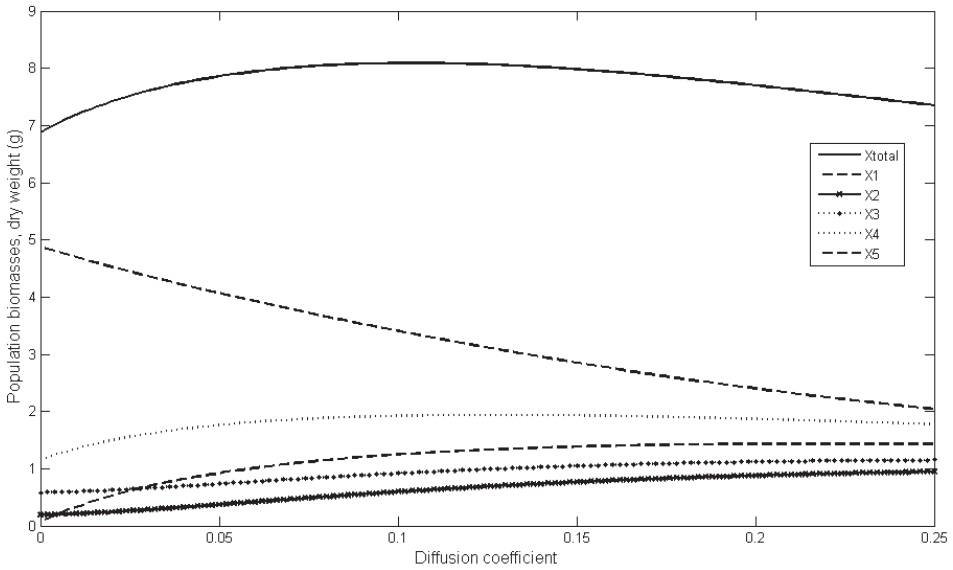

Figure 2.4. Biomasses of all five compartments and total biomass versus diffusion rate. Other estimated parameter values are the same as in Figure 2.3.

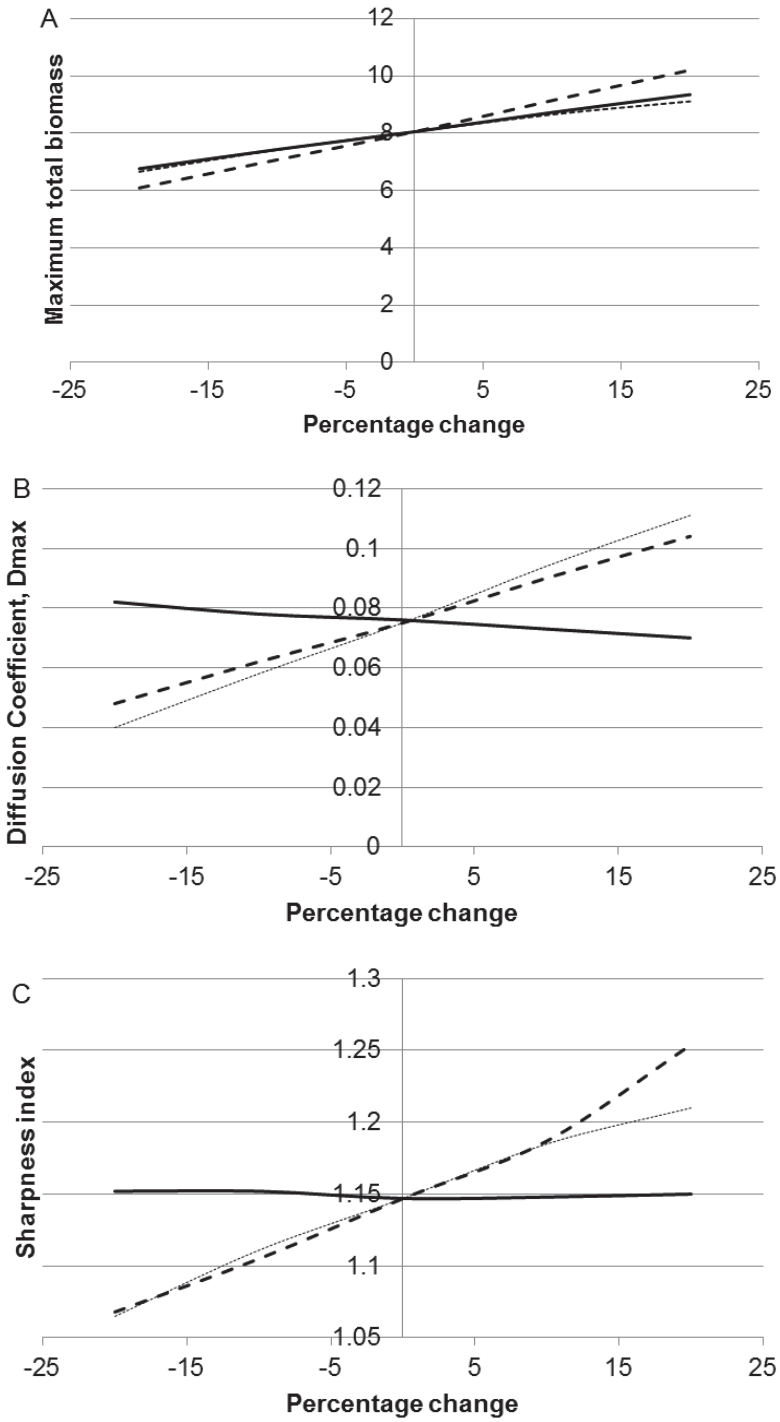

Figure 2.5. Sensitivity analysis for (a) maximum total biomass, (b) diffusion coefficient, M_{max} , at which maximum total biomass occurs, and (c) sharpness of the peak (ratio of height at M_{max} to height when $M = 0$). The values are simulated for (+, - 10% and +,- 20%) of all the r_is (solid line), all the K_is (dotted line) and slope, S, of the resource gradient across the containers, S.

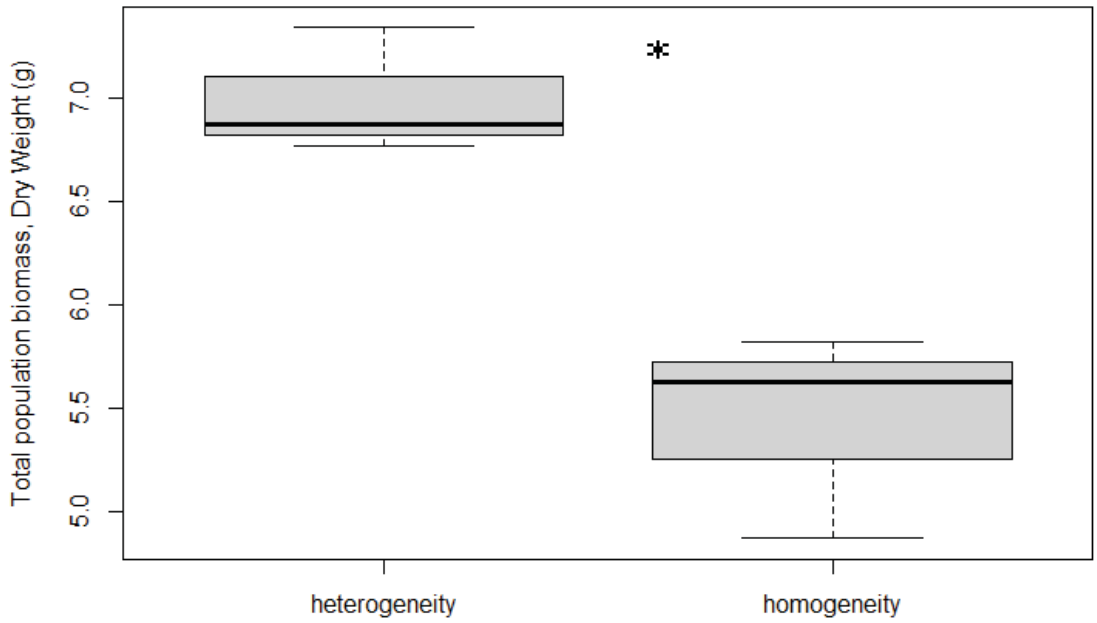

Figure 2.6. Experimental values of mean and standard deviation of total dry biomass. The left bar shows the dry weight of duckweed from the heterogeneous treatment group with 20% diffusion rate and the right bar shows the dry weight from homogeneous treatment group with 20% diffusion rate. In both treatments total nutrients were the same. Stars above the error bars indicate significant differences ($P<0.05$) between treatments. Each treatment was replicated 3 times.

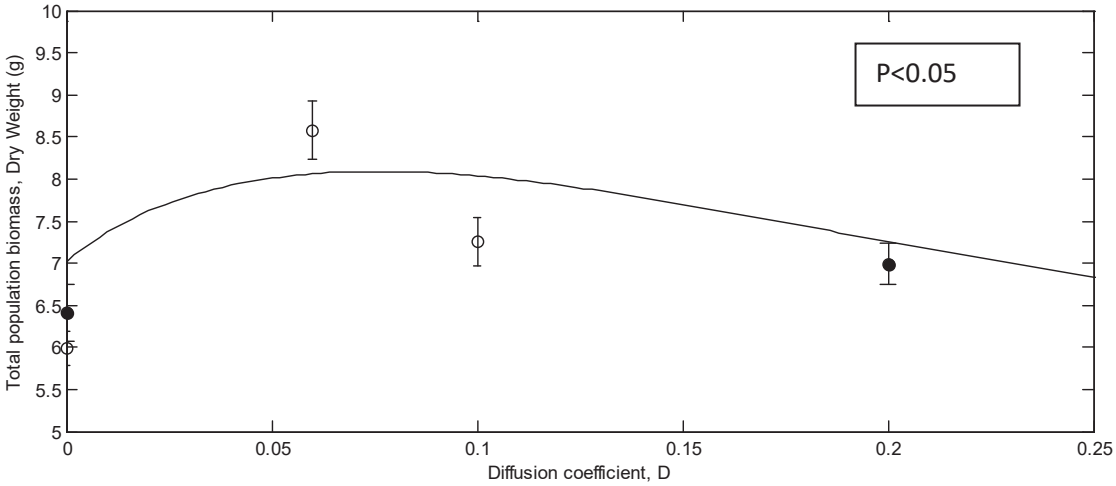

Figure 2.7. Mean and standard deviation of total dry biomass as functions of diffusion coefficient from experiment and model simulation. The dark dots show the total dry weight under heterogeneous condition with different diffusion rates (0%, 20%) from first experiment. The empty dots show the total dry weight under heterogeneous conditions with different diffusion rates (0%, 6%, 10%) from the second experiment. $P<0.05$ indicates significant differences between treatments. The solid line shows results for dry mass as a function of diffusion coefficient (from 0% to 25%) from the simulation model.

Chapter Three

Carrying capacity in a heterogeneous environment with habitat connectivity

Summary

A large body of theory predicts that populations diffusing in heterogeneous environments reach higher total size than if non-diffusing, and, paradoxically, higher size than in a corresponding homogeneous environment. However, this theory and its assumptions have not been rigorously tested. Here we extended previous theory to include exploitable resources, proving qualitatively novel results, which we tested experimentally using spatially diffusing laboratory populations of yeast. Consistent with previous theory, we predicted and experimentally observed that spatial diffusion increased total carrying capacity in heterogeneous environments, with the effect size depending on the relationship between r and K. However, in a second experiment, in which resources were maintained in a dynamic equilibrium by input rather than fixed at a static level determined at the outset, we discovered that homogeneously distributed resources support higher total carrying capacity than heterogeneously distributed resources, even with species diffusion. Our results provide rigorous experimental tests of new and old theory, demonstrating how carrying capacity in spatially distributed species depends on the interplay between growth parameters, population diffusion and resource dynamics.

Background

Carrying capacity, the steady-state upper limit on a population's size, is a fundamentally important quantity in both theoretical and applied ecology. Understanding the factors influencing carrying capacity is essential for the rational design of strategies for management of threatened or endangered species and control of invasives. In the simplest case, namely a species confined to a single point in space, carrying capacity is set by the local availability of limiting resource. For example, for a plant population, this is typically space, light, or a nutrient. However, most species in nature are spatially distributed over a diffuse geographic region with a heterogeneous (non-uniform) distribution of resources. This is true, for instance, of species whose habitat has been fragmented by human activity. For spatially distributed species, the determinants of carrying capacity are much more complex, as they depend on additional factors such as the rate of individual movement over space (dispersal or diffusion) and the spatial distribution of resources.

Indeed, mathematical theory predicts that dispersal has a remarkable effect on a population's total carrying capacity (see Supporting Information (SI), Appendix A for detailed overview of previous theory). If resources are heterogeneously distributed over space, then undirected spatial diffusion of individuals can increase the total size of the global population. That is, the upper limit on total equilibrium population size, which we will call 'realized asymptotic population size', of a spatially distributed population with dispersal is mathematically predicted to be greater than the sum of carrying capacities over each point in space. This effect was shown by Holt (1985) for a two-patch system with a logistic population model, $dN/dt = r(1 - N/K)N$. When the r's and K's differed

for the two patches and $K_j > K_i$ and $r_j/K_j > r_i/K_i$ the total population at equilibrium could exceed the sum of the carrying capacities of the two patches; that is $N_1^* + N_2^* > K_1 + K_2$ in the limit of a very high diffusion rate between the two patches. More general results for this two-patch model were derived by Arditi et al. (2016). Lou (2006) extended these results beyond a simple two-patch setting by using a reaction-diffusion model, and arrived at the same conclusion. DeAngelis et al. (2016) showed that this effect extends to weak diffusion, where increasing diffusion rate linearly increases realized asymptotic population size. In general, these results show that the realized asymptotic population size is not the same as the summed or integrated local carrying capacities, and that in certain cases, dispersal increases population size.

Most puzzling, these mathematical results imply that if the local carrying capacities are distributed over space in a heterogeneous manner, the equilibrium population of a diffusing population can exceed that attained by the population in a homogeneous environment with the same total carrying capacity. This remarkable effect has been called a 'paradox' by Holt (1985).

Importantly, these models either implicitly or explicitly assumed a positive correlation between the parameters *r* and *K* (DeAngelis et al. (2016)). DeAngelis et al. (2016) proved, using the Pearl-Verhulst reaction term, that these results require a positive relationship between *r* and *K*. With a negative *r*-*K* correlation, diffusion is mathematically predicted to decrease the realized asymptotic population size (DeAngelis et al 2016). Thus, realized asymptotic population size depends not only on dispersal rate and resource distribution, but also on the physiological capacities of a species linking reproductive rate and efficiency.

Despite the broad implications of these theoretical predictions, rigorous empirical validation is lacking. An experiment with duckweed, in which diffusion between adjacent patches of a linear five-patch system with different initial nutrient levels, provides some corroboration for the effect of diffusion on total carrying capacity (Zhang et al. 2015). However, the *r*-*K* relationship was not directly measured, nor was this relationship experimentally manipulated to test the theoretical prediction that a positive *r*-*K* correlation is necessary for the predicted effect. Furthermore, precise control of nutrient levels, measurement of *r* and *K,* small patch number, and low throughput proved to be limitations in this work. More generally, testing these mathematical predictions in the field or laboratory is complicated by the fact that real populations are usually limited by resources that are exploitable and renewed. The classic logistic model used in previous theory is phenomenological rather than mechanistic, and its population parameters (e.g., *K* and *r*) are assumed fixed, such that they are not influenced by feedback from exploitation by consumers. In reality, these parameters emerge from the interaction of consumers with exploited renewable resources (Tilman 1982).

Therefore, our objectives here are twofold. First, we analyze a mechanistic consumer-resource model to determine analytically whether it produces the same results as those described above for the phenomenological logistic model. Second, we test theoretical predictions using high throughput experimental methods in spatially diffusing laboratory populations of the heterotrophic budding yeast, *Saccharomyces cerevesiae*, limited by a single essential nutrient. In these experiments, we manipulate diffusion rate, resource distribution, and the *r*-*K* correlation. We test three hypotheses suggested by the earlier mathematical results with the phenomenological logistic. Hypothesis 1: when a

consumer exists in a region with a heterogeneously distributed input of exploitable limiting resource, the steady state population can reach a greater size when it disperses than when it does not. Hypothesis 2: the higher population in a heterogeneous environment with diffusion is associated with a positive relationship of growth rate and carrying capacity. Hypothesis 3: a consumer population diffusing in a domain with a heterogeneously distributed input of exploitable limiting resource can reach a greater steady state size than a population diffusing (or not) in a domain with the same total input of resources spread homogeneously in the domain.

Methods

Mathematical model

We first develop a mathematical model describing a diffusing population of consumers in an environment with heterogeneously distributed resources that are exploited by the consumer and externally renewed. A general pair of equations for a consumer-resource system (yeast-tryptophan in our experiments; see Experimental Methods) are:

$$\frac{\partial u(x,t)}{\partial t} = D\frac{\partial^2 u(x,t)}{\partial x^2} + \frac{r_{\max} n(x,t)u(x,t)}{k + n(x,t)} - m(x)u(x,t) - g(x)u(x,t)^2 \quad (1a)$$

$$\frac{dn(x,t)}{dt} = N_{input}(x) - \eta n(x,t) - \frac{r_{\max} n(x,t)u(x,t)}{\gamma(k + n(x,t))} \quad (1b)$$

where $u(x,t)$ is the consumer population size, $n(x,t)$ is the nutrient concentration,, D is the diffusion rate, r_{max} is the asymptotic growth rate under infinite resources, k is the half-saturation coefficient, defined as the nutrient concentration where $r = r_{max}/2$, $m(x)$ is

the mortality rate, $g(x)$ is the density-dependent loss rate, $N_{input}(x)$ is the nutrient input, η is the loss rate of nutrient from the system, and γ is the yield, individuals per unit nutrient.

For convenience, two special cases of this model were analyzed, which are intended to provide plausible quantitative representations of our experimental nutrient-yeast dynamics:

Model 1: $\eta = 0$, $m_i = 0$, $g_i > 0$ for all i. Model 2: $\eta = 1$, $m_i > 0$, $g_i = 0$ for all i

Model 1 assumes that nearly all of the nutrients are taken up by the yeast and that dead yeast cells are assumed to accumulate at a rate $g_i (U_i^*)^2$. The yeast cells are not physically lost, but they stop reproducing, with no recycling of nutrients. Model 2 is a chemostat type model.

We test these models mathematically in the limit that $D \to \infty$, in which the consumer population is well mixed on the landscape, and through computer simulations (see below) of the model for smaller values of D.

Four situations are assumed: (1) Heterogeneous distribution of nutrient inputs with no dispersal of the population, (2) heterogeneous distribution of nutrient inputs with dispersal, (3) homogeneous distribution of the same total nutrient inputs with dispersal, and (4) homogeneous distribution of the same nutrient inputs with no dispersal. It is assumed that when dispersal occurs, it occurs at a fast enough rate that there is perfect mixing of the population across the patches. The analysis is performed assuming continuous-time dynamics, whereas in the experiment, diffusing events are performed at discrete time intervals.

Simulations and Discretized Model

We augment our analytical and experimental investigations with simulations. We simulate a one-dimensional discrete-space, or "patch", version of equations (1a,b). These simulations are intended to mirror our experimental design (Experimental Methods), in which a yeast population is spatially distributed over 12 linearly arrayed subpopulations linked by periodic, nearest-neighbor dispersal (Fig. 1). The model, in general form for *n* patches, is

$$\frac{dU_i}{dy} = \frac{r_{\max} N_i}{k + N_i} - m_i U_i - g_i U_i^2 - D\left(U_i - \frac{1}{2}U_{i-1} - \frac{1}{2}U_{i+1}\right) \qquad (i=1,12)$$

(2a)

$$\frac{dN_i}{dt} = N_{input,i} - \eta N_i - \frac{r_{\max} N_i U_i}{\gamma(k + N_i)} \qquad (i=1,12)$$

(2b)

where no diffusion is assumed between the two end patches (1 and 12).

Experimental Methods

To test these hypotheses and to validate our spatial consumer-resource model, we conducted laboratory experiments in spatially distributed, single strain populations of budding yeast, where yeast serve as the consumer and the amino acid tryptophan as the renewable resource.

Yeast Strains

We used an auxtrophic, haploid (mat-a) strain of the budding yeast, *Saccharomyces cerevisiae (yMM039)*, provided as a generous gift from M. Mueller and A. Murray (Harvard University) (Mueller et al. 2014). Briefly, this strain was constructed in a prototrophic W303 background by replacement of the tryptophan biosynthesis pathway gene *TRP2* with an antibiotic resistance cassette, *KANMX*. This strain can synthesize all amino acids except tryptophan (throughout denoted as "Trp"), and therefore it requires growth medium supplemented with Trp for population growth. In all experiments, cells were propagated vegetatively (i.e., no sexual reproduction).

Culture Medium

All growth media consisted of 0.74 g/L of Complete Synthetic Medium minus Trp (CSM -Trp) (Sunrise Science) and 20 g/L dextrose. This base medium was then supplemented with different concentrations of Trp in order to manipulate the supply of the limiting resource in the growth media (specific concentrations reported below). In order to manipulate growth parameters independently of the resource level, we applied varying sublethal doses of the macrolide eukaryotic antibiotic cycloheximide (throughout denoted as Cyh) to the growth media. Cyh is a translation inhibitor that interferes with translation elongation by binding to the ribosomes, thus retarding *r.* We reasoned that, for a given Trp level, Cyh would slow *r* but have a smaller relative effect on *K*, which is set by the resource supply. Thus, Cyh would provide a means to experimentally manipulate the relationship between *r* and *K*.

Spatially Distributed Populations and Dispersal

A single "population" was composed of a single row of 12 wells ("subpopulations") in a 96-well microtitre plate. Thus, populations were spatially distributed over a 1-dimensional domain of 12 subpopulations potentially linked by nearest-neighbor diffusion (see Figure.3.1). Importantly, our experiments were designed such that consumers (yeast cells) disperse between wells, but nutrients do not. Each 12-well population had either a heterogeneous or homogeneous distribution of resources. A heterogeneous environment was designed by alternating Trp concentrations between 1.468 mg/L ("low" nutrient level, white circles) and 44.04 mg/L ("high" nutrient level, dark blue circles). A homogeneous environment was designed as having a uniform amount of Trp of 22.2 mg/L in each of the 12 wells (shown as the bottom row in Fig.1). These values provided the same total amount of Trp for the heterogeneous and homogeneous conditions. In each of the heterogeneous and homogeneous environments, we further had four concentrations of Cyh: 0 nM, 50 nM ("low"), 200 nM ("medium"), and 400 nM ("high"). Each treatment was replicated 4 times.

Experiments were initiated from an overnight culture of the strain grown in YPD (plus tetracycline and ampicillin to prevent contamination). The saturated culture was washed three times with sterile water and resuspended in the appropriate growth medium. 128 uL/well was transferred into each well of a 96-well plate, and then diluted by a factor of 2^{10} using a Biomek FXP liquid handling robot, providing an initial population size of ~10^5 cells in all wells. Each plate was incubated unshaken at 30 ºC for 24 hours.

Every 24 hours the plates were removed from the incubator and subjected to either a diffusion or a sham- diffusion protocol. The 96-well plate was shaken on a plate shaker to disperse the cell pellet. Using a Biomek FXP liquid handling robot, 3% volume was aspirated from each well and then transferred to a new plate ("Plate 2" in Figure.3.1). For the diffusion treatment, this volume was dispensed into Plate 2 in the adjacent position to the left (e.g., from well A2 in Plate 1 into well A1 in Plate 2; green arrows in Figure.3.1), thus generating 3% diffusion to the left. For the non- diffusion treatment, the volume was dispensed into Plate 2 at the same position (e.g., from A2 in Plate 1 into A2 in Plate 2), such that no diffusion of cells occurred (Figure S4.2 in Supporting Information, Appendix 4). This was repeated again, but with the 3% volume dispensed into the adjacent position to the right (e.g., from A2 in Plate 1 to A3 in Plate 2; red arrows in Figure.3.1) to generate diffusion of cells to the right. Again, for the non- diffusion treatment the volume was dispensed into Plate 2 in the same position as Plate 1. Then, the remaining volume in Plate 1 was dispensed into Plate 2 in the same position (e.g., A2 in Plate 1 into A2 in Plate 2; black arrows in Figure.3.1), constituting the non-diffusing fraction of the population. Thus, diffusion steps in our protocol did not dilute the populations. Note also that we did not implement a wrap-around boundary, such that the two perimeter columns of the 96-well plate (columns 1 and 12) only diffused in one direction. Wells from these two columns were thus excluded from all analyses to avoid edge effects.

To renew the resource and to ensure that resources do not diffuse with consumer cells, we centrifuged Plate 2 at 2400 rpm for five minutes, and "old" medium was removed using the liquid handling robot. Fresh medium was then dispensed into each

well, and the plate was shaken on a plate shaker to resuspend cells before incubating at 30 ºC for 24 hours. This procedure was repeated for 9 days, at which point the population densities for all treatments had approached an asymptote.

Population density was measured at each time point as the optical density (OD600) of the culture in each individual well using a plate reader (Tecan Infinite M200 Pro). At each time point, plates were removed from the incubator, shaken on a plate shaker to thoroughly disperse the culture in each well, and then the OD600 of each well was measured three times, with the average of these three technical replicates used as the measurement for each subpopulation (well).

Statistical Methods

A Treatment effects were estimated using a Mann-Whitney U test in the Non-parametric platform of JMP10 (SAS Institute, USA). In order to exclude the possibility of boundary effects biasing our results, since boundary wells 1 and 12 disperse in only a single direction, we further compared the diffusion effect on the total yeast population, in which two or three columns on each side were excluded respectively, at each condition, with same analysis. To estimate r and K, we used daily measurement of OD600 in each individual well of our “non- diffusion” treatments from day 1 to day 9, for three Trp concentrations (1.468, 22.2 and 44.04 mg/L) at 4 concentrations of the growth inhibitor Cyh (0, 50, 200, 400 nM) in all combinations. These *r* and *K* values were estimated by fitting the data to both the standard logistic growth and Gompertz growth (Paine et al. 2012) using custom fit in MATLAB R2015a. To describe the measured relationships between *r* and *K*, we used a linear function ($r = a*K+b$) to calculate the goodness-to-fit

for the *r* vs. *K* relationship. The overall goodness-of-fit is based on the coefficient of determination (R^2).

RESULTS

Mathematical results

The mathematical analysis of equations (2a,b) is presented in Supporting Information Appendices 5 and 6, providing total population sizes in the four cases for the two models, which are shown in Box 1, Appendix 5.

When evaluated numerically, the *Total population,heterogeneous, no diffusion* ($TPop_{hetero,\ no\ diff}$) and the *Total population,heterogeneous with diffusion* ($TPop_{hetero,\ diff}$), shown in Box 1, Appendix 5, can differ. As an example, consider Model 2 ($\eta=0$, $m_i = 0$, $g_i>0$), applied to the experimental system in which alternating wells contain nutrient (Trp) inputs of $N_{input,i} = N_{lownutrient} = 0.02$ ($i = 1, 3, 5, 7, 9, 11$) and $N_{input,i} = N_{highnutrient} = 0.6$ ($i = 2, 4, 6, 8, 10, 12$), the same proportions as in the experiment. Evaluation of equations (B19a) and (B19b) shows $TPop_{hetero,\ diff} > TPop_{hetero,\ no\ diff}$ when all values of g_i are the same (for all values of i, $g_i = 0.001$ in Figure 3.5). Assuming next that the values of g_i in low nutrient wells ($g_{lownutrient}$) can differ from those in high nutrient wells ($g_{highnutrient}$), we compare $TPop_{hetero,\ no\ diff}$ and $TPop_{hetero,\ diff}$ over a range of values of $g_{lownutrient}$, with $g_{highnutrient}$ fixed, showing $TPop_{hetero,\ diff} > TPop_{hetero,\ no\ diff}$ (compare solid and dashed curves in Figure 3.5). This range corresponds to a positive relationship between growth rate and carrying capacity. Simulations of equations (2a,b) show these results hold over the whole range of values of *D*. Similar results hold for Model 1; i.e., $TPop_{hetero,\ diff} > TPop_{hetero,\ no\ diff}$ over a range of parameter values (see Appendix 5). Thus the model results confirm Hypotheses 1 and 2 that, at steady state, a consumer population, when diffusing

in a spatial system with heterogeneously supplied exploitable resource, can exceed the total population of the population that is not diffusing when there is a positive relationship between growth rate and carrying capacity.

Next we consider the system in which the same resource inputs are spread homogeneously, again using Model 2 as the example. Hypothesis 3 states that higher population rate is obtained for the diffusing population in a heterogeneous environment than the population resulting from the same total nutrient input being distributed homogeneously (that is, *Total population, homogeneous*, or $TPop_{homo} < TPop_{hetero,\ diff}$). Actually, there are two expressions for $TPop_{homo}$, $TPop_{homo,\ diff}$ and $TPop_{homo,\ no\ diff}$, for $D \rightarrow \infty$ because these differ from each other. $TPop_{homo,\ diff}$ is given in equation (B19b), with $\sum_{i=1}^{n} \gamma N_{input,i}$ replaced by γN_{mean} where N_{mean} is the mean value averaged over wells. Thus $TPop_{homo,\ diff} = TPop_{hetero,\ diff}$, so it is given by the solid line in Figure 2.5. However, when D is close to zero, it can be proved (Appendix 6) and shown (model simulations) that $TPop_{homo,\ diff} > TPop_{hetero,\ diff}$ for values $g_{lownutrient} < g_{highnutrient}$, but $TPop_{homo,\ diff} < TPop_{hetero,\ diff}$ for $g_{lownutrient} > g_{highnutrient}$. The former case corresponds to a positive relationship between $N_{input,i}$ and g_i. $TPop_{homo,\ no\ diff}$ is given by expression (B19c). For this case of a non-diffusing population in a homogeneous environment, it is always true that $TPop_{homo,\ no\ diff} > TPop_{hetero,\ diff}$ (dotted line in Figure 3.5). Therefore, Hypothesis 3 does not hold in for a population that in non-diffusing in the homogeneous environment and only holds for the diffusing case when $N_{input,i}$ and g_i are negatively related.

Experimental Results

Figure.3.3 shows the final (nine day) total yeast concentrations (OD600) for the diffusion experiments in the heterogeneous environment. For the lowest concentrations of Cyh (0 nM and 50 nM) the final total population with diffusion (D) significantly exceeded that without diffusion (ND) (Figure.3.3a,b) (0 nM Cyh: $P = 0.0209$; 50 nM Cyh: $P = 0.0209$). For the highest two levels of Cyh (200 nM and 400 nM) no difference was observed. The daily amounts over the nine days are shown in Figure S4.3a, b, c, d in the Supporting Information, Appendix 4.

The insets in Figure.3.3 show the averages at day nine for the five lowest nutrient wells (filled triangles) and five highest nutrient wells (unfilled triangles) for both the diffusion and non- diffusion treatments. In the 0 nM and 50 nM cases there was no difference between the averages of the final subpopulation in high nutrient conditions (Trp level: 44.04 mg/L), but the averages of the final subpopulation in low nutrient conditions (Trp level: 1.468 mg/L) were higher with diffusion than without diffusion (filled triangle in Figure.3.3a). In contrast, in the high Cyh concentration treatments (200 and 400 nM), there was a weakened impact of diffusion on achieving a larger total population in heterogeneous environment than in homogeneous environment, resulting in no difference in total yeast population between diffusion and non- diffusion (Figure.3.3c,d) (200 nM *Cyh*: $P = 0.3865$; 400 nM *Cyh*: $P = 0.0833$). We hypothesize that the decreased impact of diffusion is due to the fact that Cyh inhibits yeast growth, which weakens the positive relationship between growth rate and carrying capacity and theoretically should diminish the difference between total population for diffusion and non- diffusion (see Mathematical Results). However, we found a slightly higher average

final subpopulation size in the high nutrient condition without diffusion than with diffusion.

We found a significant positive relationship between *r* and *K* through fitting a logistic growth to the non-dispersal data, with three different levels of Trp and four different levels of cycloheximide (Cyh) (Figure.3.4). We suspect that this positive relationship is mediated by the joint effect of the limiting resource on these two growth parameters. Specifically, lower concentrations of limiting resource (Trp) lead to both lower yield (low *K*) due to the lower overall abundance of growth-supporting nutrient, and to lower encounter rates between nutrient molecules and cells, which will cause slower growth (low *r*). Given the same Trp concentration, when Cyh was added, the *K* and *r* both decreased. This indicated that the addition of this toxic stressor not only reduced *r*, as expected from its mode of action (i.e., translation inhibition), but also reduced *K,* though to a lesser relative degree than it reduced *r*. The molecular and physiological mechanisms by which a translation-inhibitor can reduce yield are unclear, and suggest a deeper biological effect on the *r* and *K* relationship than resource-mediation alone. We found that the *r* and *K* relationship was more positive with 0 and 50 nM Cyh treatments than with 200 and 400 nM Cyh treatments (0 nM: $r = 1.765 *K - 0.7568$, $R^2 = 0.992$; 50 nM: $r = 1.634*K - 0.6875$, $R^2 = 0.985$; 200 nM: $r = 0.9941*K - 0.3437$, $R^2 = 0.955$ and 400 nM: $r = 0.5882*K + 0.04734$, $R^2 = 0.738$) (Figure.3.4a, b, c, d). Similar results were found based on Gompertz growth fitting.

Compared to heterogeneous case, there was no statistically significant difference of the final total population size with diffusion and without diffusion in homogeneous condition. This was consistent among all four Cyh levels (Figure.3.5a, b, c, d) (0 nM *Cyh*:

P = 0.0833; 50 nM *Cyh*: P = 0.0433; 200 nM *Cyh*:, P = 0.5637; 400 nM *Cyh*: P = 0.7728). Considering the average final subpopulation size in medium Trp level (22.2 mg/L), no difference was observed between diffusion and non-diffusion (filled triangles in Figure.3.5a, b, c, d). The average total yeast population (OD600) with (filled triangles) and without diffusion (unfilled triangles), under four Cyh concentrations at each day is shown in Figure S4.4 in the Supporting Information, Appendix 4. Also, we found that the total population size in all four levels of Cyh for no diffusion (Figure.3. 5a,b,c,d) exceeded the cases of heterogeneity with diffusion (Figure.3.3a,b,c,d).

Discussion

Both the experiments with yeast diffusing in a heterogeneous environment of exploitable resources (Figure 3.3) and the mathematical analysis (Appendices 5 and 6) confirm our Hypotheses 1 and 2 that, at steady state, a consumer population, when diffusing in a spatial system with heterogeneously supplied nutrient, can exceed the total size of a population that is not diffusing, when growth rate and carrying capacity are positively related. Both of the experiments (compare Figure 3.4 and Figure 3.3) and the mathematical analysis (Appendix 5) reject our third hypothesis, that higher population size is obtained for the diffusing population in a heterogeneous environment than the population resulting when the same total nutrient input is distributed homogeneously. This result would seem to contrast with the results of Holt (1985), Lou (2006) and DeAngelis et al. (2016), who show that diffusion allows the population in a heterogeneous system to exceed that attained in the system with homogeneously distributed local carrying capacity. However, those earlier results were derived with models in which the carrying capacities varied with spatial location yet were fixed in that

the population did not have a feedback effect on those values. Sometimes that assumption is justified, as in some cases space alone may be the main limiting factor, as for some intertidal populations (Paine 1966). But in many cases, some exploitable resource is limiting, so the feedback of the population on that resource must be taken into account.

The mathematical results were entirely consistent with our microbial experimental study. The empirical results showed a consistent and significantly higher (up to 10%) total yeast population with diffusion than without diffusion in the heterogeneous case; that is, the total population with diffusion exceeded the summation over the local observed carrying capacities. This suggests that if the resource inputs are heterogeneous by nature, creating heterogeneous carrying capacities, diffusion may be more advantageous for the population rather than not diffusion. As far as we aware, this is the first rigorous experimental support that the *r* vs. *K* relationships determined whether a diffusing population could exceed in size the sum of the local carrying capacities.

However, consistent with the mathematical models, when the same total resource inputs were distributed homogeneously, the total population size supported exceeded that of a diffusing population in an environment in which the same total resource was distributed heterogeneously. Therefore, spreading exploitable resource inputs homogeneously in space, if possible, is advantageous.

Our results also confirmed the hypothesis that there was a positive and convex relationship between carrying capacity and per capita growth rate, which was mediated by the joint effect of the limiting resource. Furthermore, the *r* vs. *K* relationship was manipulated by adding an external growth inhibitor, so that *r* vs. *K* relationship was transformed to be less convex with higher concentration of the stressor cycloheximide.

Importantly, we found that the difference in the total population size between diffusion and non- diffusion in heterogeneous environments was larger when *r* vs. *K* relationship was more convex. The growth inhibitor, by reducing the convexity of the *r* vs. *K* relationship, reduced the positive effects of diffusion on population size in the heterogeneous environment

The combination of mathematics and experiments reveal that some of the effects of diffusion in a heterogeneous environment differ when the heterogeneity is considered in terms of local resource inputs rather than in terms of local carrying capacities and growth rates. These two quantities are fundamental to ecological theory. Therefore, this study provides a new perspective, both experimentally and theoretically, for re-thinking about carrying capacity in heterogeneous environment, which has a crucial role on assessing and managing wildlife (e.g., Vasconcellos and Gasalla 2001, Goss-Custard et al. 2003, Hayward et al. 2007). Our findings demonstrate that the interaction of spatial heterogeneity and population dispersion complicates the notion of carrying capacity, which is especially important, as heterogeneous landscapes are becoming more common nowadays, due to landscape fragmentation and human activities (Pimm and Raven 2000; Pimm et al. 2006, Aviron et al. 2005; Clevenger and Waltho 2005, Denslow 1985). Therefore, such environmental heterogeneity could provide different qualities of habitats (Cosson et al. 1999; Dias 1996) and lead to different local population growth rates and carrying capacities (Basin and Thomas, 1999; Koivula and Vermeulen, 2005; Cutway and Ehrenfeld 2009; Herbener et al. 2012; Lemke and Salguero-Go´mez 2016). Our results also suggest that environmental stressor (as the function of cycloheximide in this study), such as drought, high salinity/temperature on plant (Bond-Lamberty et al. 2013;

Van Ha et al. 2013); high CO_2 on most calcifying organisms (Dineshram et al. 2012); and higher copper levels on Daphnia (Sommer et al. 2016), which usually adversely affect population growth, should also be considered as factors in the effective carrying capacity of a landscape. As a result, carrying capacity is a more complicated concept and many other factors should be involved in giving rise to an apparent carrying capacity in future studies, such as organism size (Brown et al. 2004), foraging costs (van Gils et al. 2004), and human management practices (Oesterheld et al. 2002).

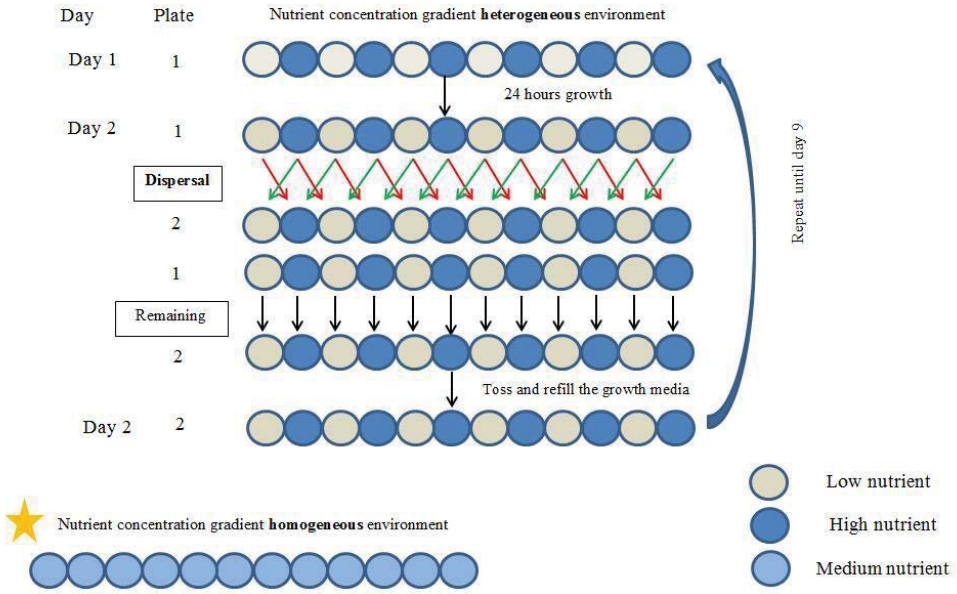

Figure 3.1. Schematic of experimental diffusion protocol. Represented is a single spatially distributed "population" composed of one row of 12 wells in a 96-well microtitre plate. Each circle is a single well. Color of a well represents nutrient (Trp) concentration. Alternating white/blue wells represents the heterogeneous environment treatment, while the population on the bottom of figure with all light blue wells represents the homogenous nutrient treatment. The initial yeast population had 24 hours growth at 30 ^{o}C, followed by a diffusion event from the original plate (plate 1) to a new empty plate (plate 2), in which 3% volume in each well was transferred to the well on the left in plate 2 (green arrows) and another 3% to the right well of plate 2 (red arrows). The remaining volume was transferred to the same well in plate 2 (black arrows). After the diffusion and transfer, plate 2 was centrifuged to create a yeast pellet at the bottom in each well, old media was removed and fresh media was added. The yeast population underwent another 24 hours growth, and the previous processes were repeated, up until Day 9. Non-diffusion treatments underwent a sham- diffusion protocol identical to the above, but instead of a well diffusing into adjacent wells on the left and right, it "diffused" into a single well so that no spatial diffusion of cells occurred.

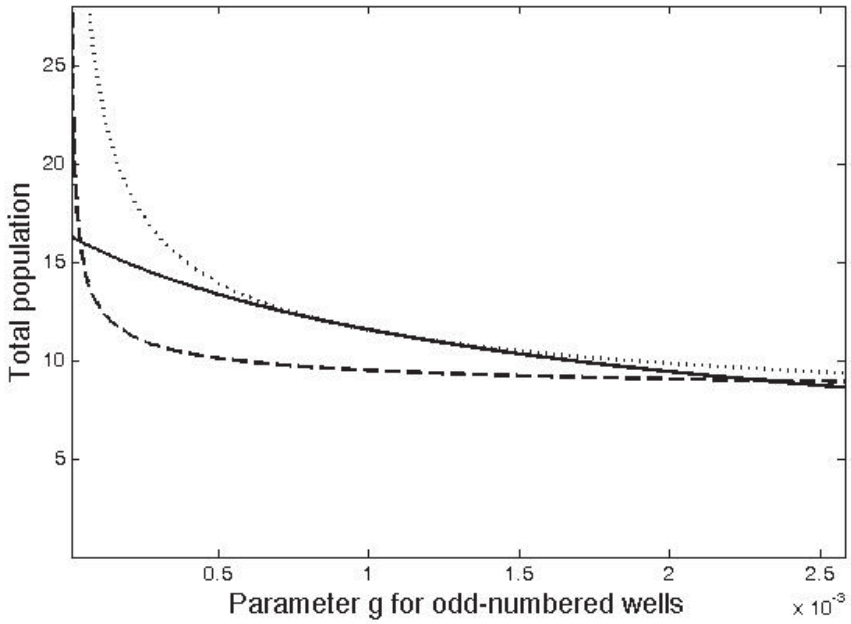

Figure 3.2. *Total population, heterogeneous, no diffusion (*$TPop_{hetero,\ no\ diff}$*,* dashed curve), *Total population, heterogeneous with diffusion (*$TPop_{hetero,\ diff}$*,* solid curve), and *Total population, homogeneous no diffusion (*$TPop_{homo\ no\ diff}$, dotted curve) as functions of the g_i value for the low nutrient input wells, $g_{lownutrient}$, (odd-numbered wells) for fixed value of the $g_i = 0.001$ for the high nutrient input wells, $g_{highnutrient}$ (even-numbered wells), for $D \rightarrow \infty$. $TPop_{homo\ diff}$ is the same as $TPop_{hetero,diff}$ (solid curve) for $D \rightarrow \infty$, but differs for small D (see text). For simplicity, the other parameters have been set to $r = 0.1$, $k = 0.1$, and $\gamma = 0.01$. The heterogeneous distribution is; $N_{input,i}$ = (0.02, 0.6, 0.02, 0.6, 0.02, 0.6, 0.02, 0.6, 0.02, 0.6, 0.02, 0.6), and the homogeneous distribution is; $N_{input,i}$ (0.31, 0.31, 0.31, 0.31, 0.31, 0.31, 0.31, 0.31, 0.31, 0.31, 0.31, 0.31).

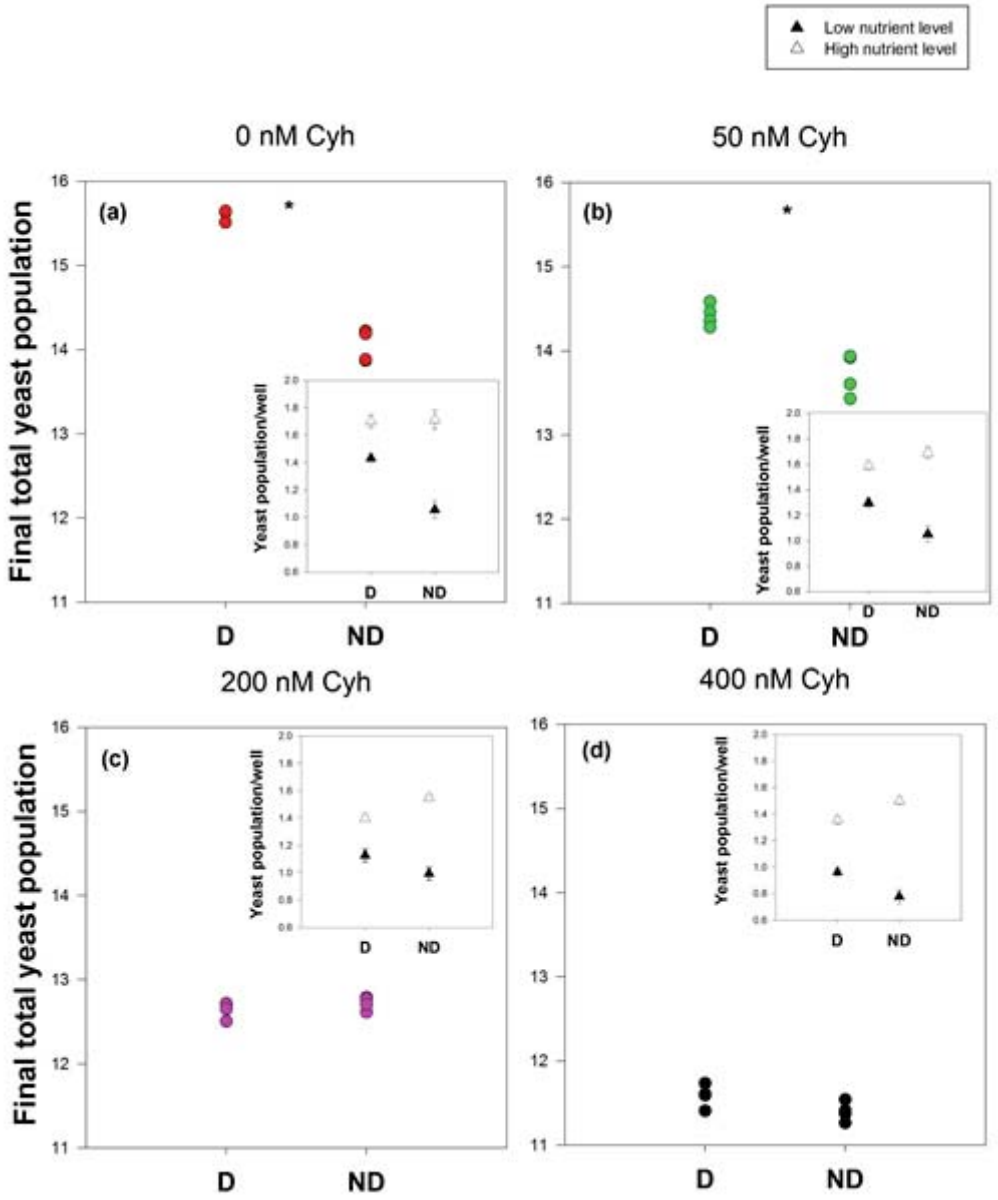

Figure 3.3. The final total yeast population (OD600) with four replicates with diffusion (D) and without diffusion (ND), at four levels of Cyh in the heterogeneous scenario: a. 0 nM, b. 50 nM, c. 200 nM, d. 400 nM. The diffusion rate is 0.06. Insets a, b, c, d: show the average final subpopulation in the low nutrient condition; that is, averaged over the five wells with lowest nutrients (1.468 mg/L of Trp) (filled triangle) and in the high nutrient condition; that is, averaged over the five wells with highest nutrient levels (44.04 mg/L of Trp) (unfilled triangle), with diffusion (D) and without diffusion (ND), with four levels of Cyh in the heterogeneous scenario (0 nM, 50 nM, 200 nM and 400 nM). Asterisks above the dots in a and b represented there was significantly higher final total yeast population with diffusion than without diffusion ($P < 0.05$). Cyh: cycloheximide, Trp: tryptophan. OD 600: optical density.

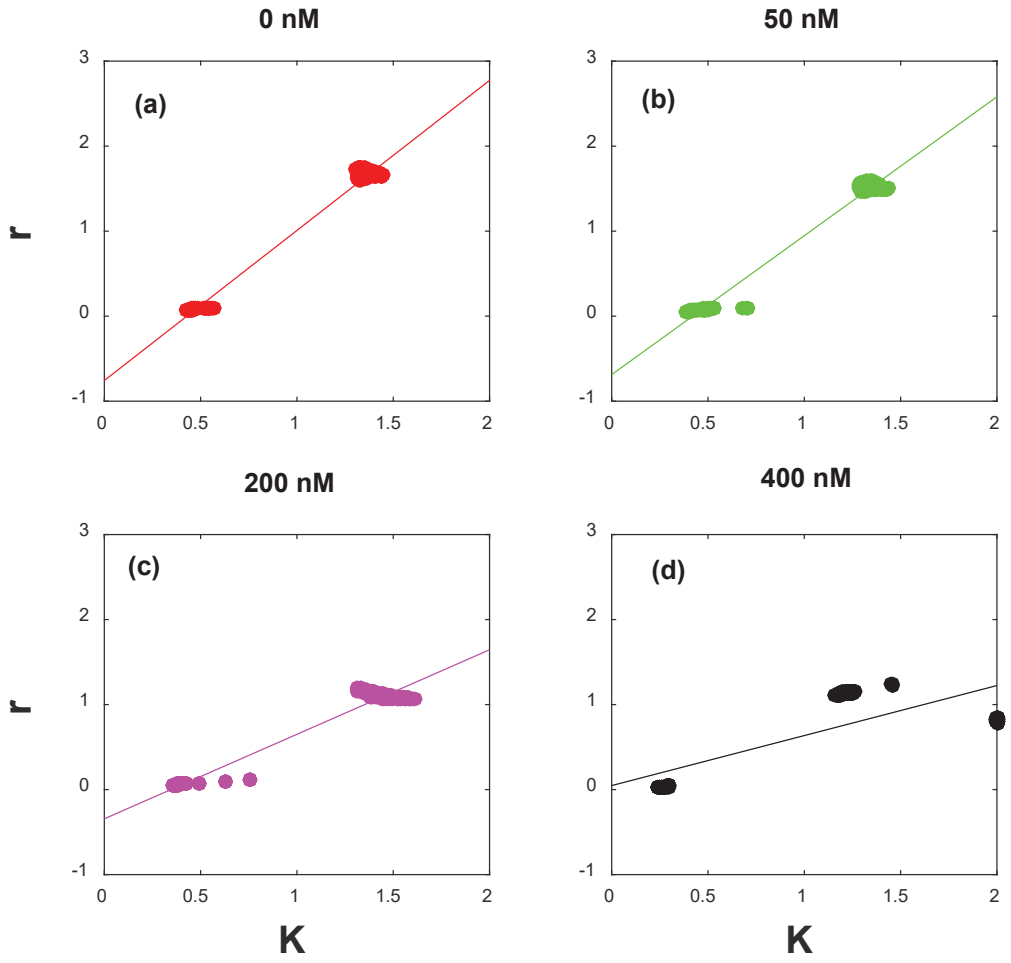

Figure 3.4. The relationship between per capita growth rates (*r)* and carrying capacity (*K*), estimated based on logistic growth. (a), (b), (c) and (d): The r and *K* were calculated from non-dispersal growth curve data at the three Trp concentrations used in the non-dispersal experiment (1.468, 22.2 mg/L and 44.04 mg/L) with four Cyh concentrations (results of the latter two concentrations converged). The solid lines represent the fitted line of the data points, using linear function (r = a*K), to calculate the goodness-to-fit for the *r* and *K* relationship.

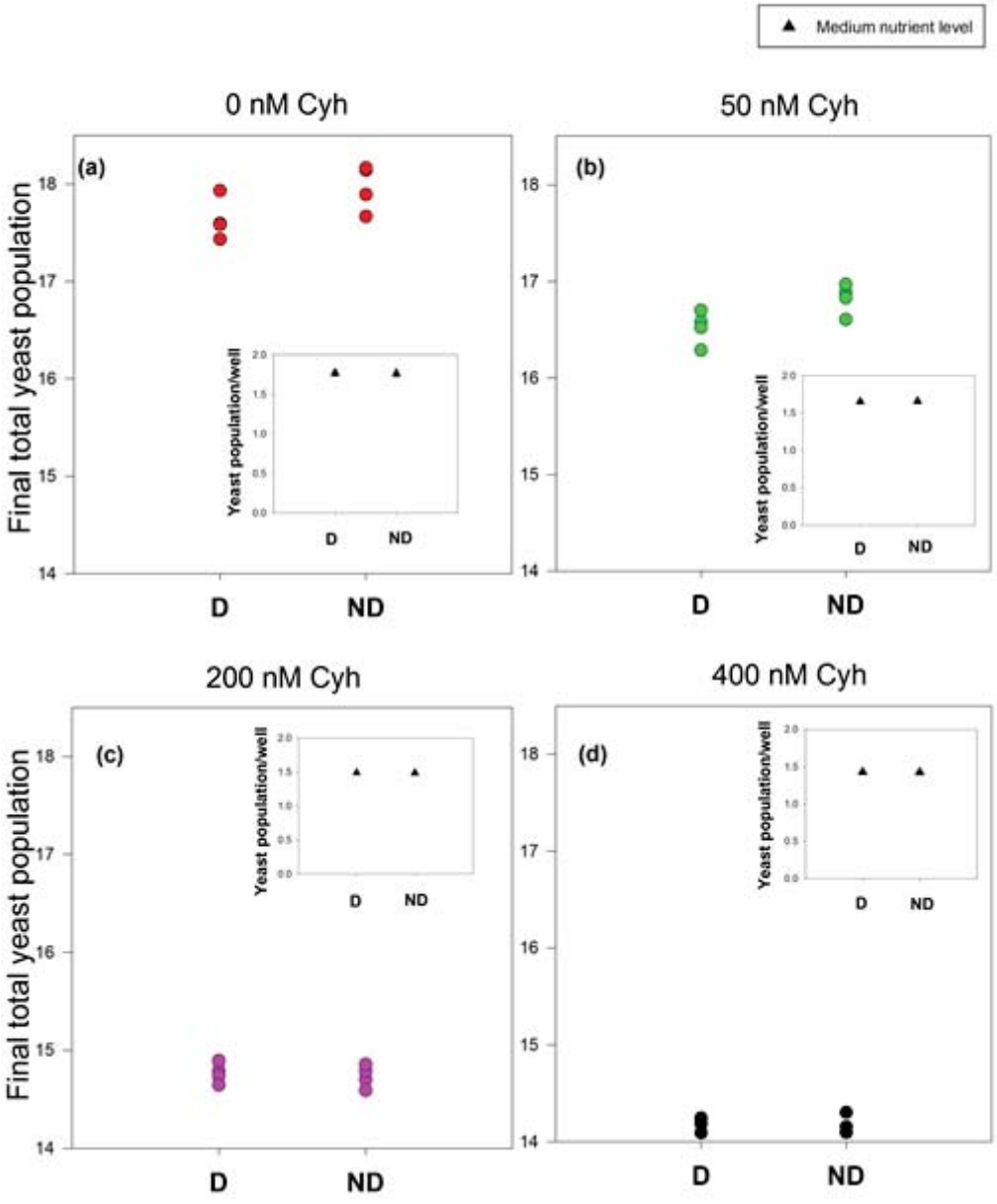

Figure 3.5. The final total yeast population (OD600) with four replications with diffusion (D) and without diffusion (ND), at four levels of Cyh in the homogeneous scenario: a. 0 nM, b. 50 nM, c. 200 nM, d. 400 nM. The diffusion rate is 0.06 per day. Insets a, b, c and d: the average final subpopulation in medium nutrient well (22.2 mg/L oft rp) (filled triangle), with diffusion (D) and without diffusion (ND), at four levels of Cyh in the heterogeneous scenario (0 nM, 50 nM, 200 nM and 400 nM). Cyh: cycloheximide, Trp: tryptophan. OD 600: optical density.

Chapter Four

Modeling the long-term effects of introduced herbivores on the spread of an invasive tree

Summary

Context*: Melaleuca quinquenervia* (Cav.) Blake (hereafter melaleuca) is an invasive tree from Australia that has spread over the freshwater ecosystems of southern Florida, displacing native vegetation, thus threatening native biodiversity. Suppression of melaleuca appears to be progressing through the introduction of insect species, the weevil, *Oxiops vitiosa*, and the psyllid, *Boreioglycaspis melaleucae*.

Objective: To improve understanding of the possible effects of herbivory on the landscape dynamics of melaleuca in native southern Florida plant communities.

Methods: We projected likely future changes in plant communities using the individual based modeling platform, JABOWA-II, by simulating successional processes occurring in two types of southern Florida habitat, cypress swamp and bay swamp, occupied by native species and melaleuca, with the impact of insect herbivores.

Results: Computer simulations show melaleuca invasion leads to decreases in density and basal area of native species, but herbivory would effectively control melaleuca to low levels, resulting in a recovery of native species. When herbivory was modeled on pure melaleuca stands, it was more effective in stands with initially larger-sized melaleuca. Although the simulated herbivory did not eliminate melaleuca, it decreased its presence dramatically in all cases, supporting the long-term effectiveness of herbivory in controlling melaleuca invasion.

Conclusions: The results provide three conclusions relevant to management: (1) The introduction of insect herbivory that has been applied to melaleuca appears sufficient to suppress melaleuca over the long term, (2) dominant native species may recover in about 50 years, and (3) regrowth of native species will further suppress melaleuca through competition.

Background

Melaleuca quinquenervia (Cav.) Blake (common names: melaleuca, paper bark, punk tree; Family, Myrtaceae, referred to as melaleuca thereafter) is a large (25-30m tall) native Australian tree introduced into the Florida landscape during the late 19th century for pulp production and ornamental purposes (Dray 2003). It has strong invasive attributes, such as ecological fire adaptation and high reproductive potential. A single 10-m tall open-grown tree can store over 20 million seeds in its capsules at any given time (Myers 1983). By the end of the 1900s melaleuca had spread over 200,000 ha of ecologically sensitive freshwater ecosystems of southern Florida (Dray et al. 2006) displacing native vegetation such as slash pine (*Pinus elliottii* Engelm.) and pond cypress (*Taxodium ascendens* Brong.), threatening native biodiversity (Serbesoff-King 2003; Martin et al. 2009, 2011). Melaleuca invasion has caused adverse economic and environmental impacts to southern Florida (Center et al. 2007), with the loss valued, 16 years ago, at nearly $30 million per year (Center et al. 2000).

The difficult work of making predictions of the establishment and spread of invading species such as melaleuca has important ecological and economic implications (e.g., Williamson 1999; Rai 2015a,b; Elliott-Graves 2016). Modeling has been applied to make predictions of future spread in many cases, including both niche modeling (e.g.,

Bradley et al. 2010) and mechanistic models (e.g., Higgins and Richardson 1996). Various control methods have been applied, including the use of biocontrol agents that are natural enemies of the pest species. Because use of both biocontrol and other methods of control are costly, prediction of the efficacy of control is needed. The long-term success of biocontrol is still uncertain, so modeling has been used in a number of cases of invasive species, including plant species (e.g. Maines et al. 2013; Krug et al. 2015)

Our objective is to apply modeling to melaleuca, for which biocontrol has been attempted. A program to suppress melaleuca, begun in 1997 with insect herbivore agents, including the melaleuca weevil *Oxyops vitiosa* Pascoe and the psyllid *Boreioglycaspis melaleucae* Moore (Myers and Bazerly 2003; Tipping et al. 2008, 2009; Center et al. 2012), appears to be highly successful. The introduced biological control agent *O. vitiosa* feeds exclusively on the foliar biomass while the sap-sucking psyllid feeds on foliage and stems (Pratt et al. 2005). The combined effects of these herbivores cause losses of leaves, forcing melaleuca to switch resource allocation from seed production to production of new, often unseasonal growth (Tipping et al. 2008). Field studies (Tipping et al. 2009) show that melaleuca weevils attack new lead tissue preferentially and relentlessly, thereby contributing to continuous defoliation and re-foliation cycles. Because complete recovery of leaf tissue is rare, the usual temporary reallocation of plant assimilates to leaf production may become permanent under this sustained herbivory. As a result, formerly pure stands of melaleuca are being re-colonized by native species (Tipping et al. 2012).

Through applications of insect herbivore agents, combined with mechanical removal and chemical treatments, melaleuca is now being removed from most public lands (Center et al. 2012). However, the extent to which melaleuca can be controlled to low levels

primarily through biocontrol is important to estimate, because of the costs of mechanical and chemical methods. Also, what the long-term recovery of native plant communities will be as melaleuca is gradually suppressed remains unknown. To investigate such possibilities, we used a modeling approach, made possible because a substantial amount of information is available on the melaleuca and stand dynamics for the period prior to the release of insect herbivores (Meskimen 1962; Myers 1983; Greenway 1994; Kaufman and Smouse 2001; Rayachhetry et al. 1998, 2001; Van et al. 2000; 2002; Serbesoff-King 2003). More recently, additional information has become available on the negative impact on melaleuca due to chronic damage inflicted by the insect agents (Pratt et al. 2005; Rayamajhi et al. 2007; Tipping et al. 2008, 2009; Martin et al. 2010). Information from these published data is sufficient to parameterize a well-known individual-based forest modeling platform, JABOWA-II (Botkin et al. 1972; Botkin 1993; Ngugi and Botkin 2011).

In JABOWA-II, establishment, growth and mortality of individual trees on small patches of land are simulated as functions of biotic factors (competition for available light) and abiotic factors (climate and soils) (Bugmann 2001). JABOWA-II and similar modeling platforms link environmental parameters to demographics and growth (Acevedo et al. 1996), and have provided successful simulations of forest succession in hundreds of cases around the world (Pausas et al. 1997). Given the compatibility of the data needed for JABOWA-II with the information available on melaleuca, JABOWA-II is well positioned to provide both understanding and forecasts on the dynamics of melaleuca-invaded forest stands in Florida. Below we describe the model and apply it to two types

of swamps that have been invaded by melaleuca, to project the long-term effects of continued control through herbivory.

Methods

Here we use the ODD (Overview, Design Concepts, and Details) approach of Grimm et al. (2006, 2010) to describe the individual-based JABOWA-II model (Botkin 1993). After that, we describe the scenarios and data analysis.

Description of JABOWA-II model

1. Purpose of the model

The purpose of using JABOWA-II in this study is to 1) simulate scenarios for two habitat types, Florida cypress swamp and bay swamp, including native species that are affected by melaleuca invasion, without and with the application of insect herbivory, 2) simulate scenarios of pure melaleuca stands (no native species are included) following the introduction of insect herbivory, and 3) project extended future changes that might occur over successional time scales in the scenarios of cypress and bay swamp.

2. Entities, state variables and scales

The entities of the model are individual trees. Besides melaleuca, these are slash pine (*Pinus elliotti*), pond cypress (*Taxodium ascendens*), dahoon holly (*Ilex cassine* L.), sweet bay (*Magnolia virginiana* L.) and loblolly bay (*Gordonia lasianthus* L.). Insect herbivores were not simulated explicitly; a constant effect level of herbivory on each melaleuca tree was assumed, by decreasing the melaleuca reproduction rate by 49% and

the growth rate by 83% based on empirical measurement in Tipping et al. (2008), which represented the maximum levels.

There are two types of variables. First there are the characteristics of the environment, which are the site variables. In this case, the light environment at different heights above ground is the main environmental state variable. Each tree is assumed to be able to affect the light environment of every other tree in the plot, through shading, depending on a combination of the relative heights of the trees and individual tree species' leaf area index. Hence, the only resource for which there is competition in JABOWA-II is light. The belowground resources, such as water and nutrients, are specified for a site. These affect plant growth but are not assumed to be affected by feedback from the tree communities, and are summarized in the $f_i(environment)$ factor of the growth equation (see Growth submodel below).

The second set of variables, the state variables, consists of the characteristics of the trees; in JABOWA-II, the diameter at breast height (DBH) is the key state variable. All other variables, such as height, vertical leaf profile, etc., are deduced from stem diameter via allometric relationships.

3. Processes

JABOWA-II simulates plant succession on yearly time steps for up to 600 years in a 0.01 hectare plot, using the life history characteristics (see Table 1 for the characteristics in the model) and environmental preferences of several woody plants and a set of environmental conditions. Each tree is simulated individually from the sapling stage. JABOWA-II includes the following basic features: establishment, growth, and mortality.

Establishment: A maximum limit on the possible number of new saplings that can be established is determined for each year. The actual number is modified by site conditions, including the light environment, and depends also on the degree of shade tolerance of the species. For less tolerant species the number of saplings would be limited, depending on light available. Within those limits, a uniformly distributed random number is used to determine the actual number of saplings established in a given year.

Growth: Diameter growth, *D*, is modeled as a deterministic process on an annual time step, based on a consideration of the maximum possible growth rate (*G*) at a given size under optimal conditions. *D* is reduced according to the canopy volume (leaf area index) and stand volume (as woody biomass) (Smith and Urban 1988), which affect available light, as well as by environmental factors. Growth is described further under Growth submodel.

Mortality: Tree mortality is modeled as a stochastic process and is assumed to consist of two components: (1) a background mortality that allows on average only 2% of the trees to survive to maximum tree age (a model parameter) where annual mortality probability is constant across tree life, and (2) a stress-related mortality that acts when diameter increment is less than 0.01 cm for any given year and species. For stress-related mortality, a tree has a 1% chance of surviving 10 stress years; as soon as there is no stress, the stress-related mortality ceases to be effective. Hence, it is assumed that there are no lags between the occurrence of stress and the associated mortality, and that stress tolerance is not species-specific.

Design Concepts

Emergence: The dynamics of tree species composition and size distribution are computed in each simulation scenario, and are emergent phenomena of the competition for light.

Adaptations: The tree species have different adaptations to shading (S), nitrogen availability (N) and ground water table depth (DT), quantified as indices of tolerance to each environmental factor.

Fitness: The fitness of a tree is defined in terms of its growth over its past several years. The greater the growth, the more fit the tree is, both in terms of competitive fitness (height advantage) and avoidance of stress-related mortality, the chance of which increases when growth decreases below 0.01 cm per year.

Interaction: The interactions between trees occur through shading. Each tree is assumed able to affect every other tree in the plot, through shading, depending on the relative heights of the trees and their leaf area indices.

Stochasticity: JABOWA-II is a Monte Carlo simulation model. Stochasticity is incorporated into establishment and mortality processes; that is, how many new saplings of each species will be added to the plot and both yearly natural mortality and stress-related mortality.

Details

1. Site description

We simulated two types of swamp habitat in Florida affected by melaleuca invasion, Florida cypress swamp and bay swamp, for which information on environment and plant demography are available from studies of two sites (Casey and Ewel 2006). Although the information used here is from cypress and bay swamps in northern Florida, we believe these are reasonable surrogates for the similar swamp types in southern Florida, which is the focal area for our simulations. These two habitats are similar to field sites used in Tipping et al. (2007, 2009).

In this region, the mean annual rainfall is about 1331 mm to 1364 mm (NOAA 1968-1977), most of which occurs from June through September. Mean monthly temperature ranges from 14.4 ºC to 28.3 ºC (NOAA 1968-1977).

Cypress swamps are relatively deep (standing water depth = 20cm), while bay swamps represent shallower (standing water depth = 8cm), peaty swamp (Penfound 1952; Ewel 1990). Cypress swamp has standing water for at least part of the year and is dominated by pond cypress (Mitsch et al. 1979; Deghi et al. 1980). The vegetation communities in cypress habitats vary along a hydrologic gradient. Cypress swamp generally forms in poorly drained to permanently wet depressions in areas of pine flatwood. Cypress-hardwood associations are defined as communities in which cypress grows in association with species such as red maple (*Acer rubrum* L.), ash (*Fraxinus sp.*), cottonwood (*Populus heterophylla* L.) and water oak (*Quercus nigra* L.). A cypress-pine association is indicative of severely drained conditions, which allow slash pine (*Pinus elliottii*) and

sweet bay (*Magnolia virginiana* L.) to invade cypress (Brown 1981). Cypress in pure stands generally indicates continuous high water (Mitsch and Ewel 1979).

At least 50% of the tree species in bay swamp are broad-leaved evergreen trees growing on acid soils high in organic matter and subjected to seasonal flooding. Canopy species include red bay (*Persea borbonia* L. (Spreng.)) and swamp bay (*M. virginiana*), as well as dahoon holly (*Ilex cassine*) and pond apple (*Annona glabra* L.) (Monk 1966, 1968).

In JABOWA-II, the main implemented differences in environmental conditions between cypress swamp and bay swamp are soil depth and standing water depth. Parameter values are listed in Supplementary Information (SI): Table S1. We selected five native species: slash pine, pond cypress, dahoon holly, sweet bay and loblolly bay, for which most information on key parameters for JABOWA-II is available (Table 1). Another reason for selecting those five native species is that pond cypress and slash pine are the dominant canopy trees, with 77% of total relative frequency in cypress swamp. Loblolly bay and sweet bay together dominate bay swamp with 76% relative frequency (Casey and Ewel 2006). All five species are present in both cypress and bay swamp.

2. Submodels

Only the Growth submodel is described here, as the other submodels are described in sufficient detail under 3. Processes.

Growth submodel

In JABOWA-II, diameter at breast height of the tree (*D*) is the key state variable. The growth equation is:

$$\delta D = \frac{\{G_i D[1-[D(137+b_{2,i}D-b_{3,i}D^2)/(D_{max.i}H_{max.i})]]\} * f_i(environment)}{274+3b_{2,i}D-4b_{3,i}D^2}, \quad (1)$$

where δD is the annual growth increment and

$D_{max,i}$ = maximum diameter of tree of species i

$H_{max,i}$ = maximum height of tree of species i

G_i = maximum growth rate parameter

b_2, b_3= parameters in height vs. diameter relationship

and where $f_i(environment)$ (< 1) incorporates the effects of environment, causing δD to decrease from the value it would have under optimal environmental conditions. Specifically,

$$f_i(environment) = f_i(AL)*Q_i*s(BAR), \quad (2)$$

where available light, $f_i(AL)$, is a function of leaf area index (AL) and Q_i measures site quality, which depends on the effects of several factors;

$$Q_i = TF_i*WiF_i*WeF_i*NF_i, \quad (3)$$

where TF_i is the effect of temperature on tree growth as a function of growing degree-days during current year at site ($DEGD$), WiF_i is the effect of soil moisture on tree growth, or the wilting factor for effect of drought, and WeF_i is the wetness factor for the effect of soil wetness, including flooding. In particular, WiF_i is related to water depth and WeF_i is related to the height of the water table tolerable for the species. NF_i is the nitrogen factor for the effect of soil nitrogen, which is based on the species-specific concentration of

nitrogen in leaves and the concentration of available nitrogen in the soil. The function $s(BAR)$ represents the density-dependent limitation on the total basal area of the stand.

3. Parameterization of model

Key life cycle parameters used for each species in JABOWA-II are listed with definitions in Table 1, and values are in SI: Table S2. The values of all the parameters are from literature, based on field studies (see SI: Table S3); for example, the studies of Rayachhetry et al. (2001); Serbesoff-King et al. (2003) and Tipping et al. (2013) were used for the melaleuca parameterization. All parameters in JABOWA-II can be adjusted to apply to a particular situation. We assigned all parameter values for which data could be found for the cases modeled here, but a few that were not known were left as default values of JABOWA-II.

4. Initialization

The initialization for each type of simulation is noted in the scenario descriptions.

Descriptions of scenarios

The scenarios that are evaluated by model simulations are designed to both show the effects of melaleuca on the native forest, which can be compared with data, and project how the impact of herbivory may reverse these effects and allow the native forest to recover. We begin by simulating the cypress swamp and bay swamp forests without melaleuca to help calibrate the model. We then simulate the invasion of melaleuca in both forest types over 600 years, along with simulations in which biocontrol is added at year 300. We also simulate the effects of herbivory on pure melaleuca stands, as there are

short-term empirical data that can be used for comparison. Finally, we do a sensitivity analysis by assuming the herbivory is less efficient than the estimates we used based on empirical data.

Scenario 1. This scenario was used for calibration with densities and size distributions of native species in cypress and bay swamps without melaleuca, based on Casey and Ewel (2006). (More description, see SI, Appendix S1).

Scenario 2. These simulations started with a cypress swamp community with the size distributions of native species in cypress swamps after 300 years from scenario 1. We allowed melaleuca to invade this community at year 1 and simulated its invasion for 600 years. The simulation provided a test of whether the model agrees with recently observed effects of melaleuca on the native community, and projected the effects of melaleuca with no herbivory on the native community 600 years into the future. In an accompanying simulation, insect herbivory was added beginning at 300 years, via decreasing the melaleuca reproduction rate 49% and the growth rate 83%, based on empirical measurement in Tipping et al. (2008).

Scenario 3. These simulations were the same as scenario 2, but simulated bay swamp.

Scenario 4. These simulations projected the long-term effects of herbivory (600 years) on the pure melaleuca stands (i.e., no other species were included in the simulation), starting from saplings. There were four sub-scenarios; no herbivory impact; the addition of herbivory on melaleuca-dominated stands starting with small-sized (54 cm^2/m^2 in basal area); with medium-sized (76 cm^2/m^2 in basal area); and with large-sized

trees (134 cm^2/m^2 in basal area). We compared model simulation with empirical data (Rayamajhi et al. 2007).

Sensitivity analysis. Sensitivity analysis was applied to two parameters regarding the effectiveness of herbivory; SAP (maximum number of saplings of species that can be added in any one year to the 0.01 hectare plot) and *G* (maximum growth rate of tree of species) in pure mature-grown melaleuca stands. In scenario 4, reductions in SAP and G were 49% and 83% respectively, here, we reduced these to 25% & 40% and 10% & 10%.

Data analysis

All simulations were replicated 50 times. The relative proportion of each species in both cypress swamp and bay swamp was calculated directly as (the number of stems by species÷the total number of stems in all the species)*100.

Results

Scenario 1. The results of scenario 1 simulations showed the model's expected dynamics of native species without melaleuca's invasion under the current climate, which agreed with field measurements (Figure. 4.1, note a log scale is used). For more description, see Appendix 7.

Scenario 2. Simulations of melaleuca's invasion in cypress swamp without and with herbivory were started with the densities of the mature cypress swamp community projected in scenario 1. We first describe the simulation without herbivory, shown for a typical simulation with solid data markers in Figure. 4.2a and b. External input of melaleuca, as saplings, started from year 1 and continued until the melaleuca in the site

were large enough to reproduce. The simulation demonstrated that melaleuca stem density grew from 100 to 350 trees/100m^2, then dropped to 50 trees/100m^2 due to intraspecific competition (self-thinning) and interspecific competition from native species, especially pond cypress (Figure. 4.2a; error bars shown in Figure. S7.1a). Melaleuca recovered, with oscillations, toward a steady state density of about 200 trees/100m^2 (filled circles). Overall, melaleuca had greater stem density of individuals than the other species, including pond cypress. Slash pine lost half its original density due to melaleuca invasion in the simulations (Figure. 4.2a. filled trianglesup). Pond cypress was able to maintain dominance in basal area over melaleuca during most of the 600-year simulation without herbivory, though melaleuca slightly exceeded cypress in basal area for several decades (Figure. 4.2a), roughly years 120 to 200, when large numbers of melaleuca saplings were growing in size. After that period, melaleuca's basal area decreased from 40 to 25 due to interspecific competition with cypress and mortality of larger, older trees (Figure. 4.2b, filled circles).

At year 300, insect herbivory was added in the simulation, by decreasing the melaleuca reproduction rate by 49% and growth rate by 83%. In contrast with the simulated case without the herbivores (Figure. 4.2a, filled circles), melaleuca stem density declined from 80 to 30 trees/100m^2 within 50 years of herbivory application (Figure. 4.2a, unfilled circles), and thereafter melaleuca's density remained below 100 trees/100m^2. Pond cypress started to rapidly increase in basal area, due to decreased competition for light, so existing cypress individuals were able to grow larger in size and accumulate greater basal area, although stem density changed little. Melaleuca's basal area decreased from its previous level of 30 to very low levels (2-3 cm^2/m^2) (Figure. 4.2b, unfilled circles).

Although there was some increase in melaleuca stem density from its low by 600 years, its basal area did not recover. In order to make it easier to see the values of slash pine, sweet bay and loblolly bay, which are at very low levels, their densities and basal areas are plotted separately at a finer scale in Figure. 4.2c, d. We found the three species all had higher basal area (unfilled line) after insect herbivory was applied, compared to without herbivory (filled line).

Scenario 3. As in the cypress swamp scenarios, we first considered the 600-year simulations without herbivory impact, starting with the mature bay swamp community projected from scenario 1, which was dominated by understory trees or shrubs (sweet bay and loblolly bay) beneath the cypress canopy. Compared with cypress swamp, melaleuca rapidly invaded bay swamp, due to its stronger competitive capacity in bay swamp than cypress swamp, as shown in a typical simulation (Figure. 4.3a; and finer scale in Figure. 4.3c; error bars in Figure. S7.2a). Melaleuca reached a peak density (saplings plus trees) of about 2800 trees/100m^2 (Figure. 4.3a. filled circle line) by year 50. Its density then dropped to 200 trees/100m^2 by year 200, mainly due to intraspecific competition (self-thinning), and then oscillated around 400 – 800 trees/100m^2. Melaleuca basal area increased to a high of 90 cm^2/m^2 at year 100 (Figure. 4.3b; error bars in Figure. S7.2c), and then decreased to roughly 55 cm^2/m^2 at year 250 (Figure. 4.3b, filled circles). The native species survived at lower densities in the simulations (Figure. 4.3a, filled trianglesup, stars, diamonds and trianglesdown) and all decreased in basal area during the first 100 years, in response to melaleuca's increase (Figure. 4.3b, filled trianglesup, stars, diamonds and trianglesdown).

The addition of herbivory on melaleuca at year 300 suppressed melaleuca's reproductive rate by 49% and growth rate by 83%. Melaleuca declined in density from 700 to 100 trees/100m^2 at year 320, though it then recovered to about 200 trees/100m^2 (Figure. 4.3a, unfilled circles) by year 400. This stem density was close to the simulated density without herbivory, but these were very small stems, as the results for basal area (below) show. Meanwhile, dominant native species in bay swamp, especially loblolly bay, started to grow back after melaleuca growth was restricted by herbivory. Compared to loblolly bay, the density of sweet bay was still low even when herbivory was applied, because it is less shade-tolerant than loblolly bay. Slash pine also dropped its density because of its low reproduction rate and perhaps shading. With herbivory the basal area of melaleuca declined rapidly from 45 to less than 5 cm^2/m^2 in 100 years, as the application of herbivory killed larger trees through chronic damage to leaves (Figure. 4.3b, unfilled circle line) and melaleuca did not grow back as sizable trees. After melaleuca lost its dominant position, native species that had been suppressed started to grow back in numbers and basal areas, reaching their typical observed levels in stands without melaleuca in about 100 years (Figure. 4.3b, d, unfilled trianglesup, stars, diamonds and trianglesdown).

No empirical data are available to compare with these long-term effects of herbivory for either cypress or bay swamp, which suggests that it is important to continue long-term field observations of the impact of herbivory to further test and improve the model.

Scenario 4. This 600-year simulation was started from a plot with only melaleuca saplings. Starting with an external input of saplings during the first few decades, there was a continuous increase of melaleuca density until it reached a maximum of about 800

trees/100m^2 at year 50, followed by a sharp decrease due to both self-thinning and mortality of old-aged trees (Figure. 4.4a, red dashed line; error bars in Figure. S7.3a), then an oscillating recovery towards a steady state of between 100 and 200 trees/100m^2. Concomitant with the increase in stem density, the melaleuca increased in basal area during the first 100 years, to the maximum amount of 135 cm^2/m^2 (Figure. 4.4b. red dashed line; error bars in Figure. S7.3b). Then basal area declined with stem density from 130 to 45 cm^2/m^2 during the next 200 years, and began an oscillating trend towards a steady state. Empirical data from Rayamajhi et al. (2007) in three study sites in southeastern Florida were available for a melaleuca-dominated site without insect herbivory, shown as red dots in Figure. 4.3a and b. The model followed the increase in basal area very well over about 60 years (Figure. 4.4b), but did not fit the observed rapid decline in stem density, which declined faster than the simulated density.

Empirical data from Rayamajhi et al. (2007) were also collected following herbivory in nearly pure melaleuca stands. We attempted to match these empirical data, with points in time along our simulation that corresponded to stands of approximately the same ages and basal areas as when those studied in the field were affected by herbivory. These empirical data points are shown as blue, purple, and green dots in Figure. 4.4a and b. Herbivory in the simulation was applied by decreasing the melaleuca reproduction rate by 49% and the growth rate by 83%, in each of three different melaleuca stands, having basal areas of roughly 50, 80, and 130 cm^2/m^2 (black arrows in Figure. 4.4b). We concentrate here on Figure. 4.4b, as the model fits basal area better than stem density. Note that the rate at which the basal area declines following introduction of herbivory in the simulation depends on the initial basal area of the stand. In the model it is possible

that older, larger individuals are more strongly affected by the herbivory (perhaps because they are already stressed from competition), which slowed their rate of growth and increased their mortality rate, so that the stand with larger basal area (i.e., larger trees) experienced a greater rate of decline (Figure.4.4b blue and green solid lines). Simulated impact of herbivory caused slowest decline in stands with younger, smaller individuals (Figure. 4.4b, black solid line). During the course of the simulation, herbivory decreased melaleuca's basal area from both the 135 cm^2/m^2 (Figure. 4.4b blue solid line) and 80 cm^2/m^2 (Figure. 4.4b, green solid line) starting values down to 5 cm^2/m^2, when applied to stands with larger trees. However, during the same period, the simulated melaleuca stand starting from a basal area of 45 cm^2/m^2 declined only to 25 cm^2/m^2 (Figure. 4.4b, black solid line). We did not observe recovery of melaleuca from these low values in any of the three sub-scenarios simulations, and herbivory significantly decreased melaleuca's basal area compared to stands without its application (Figure. 4.4b, red dashed line). All three sub-scenario simulation results fit field data from Rayamajhi et al. (2007) well (Figure. 4.4b blue, green and black dots), although these field data span too short a time interval to be a strong test of the model. Similar results were found in the changes of melaleuca stem density with application of herbivory on different size stages (Figure. 4.4a), though they are not as clear as in the case of basal area densities.

Scenario 5. The sensitivity analysis results showed that a mere 10% decrease of both reproduction rate (SAP) and growth rate (G) lead to lack of control melaleuca's invasion (Figure. 4.5). In fact, density and basal area levels were found to be the same as the field observations of uncontrolled melaleuca now. A 25% reduction of reproduction rate (R) and a 40% decrease of the growth rate were shown to keep melaleuca somewhat lower

than the non application of herbivory case. But we found that only application of herbivory impacts much closer to a 49% reduction of reproduction rate (R) and a 83% decrease of the growth rate (G) were able to control melaleuca to a very low level.

Discussion

Effects of the biological control agent on recovery of native woody plant communities

The model projects substantial herbivory-mediated reduction in survival and reproductive potential of melaleuca. Introducing herbivory in our simulations led to large reductions of stem density and basal area of melaleuca. This agrees with Rayamajhi's (2007) field measurements. Native plants are projected to recover basal area and stem density comparable to the pre-melaleuca invasion state (although slash pine and sweet bay did not completely recover in bay swamp). The simulations also show that as native plants recolonize the habitat, melaleuca is further suppressed, since melaleuca trees are rendered less competitive due to chronic damage inflicted by insect herbivores. Because of the short time available for field observations following the introduction of specialized herbivores, no significant recolonization by natives has been recorded. However, Rayamajhi (unpublished data) found increases in native plant diversity and abundance following herbivore-mediated declines for melaleuca growing in wetter, higher organic soils.

This relates to the problem of specialist biocontrol agents in general. These require some persistent population of their host species to remain as effective control agents (Murdoch and Briggs 1996, Ewel et al. 1999, Fagan et al. 2002, Symondson et al. 2002, Stiling and

Cormelissen 2005). A general strategy in such cases has been the augmentation of the biocontrol agents through periodic mass rearing and reintroduction (DeBach 1974), Reduction of melaleuca to a relatively minor component of future tree communities could also facilitate application of other methods (e.g., mechanical removal and chemical treatment) to reduce it further.

Effects of biological control agent on different size staged pure melaleuca stands; management implications

Simulation results (Figure. 4.4 a, b) showed good fits to empirical data, especially basal area, when no herbivory was applied to these stands. Projections show that without control melaleuca has higher stem density and basal area in pure stands than when it is mixed in cypress- and bay-swamps (figures 4.2, 3), due to the lack of interspecific competition with native species. Oddly, the introduction of herbivory to the early-age pure melaleuca stand (starting at 54 cm^2/m^2 in basal area) did not reduce basal area as much as its application to older stands (starting at larger than 76 cm^2/m^2 in basal area) (Figure. 4.4b). This greater reduction of the older stands may reflect that these are already under stress due to high basal area density.

The sensitivity analysis shows a large drop in effectiveness of control would occur if negative effects of herbivory on growth and reproduction (such as only 10% decrease of both reproduction rate and growth rate) were appreciably less than estimated from empirical data. This suggests that managers should attempt to maintain reductions on reproduction and growth as close to the levels of 49% and 83%, respectively, as possible, to have the level of effects shown in our simulations.

Three conclusions relevant to management can be drawn from our model findings: (1) The introduction of insect herbivory applied to melaleuca is sufficient to suppress melaleuca to a low density and basal area level over the long term. (2) It takes about 50 years for native species to recover in the system and gain higher basal area. Thereafter, the density of melaleuca remains lower than if there are no native species in cypress swamp, suggesting that cypress will aid control by shading the melaleuca saplings. (3) Fostering native species reinvasion will help control melaleuca through competition.

Model limitations

Parameters of both plants and environment are limited by the available field measurements and observations. We have not included all the species and environmental conditions in southern Florida. We have only been able to test the model's usefulness on a small set of selected species, and the effect of herbivory on melaleuca-dominated stands. We could improve the model via recoding JABOWA-II to include more site variables, such as available phosphorus. One model conclusion that needs further consideration is that pond cypress maintained dominance over melaleuca in the cypress swamp simulation (Figure. 4.2a), as melaleuca has been found to take over in some cases (K. C. Ewel, personal communication). Absence of fire in the model is one possible explanation. Another limitation of the present simulations is that the climate is assumed constant, which is unlikely over the 600-year scenarios. Our future plan is to use 100-year climate projections to refine model output.

Implications of using an individual based forest model on other invasive plant issues

Biological control offers long-term, economically viable management potential, by reducing the rate of spread, vitality and growth rate of plants, thus rendering them more vulnerable to other environmental stresses and other control methods (Turner et al. 1998). Models that can accurately predict the long-term impact of such control on performance of native species in melaleuca-invaded habitats will be especially useful for freshwater systems that were previously dominated by melaleuca.

Table 4.1: Definitions of key parameters in the model

Notation	Definition
S	Shade tolerance. This is input as categorical values; 1 (intolerant), 2 (moderately tolerant), or 3 (tolerant)
N	Tolerance to low nitrogen availability. This is input as categorical values; 1 (intolerant), 2 (moderately tolerant), or 3 (tolerant)
SAP	Maximum number of saplings of species that can be added in any one year to the 0.1 hectare plot
R	Maximum possible relative growth rate of tree
C	Relationship between total foliage weight, W, and diameter at breast height, D
DMAX	Maximum possible diameter at breast height (dbh)
HMAX	Maximum possible height of tree
AMAX	Maximum age tree can reach
AINC	Minimum diameter growth in a year that a tree can grow and still be considered healthy
DDMIN	Minimum growing degree days for species
DDMAX	Maximum growing degree days for species
DT	Maximum depth of water table possible for species to persist
WLTMX	Maximum wilt possible for species
LT_MIN	Minimum light (as a fraction of full sunlight) under which a tree can grow

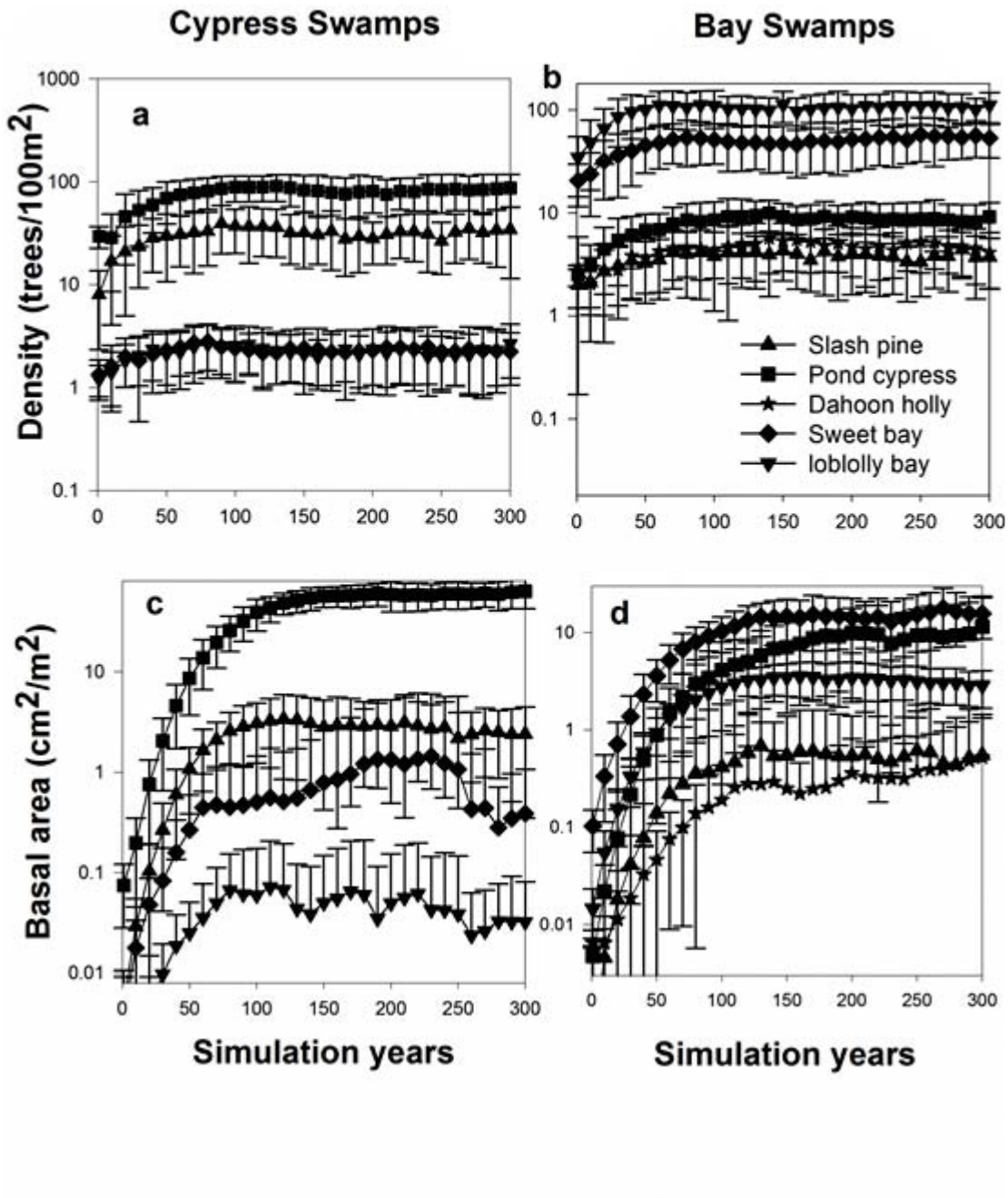

Figure 4.1 a the stem densities and **b** the basal areas of the four woody plant species included in modeling in cypress swamp without melaleuca. **c** Projected densities and **d**: Projected basal areas of the five woody plant species included in modeling in bay swamp without melaleuca.

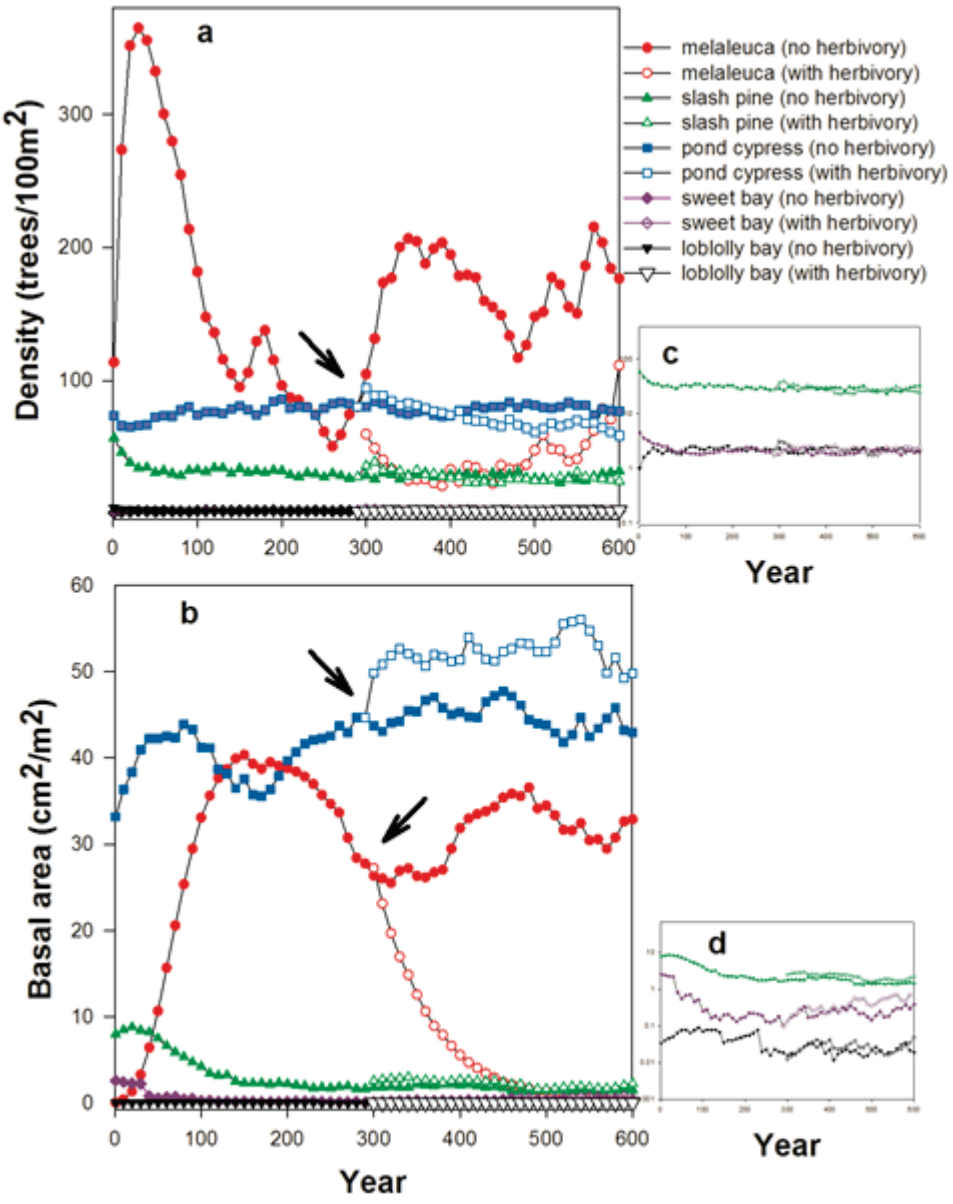

Figure 4.2. Results of scenario 2 **a.** densities; **b**. basal area of woody plant species in melaleuca-invaded cypress swamp of Florida with and without insect herbivory. Arrows show when herbivory starts to be applied. Because slash pine, sweet bay, and loblolly bay are difficult to see in this plot, they are plotted separately in **c.** densities and **d.** basal areas at a finer scale. (This figure is shown with error bars for 50 simulations in the SI: Fig. S7.1a,b,c,d.)

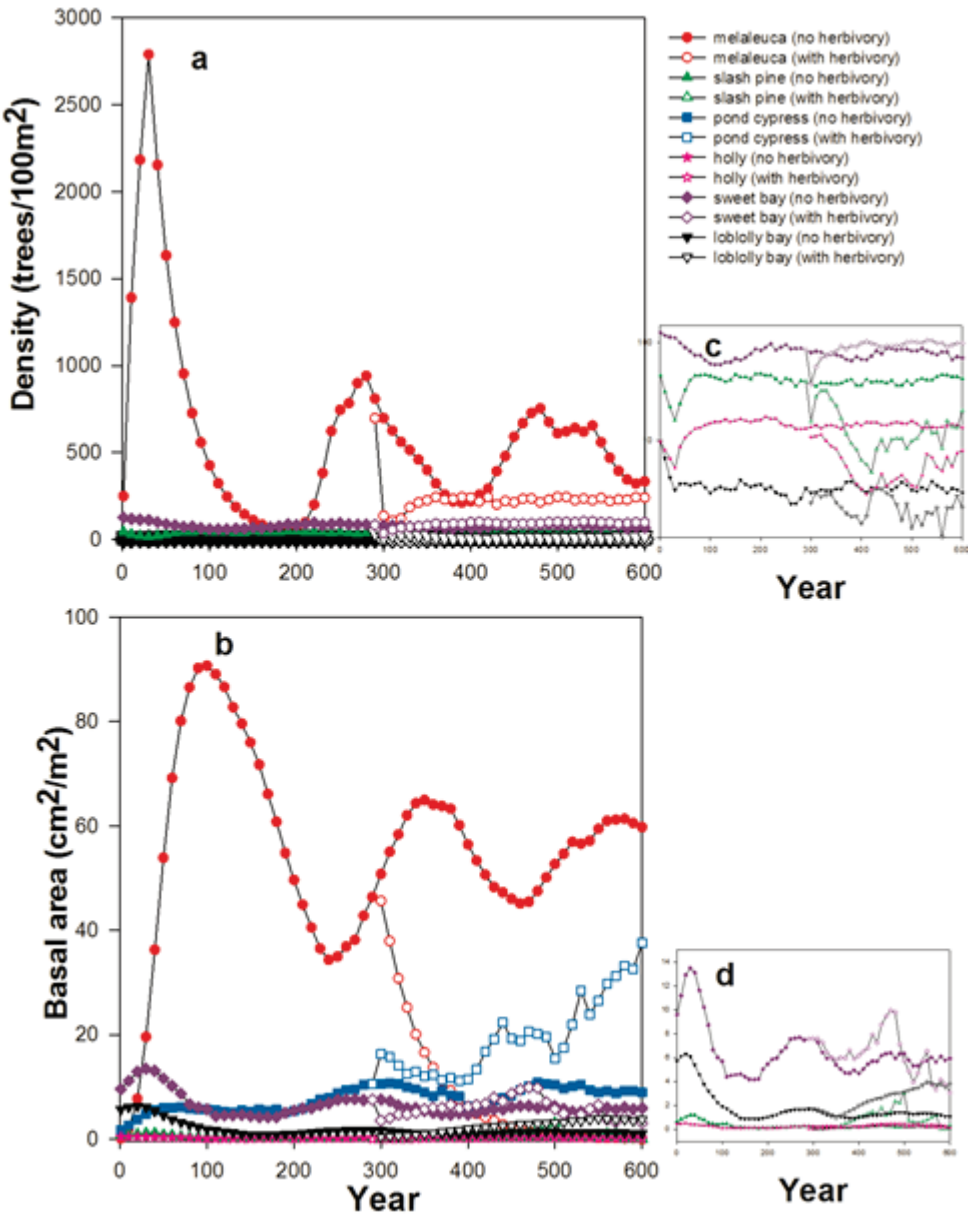

Figure 4.3. Results of scenario 3 **a.** densities; **b.** basal area of woody plant species in melaleuca-invaded bay swamp of Florida with and without herbivory. Arrows show when herbivory starts to be applied.The density and basal area of slash pine, dahoon holly, sweet bay, and loblolly bay are plotted separately in **c.** and **d.** at a finer scale (This figure is shown with error bars for 50 simulations in SI: Fig.S7.2a, b,c,d.)

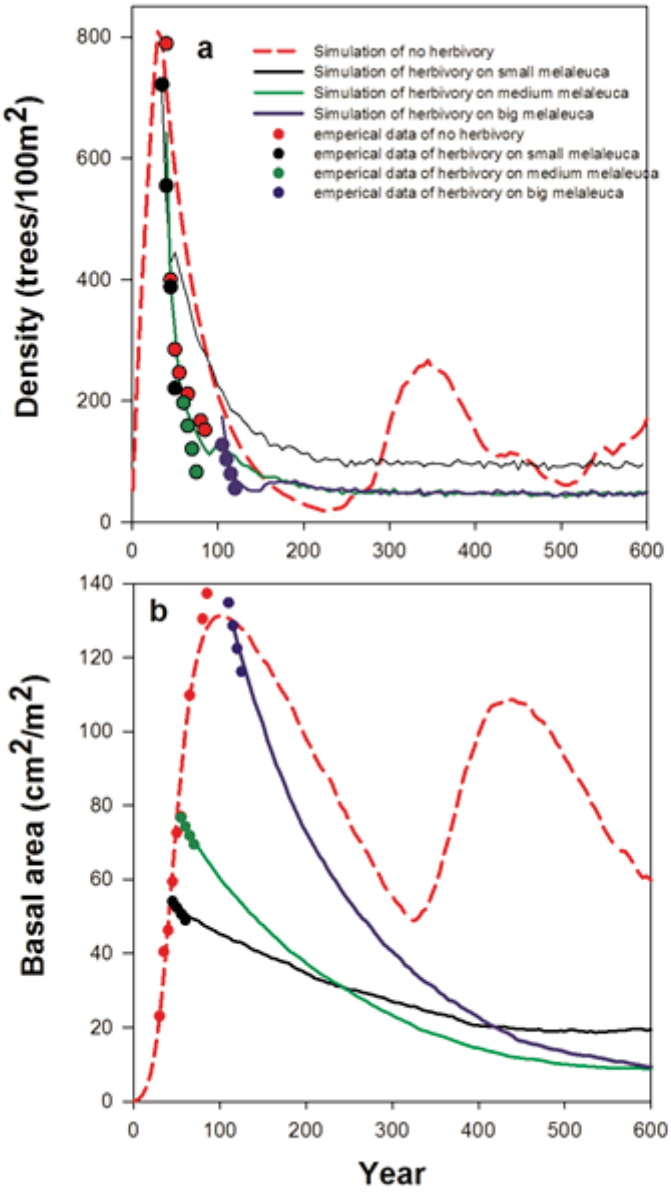

Figure 4.4.
Result of scenarios 4 **a.** densities; **b.** basal area of pure melaleuca stand with and without herbivory. Arrows show when herbivory began to be applied. (Figures are shown with error bars in the SI: Fig. S7.3.a,b.)

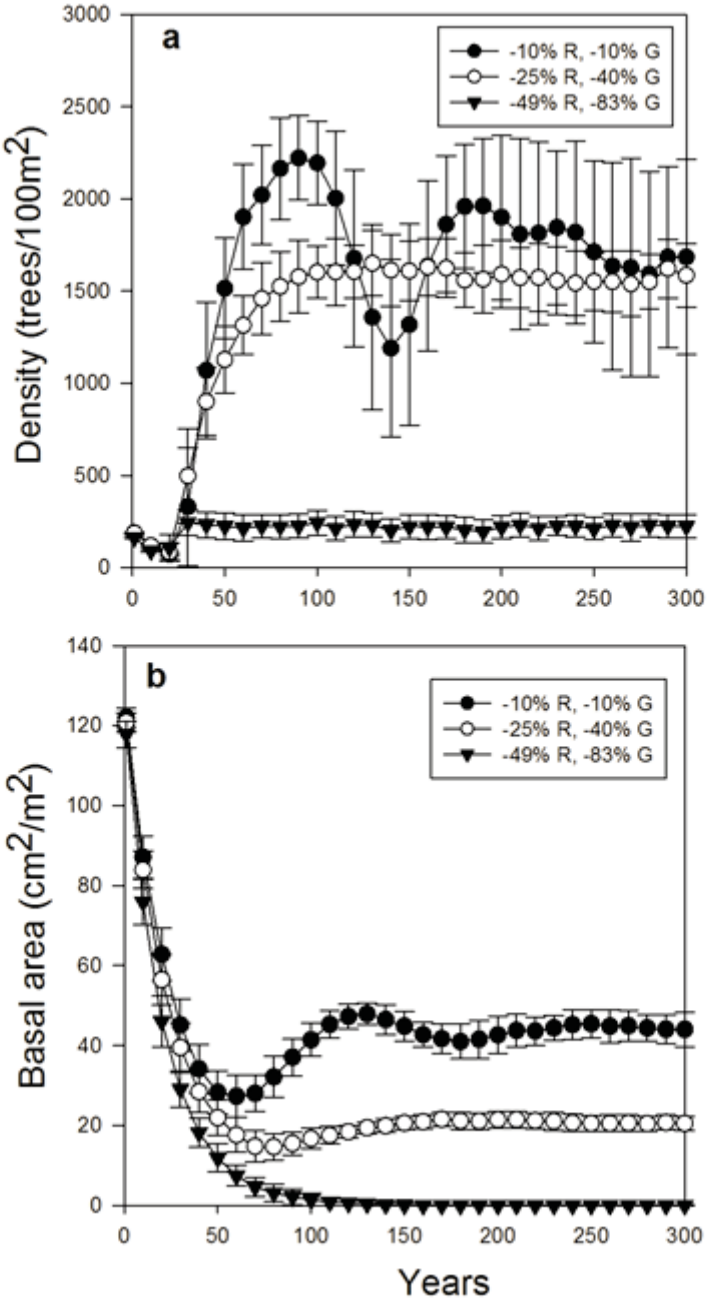

Figure 4.5. Results of sensitivity analysis **a**: the stem density; **b**: the basal area of pure melaleuca stands with different levels of biocontrol.

Chapter Five

Plant compensation and the effects of biocontrol herbivory an invasive plant

Summary

The effect of herbivory on plant fitness can be highly variable, as plants are able to compensate for herbivory up to some level. This is an important component of the ecological fitness in many plants and is of interest to agricultural scientists from the point of view of plant yields. In addition, it is of interest of the management of weedy invasive plants through defoliation, including herbivorous arthropods introduced for biocontrol.

This study used a model of tree growth and nutrient allocation to estimate the effect of different levels of herbivory on reducing the growth rate of an invasive tree species, *Melaleuca quinquiveria* in which the tree could change its carbon and nutrient allocation strategies in order to mitigate effects of increasing herbivory. The model predicted that melaleuca should reallocate more resources to production and maintenance of photosynthetic tissues (foliage), at the expense of roots, to compensate and tolerate a certain level of herbivory. This compensation buffered the severity of the defoliation effect, but there was a limit to the maximum herbivory level melaleuca could sustain and still survive. The model also showed that the level of available soil nutrient plays an important role in a tree's ability to compensate for herbivory. However, counterintuitively, when nitrogen is more limiting than carbon, it is favorable for the plant to increase biomass allocation to roots.

This study has management implications for the level of biological control, or other means of defoliation, that should be applied to obtain a desired level of growth reduction and thus control of an invasive species.

Background

The effects of herbivory on plant fitness can be highly variable, as plants are able to respond in different ways to the effects of herbivory. McNaughton (1983) pointed out three alternative hypotheses: (1) plant fitness declines consistently as the intensity of herbivory increases; (2) plants are able to compensate for herbivory up to some levels, then fitness declines with increasing herbivory; (3) plant fitness is increased by moderate levels of herbivory, then declines and goes negative at higher level of herbivory (herbivory optimization hypothesis, e.g., Hilbert et al. 1981). The second of these responses of plants by compensatory regrowth following insect herbivory is widely reported in the literature (e.g., Kulman 1971, Trumble et al. 1993). This is an important component of the ecological fitness in many plants, and is of interest to agricultural scientists from the point of view of plant yields (Southwood et al. 1973). But it is also a matter of interest of the management of weedy invasive plants through defoliation, such as by herbivorous arthropods introduced for biocontrol. For instance, Sevillano (2010) reported empirical evidence of compensation for herbivory by biocontrol agents in melaleuca. The degree to which plants can compensate for herbivore damage is important to understand in planning control efforts, as it would indicate the intensity of control measures needed to reduce the plant to a desired level.

Plant compensation for arthropod herbivory can be highly complex, involving the way that internal resources are allocated, changes in canopy architecture, changes in leaf morphology, and changes in phenology. It is also affected by extrinsic factors such as resource availability (Zhao and Chen 2012). Our model attempts to take into account only a few of these mechanisms and factors. One mechanism of compensation arises naturally from defoliation. Consider a control measure, that can be a form of mechanical, chemical, or biological control that reduces a tree's foliage by some amount. Although this reduces the surface area of the foliage, the actual rate at which light is captured might be only slightly affected, as the self-shading of leaves is reduced. This effect can be expressed mathematically in a simple model representing the relationship between leaf foliage and the growth rate, G;

$$G = R_0 [1 - exp(-k F)],$$

where R_0 is the maximum possible rate of growth based on photosynthesis, F is the amount of foliage, that is, the Leaf Area Index (*LAI)*, the total area of leaf per area of ground, and k is the rate of extinction of light per leaf layer passing through the foliage (typically between 0.3 and 0.7 . The terms $1 - exp(-kF)$ represent the amount of light captured as a saturating response to light. If F is initially large, say about 5 or 6 for many closed canopies, such that $[1 - exp(-k F)]$ is very close to 1, even reducing F by one half might not appreciably reduce the light captured. This is a compensatory mechanism reflecting the fact that trees commonly have much foliage that is relatively shaded, which can compensate for the loss of foliage above it by being exposed to a higher level of radiation. The above expression could represent increased efficiency of the remaining

leaves in other ways as well, such as reduced transpiration surface that improves the water status of those leaves (Ericsson et al. 1980).

A second compensatory mechanism is that a tree can change the way it allocates its carbon and nutrient resources to capture not just light, but water and nutrients as well. Woody plants allocate their acquired resources, energy (or carbon) and nutrients, to meet their several essential functions. Ability to adjust carbon allocation in response to environmental conditions is widely documented (Friend et al 1994). In particular, the trade-off in investment between root and shoot (foliage) is well known and has been the subject of many studies and models (e.g., Wilson 1988, Ingestad and Agren 1991, Thornley 1995, Hermans et al. 2006). This allocation can be adjusted to optimize growth taking into account the added level of defoliation, as more resources can be allocated to foliage by reducing the amount going to roots and/or wood, due to leaves serve as the primary producers of photosynthetic products in most woods plants (Morath et al. 2006). An additional compensatory effect is that, as a tree reduces its uptake of nutrients from the soil, nutrient concentration in the plant's rooting can increase, partly offsetting the reduction in intensity of exploitation. All these effects can be significant, so it is necessary to study the net effect of defoliation by considering the whole plant and soil as a system in which the plant can alter the way it allocates resources in an optimal way.

Here, we will use modeling to study the specific case of use of biocontrol to decrease the growth rate of a weedy invader, *Melaleuca quinquenervia* (Cav.) Blake (common names: melaleuca, paper bark, punk tree; Family, Myrtaceae, referred to as melaleuca thereafter), which has strong invasive attributes and had spread over 200,000 ha of the ecologically sensitive freshwater ecosystems of southern Florida by the end of the 1900s (Dray 2003;

Dray et al. 2006). The melaleuca weevil (main biocontrol agent) has been effective in consuming leaves, furthermore, it attacks new lead tissue preferentially and relentlessly, thereby contributing to continuous defoliation and re-foliation cycles (Tipping et al. 2008; 2009). Because complete recovery of leaf tissue is rare, the usual temporary reallocation of plant assimilates to leaf production may become virtually permanent under this sustained herbivory. As a strategy for success, melaleuca might be assumed to allocate more energy to foliage while it's facing to a higher level of defoliation to maximize growth rate.

In this study, we will consider as model variables only the plant's components (foliage, root and wood) and it allocation strategy among the three components, the dynamics of the herbivore that feeds on the plant's foliage is not included, as we keep its effect as a constant defoliation rate. This model has an advantage over simpler analytic models, as it is possible to study the effects of different levels of herbivore on allocation strategies of trees' energy to foliage, fine roots, and wood. We tested three hypotheses with regard to the effects of herbivore on reducing melaleuca's growth rate: (1) melaleuca has different growth rates, biomass and nitrogen contents when its energy allocation among the three components is different. (2) Melaleuca can tolerate higher level of herbivore because of allocating more energy to foliage and less to root. (3) Melaleuca can tolerate higher level of herbivore when soil nutrient is richer. Therefore, our goal is to estimate the rate of defoliation needed to achieve a specified reduction in the growth rate under various conditions of nutrient availability to the tree and how it might change its allocations to foliage and roots in an optimal way.

Methods: Mathematical Model

We use a tree dynamics model to determine the allocation strategy that maximizes growth under given conditions of light, nutrient availability, and defoliation. A well known model of tree growth and nutrient cycling is the G'DAY model (Comins & McMurtrie 1993). This model simulates both carbon and nitrogen in tree and soil compartments. Ju and DeAngelis (2009, 2010) used a variation of this model that was enhanced by adding an explicit compartment for soil pore nutrient (Figure 5.1). To avoid soil process complexity the compartments for litter and soil in the original model were removed and mineralization of nutrient from litter was assumed to occur instantaneously, going straight to the soil pore water, where it is available for uptake. It was also assumed that some nutrient could be lost during recycling at a rate proportional to its flux through the plant biomass. Of course, if a biocontrol agent, such as an herbivorous insect, is used to consume foliage, the plant might also respond by allocating carbon and nutrient to chemical defenses to deter the herbivore, or it might reduce the nutrient: carbon ratio in its leaves to make the leaves less palatable to the agent. Here, only the compensatory effects, and not anti-herbivore defenses, will be taken into account in the model.

With the above assumptions the G'DAY model reduces to six equations for carbon and nutrient (e.g., nitrogen or phosphorus) in the three tree components, foliage (C_f and N_f), fine roots (C_r and N_r), and wood (C_w and N_w);

$$\frac{dC_f}{dt} = \eta_f \; G \; - \gamma_f \; C_f - \varphi_f C_f \tag{1a}$$

$$\frac{dC_r}{dt} = \eta_r G \; - \gamma_r C_r \tag{1b}$$

$$\frac{dC_w}{dt} = \eta_w G - \gamma_w C_w \quad (1c)$$

$$\frac{dN_f}{dt} = (U - \eta_w v_w G)\frac{\eta_f}{\eta_f + \rho\eta_r} - \gamma_f N_f - \varphi_f N_f \quad (1d)$$

$$\frac{dN_r}{dt} = (U - \eta_w v_w G)\frac{\rho\eta_r}{\eta_f + \rho\eta_r} - \gamma_r N_r \quad (1e)$$

$$\frac{dN_w}{dt} = \eta_w v_w G - \gamma_w v_w C_w, \quad (1f)$$

plus a seventh equation for the soil pore water nutrient concentration, N_{pore};

$$\frac{dN_{pore}}{dt} = Q(N_{input} - N_{pore}) - U + \lambda(\gamma_f N_f + \varphi_f N_f + \gamma_r N_r + \gamma_w v_w C_w). \quad (1g)$$

N_{pore} is the equivalent of R of the simple model. Separate equations for carbon and a limiting nutrient allow the $N{:}C$ ratio in foliage, fine roots, and wood to be variable.

In the above equations, the function G represents net carbon production, or growth rate. In particular,

G = net carbon production, or growth per unit time (kg m^{-2} yr^{-1})

$$= R_0 I(C_f) E(v_f) \quad (2)$$

$I(C_f)$ = light interception factor

$$= 1 - exp(-k_f b_f C_f) \quad (3)$$

$E(v_f)$ = rate-limiting effect of low nutrient concentration on growth, where

v_f = N:C ratio in foliage = N_f/C_f

$$E(v_f) = E(v_f) = v_f/(v_0 + v_f) \quad (4)$$

The parameter R_0 is the maximum possible primary production, b_f is the foliage per unit carbon, and k_f is the light extinction factor. The factor $E(v_f)$ represents the assumption that the photosynthetic efficiency of foliage is dependent on the N_f:C_f ratio. The three parameters γ_f, γ_r, and γ_w are the loss rates, through litterfall, of foliage, fine roots, and wood, while φ_f is the loss rate of foliage through herbivory. The three parameters, η_f, η_r and η_w, govern the allocation of energy between foliage, fine root biomass, and wood, respectively, where $\eta_f + \eta_r + \eta_w = 1$. For convenience, we assume here that η_w is fixed; that is, whatever the relative allocations to foliage and roots, the fraction allocated to wood stays the same. The constants γ_f, γ_r, and γ_w are senescence (i.e., litterfall) rates. The constant φ_f represents additional loss rate of foliage due to herbivory. It is assumed that a fixed ratio, v_w, of N to C, is first allocated to wood, and then the rest of the nutrient is allocated to foliage and fine roots in the proportions $\eta_f/(\eta_f + \rho\eta_r)$ and $\rho\eta_r/(\eta_f + \rho\eta_r)$, respectively.

The function U represents nutrient uptake,

U = uptake rate of plant-available nutrient (kg m^{-2} yr^{-1}),

where

$$U = \left(\frac{g_N N_{pore}}{k_N + N_{pore}} \right) \left(1 - e^{-b_r k_r C_r}\right), \quad (5)$$

where we assume a saturated response of uptake to pore water concentration, and that there is a 'resource extinction' rate, k_r, that multiplies fine root biomass, analogous to light extinction. The parameter k_r multiplies a coefficient of fine root length per unit carbon, b_r, and the amount of carbon in fine roots, C_r (see Herbert et al. 2004), and where g_N is the maximum possible nutrient uptake rate and k_N is the half saturation constant. In eqn 1g,

Q = flow of water through the soil (kg m^{-2} yr^{-1})

N_{input} = nutrient concentration in input water (kg nutrient kg^{-1}water)

λ = fraction of nutrient recycled; the remainder is assumed tied up in recalcitrant forms or, if nitrogen, also lost to gaseous forms.

If some loss of available nutrient to recalcitrant forms or to the atmosphere potentially occurs during decomposition of litter, then $0 \leq \lambda \leq 1$. The model does not assume any carbon or nutrient storage within the plant.

The mathematical analysis of the model to find the equilibrium value of G, as a function of parameters, is presented in Ju and DeAngelis (2010) and also in our On-line Supplementary Material Appendix 8. The analysis produces an implicit equation for the plant production as a function of herbivory, nutrient availability and other factors, to ask question about the allocation of energy and nutrients to different tissues under different amounts of herbivory, to help us quantify plant production under different levels of herbivory.

Application to Melaleuca

This study focuses on understanding the optimal carbon allocation under a range of defoliation rates by herbivory. To start this, we set φ_f as 0.25, meaning that 25% of foliage was removed, as natural defoliation. Adding 25% more defoliation represented low intensity level and 75% more meant high intensity level (Erbilgin et al. 2014). All parameters are defined in Table 5-1 for the simulation. Most were determined for melaleuca, though a few that could not be estimated were left as in Comins and McMurtrie (1993).

Results

We simulated the change of the equilibrium value of the growth rate (left as *G* here for simplicity), along a range of the carbon allocation fractions to foliage (η_f), from 0.0 to 1.0, for four defoliation rates (φ_f), when nutrient input level is intermediate (baseline) (N_{input} = 0.00001). Note we only plotted when $\eta_f < 0.6$, because though in all the cases considered here, at levels of $\eta_f > 0.6$ the tree has a negative growth rate and cannot survive. In general, we found that *G* was consistently changing with different φ_f, indicated that *G* was related to carbon allocation ratio. When no herbivore defoliation was included in the simulation ($\varphi_f = 0.0$, so that there was only a natural foliage loss rate, $\gamma_f = 0.25$), *G* reached its maximum value (*Max(G))* when $\eta_f = 0.15$ (Figure 5.2A, blue dotted line), then decreased with higher η_f. When φ_f was increased to 0.25, to simulate moderate herbivory impact, *Max(G*) occurred at $\eta_f = 0.25$, indicating that melaleuca allocated a larger fraction of carbon to produce foliage to maximize growth rate (Figure 5.2A red dotted line). When herbivory became stronger, to $\varphi_f = 0.75$ and 1.25, *Max(G*) occurred at still higher levels of η_f. *Max(G*) was then substantially lower compared with zero or

moderate herbivory (Figure 5.2A, yellow and purple dotted lines, respectively). The carbon biomasses in foliage, fine roots and wood are linear functions of G and, like G, they reach maxima as functions of η_f, though the peaks occur at different values of η_f than does *Max(G)*, with the peak of C_f skewed to larger values of η_f (Figure 5.2B) and C_r skewed toward smaller values (Figure 5.2C). Only the peak in wood was identical to that of *Max(G)* because the fraction allocated to wood does not vary (Figure 5.2D).

The trends for nutrient content in foliage and fine roots differed from that of carbon because the tree compensated for defoliation by allocating less carbon to roots, decreasing the amount of nutrient uptake (Figure 5.3). This resulted in lower ratios of N/C in both roots and foliage. For each of the four levels of herbivory the N_f/C_f ratio in leaf decreased with increasing η_f, reflecting the smaller uptake of nutrient. For a given value of η_f, the ratio N_f/C_f was higher for greater herbivory, reflecting the fact that leaf carbon was affected more than leaf nutrient by the herbivory (Figure 5.3D).

An important question is whether changed levels of available nutrient change the ability of the plant to compensate, so we considered an increased value of nutrient input N_{input}. Instead of plotting G along a range of η_f as showed in Figure 5.2, we used the maximum value of G (*Max(G)*) varied with φ_f (from 0.25 – 4) at each N_{input} level (0.0000005, 0.000001, 0.000004, and 0.000015). The herbivory intensities, φ_f,, were extended from 0.0 up to a value of 4 to give a better visualization of the results. First, for each level of N_{input}, *Max(G)* decreased approximately linearly with increasing foliage loss, $\gamma_f + \varphi_f$, eventually reaching a negative growth rate ($G < 0$), at which point the tree is assumed dying (Figure 5.4A). Second, with higher N_{input}, a higher rate of herbivory, φ_f, could be reached before melaleuca suffered negative growth rate and died (Figure 5.4A). For

instance, Figure 5.4A showed that the tree's growth cannot be sustained when N_{input} is 0.0000005 and φ_f exceeds 0.75. This led to similar trends in carbon amount in foliage and root (Figure 5.4C and D). In conclusion, the same herbivory intensity had weaker impact on decreasing plant growth rate if nutrient was more available, suggesting that stronger herbivory was necessary for better limiting growth rate of melaleuca, especially at better nutrient condition.

With the increasing φ_f, we showed that the η_f value for *Max(G)* increased, as melaleuca increased its fraction allocated to foliage with increasing η_f to achieve *Max*(*G)* (Figure 5.4B), although at a saturating rate. Comparing the five nutrient levels, remarkably, at given low levels of defoliation, $\gamma_f + \varphi_f$, the melaleuca actually allocated less to foliage, η_f , as opposed to fine root at higher nutrient inputs, N_{input}. This maybe counterintuitive at first, as it would seem that greater nutrient availability would allow the melaleuca to divert more carbon from roots to foliage to compensate for foliage loss. However, at these relatively low levels of defoliation, nutrient was limiting the growth rate, through the function $E(v_f)$ (see eq. 4), so that it is advantageous to grow more fine roots to absorb nutrient when nutrient was limiting in this parameter range. When herbivory becomes strong enough ($\gamma_f + \varphi_f$ greater than about 2), the defoliation is great enough that it is optimal for the melaleuca to increase allocation to foliage when N_{input} increases.

Discussion

Few theoretical studies have examined the influence of herbivory on the resource allocation and compensation in woody perennials with the explicit aim of estimating the possible way that plant compensation alters the effects of defoliation on an invasive plant,

although relevant empirical work has been done (Holland et al. 1996; Pratt et al. 2005; Tipping et al. 2008; Rayamajhi et al. 2010 and Sevillano 2010). This study provides results of a model of plant growth as a function of allocation when allocation is a function of herbivory. It reveals the possible compensatory response of a tree, melaleuca in this case, to increased defoliation. Compensatory mechanisms include the fact that there is substantial self-shading of leaves of trees, so that loss is somewhat compensated for by the greater light-capturing efficiency of the remaining foliage. A second compensatory mechanism that a plant has to increase its allocation to the component, in this case foliage, that suffers damage. Melaleuca's optimization of growth resulted in a shift in allocation to foliage in the model. The net effect of compensation was to greatly buffer the effect of the of defoliation, as can be seen in Figure 5.4A. For example, for a nutrient input of *Ninput* = 0.000004, an increase in defoliation rate from 0.25 to 3 results in only a halving of the *Max(G).* This finding has significant management implications, in particular that the degree of biocontrol herbivory to reduce the plants growth to a desirable level will depend on the environmental conditions in which the plant is growing, which means selecting the best control for the specific environment condition (Sevillano et al. 2010).

Comparing the three herbivory levels (low, medium and high), we found that growth rate consistently decreased with higher rate of defoliation (Rayamajhi et al. 2008), and the maximum growth rate appeared at higher foliage allocation ratio when defoliation increased. Besides growth rate, foliage carbon and nitrogen contents all decreased with stronger herbivory, which agreed with Rayamajhi et al. 2010, that nitrogen and carbon are both removed from affected leaf tissues. In addition, by compacting foliage N/C ratio, we actually noticed that there was a relatively low difference between no and low

herbivory especially at high value of η_f. However, when herbivory became stronger, N/C ratio increased more apparently, indicated that leaf carbon was affected more than leaf nutrient by the herbivory.

Additional, the optimal allocation strategy, defined as the allocation ratio that gave the maximum growth rate at certain level of herbivory, increased while defoliation rate increased, suggested that melaleuca reallocated more resources to production and maintenance of photosynthetic tissues to compensate and tolerate a certain level of herbivory (Pratt et al. 2005). The reason reallocation from roots to foliage might be effective in some cases is that the tree's initial capacity for water and nutrient uptake through roots might be in excess of its needs. Just as we noted above that it can have more foliage than it needs, it may have enough initial fine root area, such that transferring a greater fraction of resources from roots to foliage does not come at a high a cost to nutrient uptake. However, there was a limit of the maximum ratio melaleuca can allocate to foliage, once defoliation exceeded certain level, melaleuca decreased its growth rate rapidly down to zero with the impact of sufficient herbivory (Pratt et al. 2004; Rayamajhi et al. 2010). Therefore, with sufficient levels of herbivory, melaleuca compensates for herbivory by predicting new stems and replacing foliage, but at a significant cost to reproduction. In conclusion, the resulting loss in reproductive capacity should ultimately lead to decline in melaleuca population (Pratt et al. 2005).

This study supported that nutrient condition plays an important role on how successful melaleuca defends to herbivory through compensation (Dickson 1989). In this study, we simulated five levels of nutrient inputs and we found that growth rate and carbon production were lower under lower nutrient condition, this was because

photosynthetic rate and biomass production were lower with less nutrient (Goolsby et al. 2004; Steven et al. 2008). Possible mechanisms by which this occurs are through herbivory enhancing nitrogen contents of root litter, through herbivory affecting production of secondary metabolites and concentrations of nutrients in foliage and thus in leaf litter and through selective foliar feeding causing shifts in plant community structure and thus the nature of litter input to the soil (Bardgett et al. 1998). In addition, we found that when herbivory was weaker, melaleuca had lower optimal carbon allocation ratio to foliage, but more to fine roots under higher nutrient level, suggested that it is more beneficial for melaleuca growing more roots for nutrient absorption; however, when herbivory became stronger, then melaleuca allocated more carbon to foliage under higher nutrient level. As a result, this study supported that adding high soil nutrient level ameliorated the impact of herbivory and increase tolerance.

Our finding supported that herbivory impact can successfully reduce melaleuca growth rate, to further limit its invasion (Tipping et al. 2008). Moreover, the effect of defoliation on growth seems to follows McNaughton's first alternative hypothesis, that plant growth (or fitness) declines consistently with the level of herbivory. The model does not show any sort of 'herbivore optimization', that is, increase in growth rate for low levels of herbivory. This may be due to some limitations of the way the model is constructed that we would like to modify in the future work. For instance: the model does not have a carbon storage component that can be utilized for short-term response to herbivory. Also, the model does not show a 'threshold' behavior in which increasing herbivory leads to a sudden drop in the growth rate.

Table 5.1. Variables and parameters used in the model.

Variables	
C_f, C_r, C_w = carbon pool for foliage, root and wood (kg m^{-2})	
N_f, N_r, N_w = nitrogen pool for foliage, root and wood (kg m^{-2})	
N_{pore} = soil pore water nitrogen pool (kg nutrient kg^{-1} water)	
η_f , η_r = allocation fraction of carbon to foliage and root	
Parameters	**Value(s) or Range(s)**
R_0 = maximum possible growth rate (kg m^{-2} yr^{-2})	7.03
η_w = allocation fraction of carbon to wood	0.40
ρ = ratio of root *N:C* to foliage *N:C* ratio (assumed constant)	0.70
v_w = N:C ratio for wood, N_w /C_w	0.0001
γ_f = senescence rate for foliage (yr^{-1})	0.25 (no herbivory; 0.5, 1 and 1.5, low, medium and high herbivory, respectively)
γ_r = senescence rate for root (yr^{-1})	0.60
γ_w = senescence rate for wood (yr^{-1})	0.005
λ = recycling ratio	0.98
v_0 = foliar N:C half-saturation constant	0.02
g_N = maximum possible steady nutrient uptake rate per ground area	3.00

k_N = half-saturation coefficient for N plant uptake

0.00002

b_f = foliage area per unit C 10.0

b_r = root length per unit C 2.0

k_r = soil resource extinction 0.1

k_f = radiation light extinction coefficient 0.50

N_{input} = input nutrient concentration (kg nutrient kg^{-1} water)

0.0000005, 0.000001, 0.000002 and 0.000004, four nutrient levels

Q = flow of water (kg m^{-2} yr^{-1}) 100

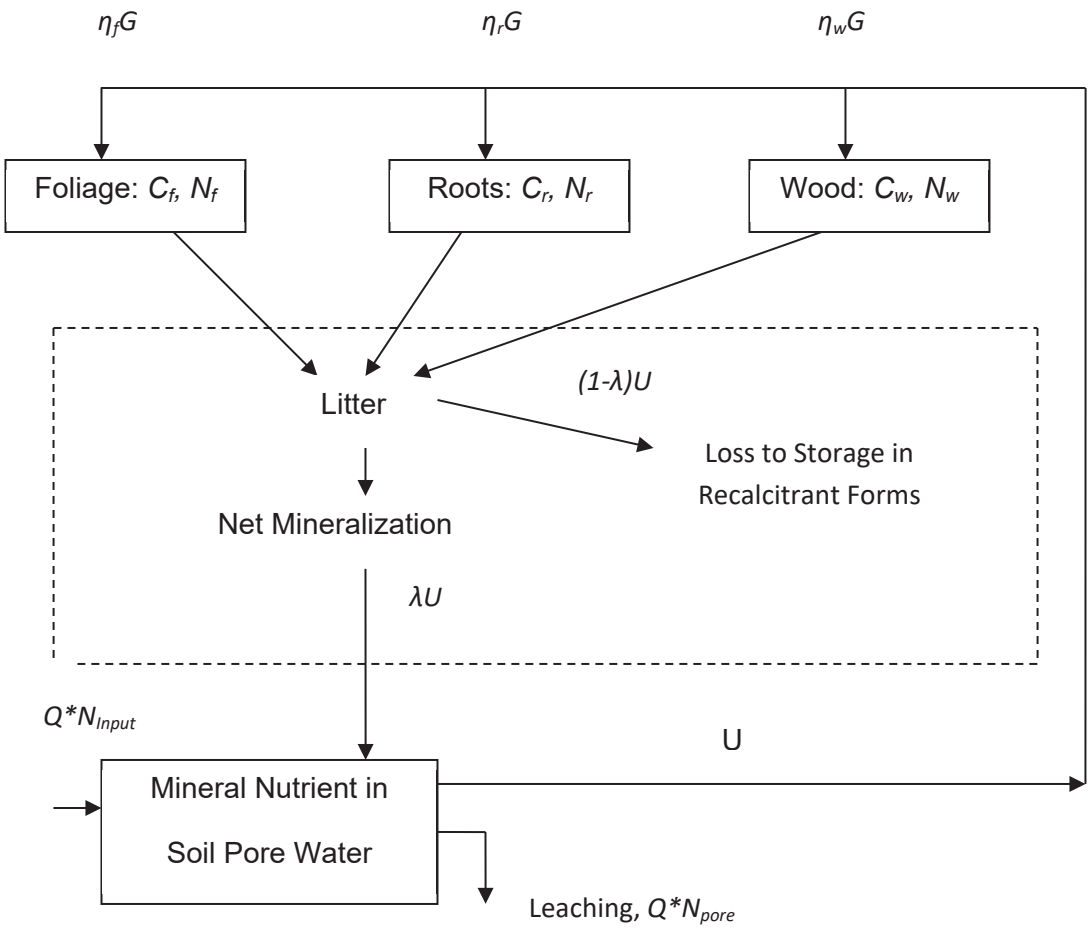

Figure 5.1. Schematic of model for allocation of carbon and for nutrient cycling. The solid lines represent the flow of the limiting nutrient, while the dashed lines represent the allocation of carbon that is produced through photosynthesis. Storage outflows are not explicitly represented.

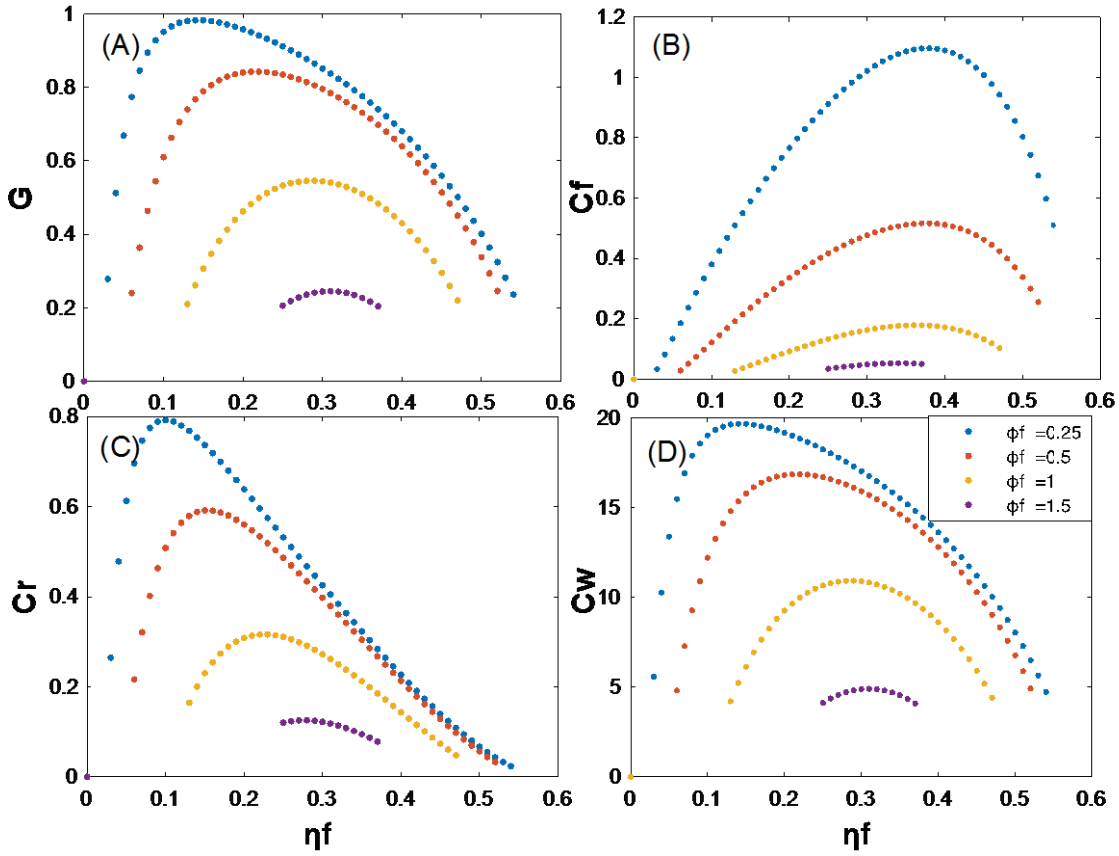

Figure 5.2. Simulated relationships between carbon allocation to foliage, η_f (0-0.6) and (A) *G*, (B) carbon amount in foliage, (C) carbon amount in fine roots and (D) carbon amount in wood, at four levels of herbivory intensity ($\varphi_f = 0.$; $\varphi_f = 0.25$; $\varphi_f = 0.75$ and $\varphi_f = 1.25$). Nutrient input $N_{input} = 0.000001$, the baseline nutrient level.

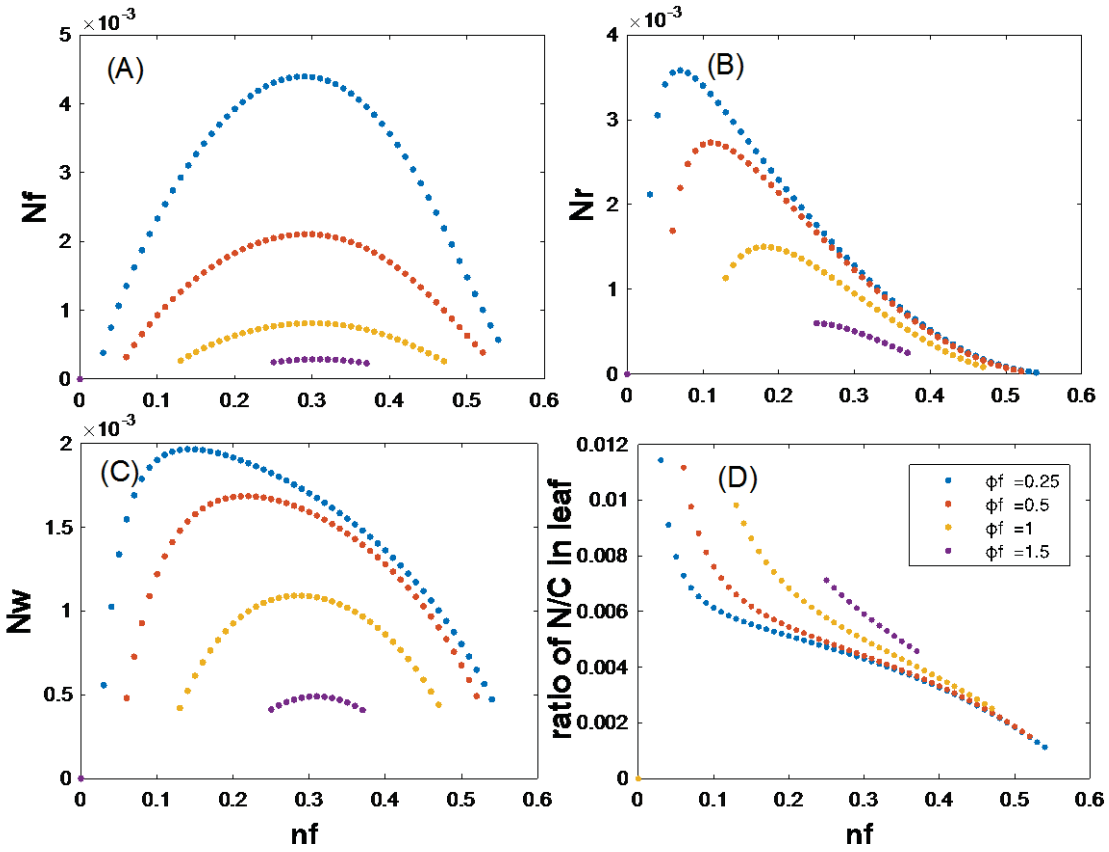

Figure 5.3. Simulated relationship between carbon allocation to foliage, η_f (0-0.6) and (A) nutrient content in foliage, (B) nutrient content in fine roots, (C) nutrient content in wood and (D) nutrient/carbon ratio in foliage, at four herbivory intensities ($\varphi_f = 0.0$; $\varphi_f = 0.25$; $\varphi_f = 0.75$ and $\varphi_f = 1.25$). Nutrient input $N_{input} = 0.000001$, the baseline nutrient level.

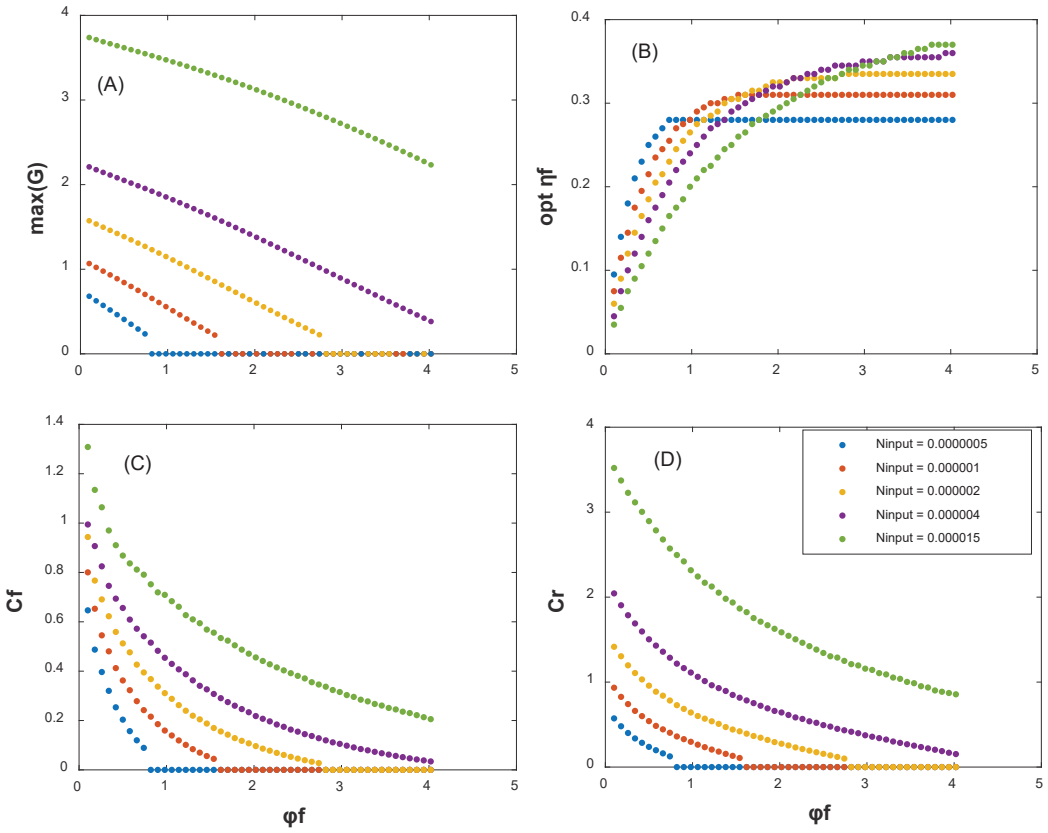

Figure 5.4. Simulated relationship between defoliation ratio (0.1-4) and (A) *max(G),* (B) carbon amount in foliage, (C) carbon amount in root and (D) carbon amount in wood, at four soil nutrient inputs (N_{input} = 0.0000005; N_{input} = 0.000001; N_{input} = 0.000002; N_{input} = 0.000004, N_{input} = 0.000015).

Chapter 6

Overall Conclusions

The research in this dissertation utilized different types of mathematical modelling to answer two major and crucial ecological questions, which are (1) how to understand total carrying capacity in a heterogeneous environment; (2) how to manage invasive species in a better strategy. Additionally, I tried my best to combine empirical data with model simulation, to have stronger results to support my hypothesis or give more convincible suggestions. First, I conducted a novel green-house experiment to test a very interesting mathematical theory on total carrying capacity in a heterogeneous system with diffusion connection. Second, showed clear evidence on why total population could be actually higher than total carrying capacity, with a rigorous laboratory microbial experiment and a new model/mathematical analysis. Third, I applied a famous and well-applied individual based model to project the long-term impact of biological control on an invasive species, in different native communities, this work provided important suggestions on invasive species management. Finally, I used a nutrient-allocation model to simulate the optimal allocation strategy of invasive species when it is under multiple intensities of biological control, to imply if invasive species can compensate and tolerate certain level of biological control, so that it is crucial to be considered when field managers select best biological control agent at different habitats.

The effects of spatial heterogeneity and dispersal on populations and on ecosystem properties such as productivity are key issues in ecology. An interesting

recent result from mathematics is that a population in an environment in which resources vary spatially will reach a higher total equilibrium biomass than the same population in an environment with the same total resources but where resources are distributed homogeneously. This result from mathematical theory have implications for ecology, however, to our knowledge, rarely been tested empirically. Therefore, in my chapter two, I conducted a green-house experiment to study the total biomass growth of duckweed (*Lemna minor* Linn), in where the resources (nutrients added to water) were distributed homogeneously or heterogeneously. Both the experimental and simulation results showed that total biomass peaked at an intermediate, relatively low, diffusion rate, higher than the total carrying capacity of the system.

While, the experiment was not rigorous due to difficulty of controlling nutrient levels and it did not show the basic reason that caused the previous results. So beyond that, in chapter three, I utilized a budding yeast population to test a clear hypothesis that the higher population in a heterogeneous environment with diffusion is determined by the positive relationship of growth rate and carrying capacity. And, thereafter, I used mathematical analysis to extend previous mathematical models to the case of exploitable resources. Consistent with previous theory, both predicted and experimentally observed that spatial diffusion increased total carrying capacity in heterogeneous environments, with the effect size depending on the relationship between r and K. Surprisingly, however, we discovered that homogeneously distributed resources support higher total carrying capacity than heterogeneously distributed resources, even with species diffusion. The results provide rigorous experimental tests of new and old theory, demonstrating how

carrying capacity in spatially distributed species depends on the interplay between growth parameters, population diffusion and resource distribution.

Later on, I finished another two chapters to understand the long term impact of biological control on an invasive species (melaleuca) and the mechanism of melaleuca tolerating biological control via compensation and nutrient re-allocation. In my fourth chapter, I projected likely future changes in plant communities using the individual based modeling platform, JABOWA-II, by simulating successional processes occurring in two types of southern Florida habitat, cypress swamp and bay swamp, occupied by native species and melaleuca, with the impact of insect herbivores. Computer simulations show melaleuca invasion leads to decreases in density and basal area of native species, but herbivory would effectively control melaleuca to low levels, resulting in a recovery of native species. When herbivory was modeled on pure melaleuca stands, it was more effective in stands with initially larger-sized melaleuca. Although the simulated herbivory did not eliminate melaleuca, it decreased its presence dramatically in all cases, supporting the long-term effectiveness of herbivory in controlling melaleuca invasion. The results provide three conclusions relevant to management: (1) The introduction of insect herbivory that has been applied to melaleuca appears sufficient to suppress melaleuca over the long term, (2) major native species may recover in about 50 years, and (3) strong regrowth of native species will help suppress melaleuca through competition.

Interestingly, the sensitivity analysis showed that changes in reductions of reproduction and growth from, respectively, 49% and 83%, to 25% and 40% and 10% and 10% reductions, greatly decreased the ability of the herbivory to control melaleuca. Therefore, I did chapter five, to understand why weak level of biological control is not

efficient enough on controlling melaleuca in a long-term. This study used a modeling approach to estimate the effect of different levels of herbivory on foliage by biocontrol agents on an invasive tree species, *Melaleuca quinquiveria* in which the tree could change its carbon and nutrient allocation strategies in order to mitigate effects of increasing herbivory. The model predicted that melaleuca should reallocate more resources to production and maintenance of photosynthetic tissues, at the expense of roots, to compensate and tolerate a certain level of herbivory. This compensation buffered the severity of the defoliation effect, but there was a limit of the maximum herbivory level melaleuca could survive. The model also showed that the level of available soil nutrient plays an important role in a tree's ability to compensate for herbivory. However, counterintuitively, under some circumstances in which nutrient is more limiting than carbon, it may be more favorable for the plant to increase the fraction of carbon going to roots if there is an increase in nutrient availability for a given level of herbivory.

Work Cited

Acevedo, M. F., D. L. Urban, H. H. Shugart. 1996. Models of forest dynamics based on roles of tree species. Ecological Modelling **87**: 267-284.

Amarasekare, P., and R.M. Nisbet. 2001. Spatial Heterogeneity, Source-sink dynamics, and the local coexistence of competing species. The American Naturalist **158**: 572-584.

Amarasekare, P. 2004. The role of density-dependent dispersal in source-sink dynamics. Journal of Theoretical Biology **226**: 159-168.

Amezcua, A.B., and M. Holyoak. 2000. Empirical evidence for predator-prey source-sink dynamics. Ecology **81**: 3087-3098.

Arditi, R., C.Lobry, T. Sari. 2015. Is dispersal always beneficial to carrying capacity? New insights from the multi-patch logistic equation. Theoretical Population Biology **106**: 45-59.

Aviron, S., P. Kindlmann, F. Burel. 2005. Conservation of butterfly populations in dynamic landscapes: the role of farming practices and landscape mosaic. Ecological Modelling **205**: 135-145.

Balentine, K. M., P. D. Pratt , F. A. Dray, M. B. Rayamajhi, T. D. Center. 2009. Geographic distribution and regional impacts of *Oxyops vitiosa* (Coleoptera: Curculionidae) and *Boreioglycaspis melaleucae* (Hemiptera: Psyllidae), biocontrol agents of the invasive tree *Melaleuca quinquenervia*. Environmental Entomology **38**: 1145-1154.

Bardgett, R. D., D. A. Wardle, G. W. Yeates. 1998. Linking above-ground and below-ground interactions: how plant responses to foliar herbivory influence soil organisms. Soil Biology and Biochemistry **30**: 1867-1878.

Basin, L. and C. D. Thomas. 1999. The distribution of plant species in urban vegetation fragments. Landscape Ecology **14**: 493-507.

Bond-Lamberty, B., A.V. Rocha, K. Calvin, B. Holmes, C. Wang, M.L. Goulden. 2013. Disturbance legacies and climate jointly drive tree growth and mortality in an intensively studied boreal forest. Global Change Biology **20**: 216-227.

Botkin, D. B., J. F. Janak, J. R. Wallis. 1972. Some ecological consequences of a computer model of growth. Journal of Ecology **60**:849-872.

Botkin, D. B. 1993. Forest Dynamics: An Ecological Model. Oxford University Press. Oxford and New York. 309 pp.

Brown, S. 1981. A comparison of the structure, primary productivity and transpiration of cypress ecosystems in Florida. Ecological Monographs **51**: 403-427.

Brown, J.H., J.F. Gillooly, A. P. Allen, V.M. Savage, G.B. West. 2004. Toward a metabolic theory of ecology. Ecology **85**: 1771-1789.

Brawn, J.D., and S.K. Robinson. 1996. Source-sink population dynamics may complicate the interpretation of long-term Census Data. Ecology 77: 3-12.

Bradley BA, Blumenthal DM, Wilcove DS, Ziska LH (2010) Predicting plant invasions in an era of global change. Trends of Ecology and Evolution **25**:310-8.

Breininger, D.R. and G.M. Carter. 2003. Territory quality transitions and source-sink dynamics in a Florida scrub-Jay population. Ecological Applications **13**: 516–529.

Bugmann, H. 2001. A review of forest gap models. Climatic Change 51: 259-305.

Cantrell, R. S., and Cosner, C. 1998. On the effects of spatial heterogeneity on the coexistence of competing species. Journal of Mathematical Biology **37**: 103-145.

Casey, W. P., and Ewel, K. C. 2006. Patterns of succession in forested depressional wetlands in north Florida, USA. Wetlands **26**: 147-160.

Center, T. D., T. K. Van, M. Rayachhetry, G. R. Buckingham, F. A. Dray, S. A. Wineriter, M. F. Purcell, P. D. Pratt. 2000. Field colonization of the melaleuca snout beetle (*Oxyops vitiosa*) in south Florida. Biological Control **19**: 112-123.

Center, T. D., P. D. Pratt, P. W. Tipping, M. B. Rayamajhi, T. K. Van, S. A. Wineriter, F. A. Dray. 2007. Initial impacts and field validation of host range for *Boreioglycaspis melaleucae* Moore (Hemiptera: Psyllidae), a biocontrol agent of the invasive tree *Melaleuca quinquenervia* (Cav.) Blake. Environ. Entomol **36**: 569-576.

Center, T. D., M. F. Purcell, P. D. Pratt, M. B. Rayamajhi, P. W. Tipping, S. A. Wright, F. A. Dray Jr. 2012. Biological control of *Melaleuca quinquenervia*: an everglades invader. BioControl **57**:151-165.

Chesson, P.L. 1985. Coexistence of competitors in spatially and temporally varying environments: a Look at the combined effects of different sorts of variability. Theoretical Population Biology **28**: 263-287.

Clevenger, A. P. and N. Waltho. 2005. Performance indics to identify attributes of highway crossing structures facilitating movement of large mammals. Biological Conservation **121**: 453-64.

Comins, H. N., and R. E. McMurtrie. 1993. Long-term response of nutrient-limited forests to CO_2 enrichment; equilibrium behavior of plant-soil models. Ecology Applications **3**: 666-681.

Cosson, J. F., J.M. Pons, D. Masson. 1999. Effects of forest fragmentation on frugivorous and nectarivorous bats in French Guiana. Journal of Tropical Ecology **15**: 515-534.

Cutway, H. B. and G. J. Ehrenfeld. 2009. Exotic plant invasions in forested wetlands: effects of adjacent urban land use type. Urban Ecosyst **12**: 371-390.

DeAngelis, D., W. Ni, B. Zhang. 2016. Dispersal and spatial heterogeneity: single species. The Journal of Mathematical Biology **72**: 239-254.

DeAngelis, D. L., Wei-Ming Ni, and Bo Zhang. 2016. Effects of diffusion on total biomass in heterogeneous continuous and discrete-patch systems. Theoretical Ecology **9**: 443-453.

Deghi, G. S., K. C. Ewel, and W. J. Mitsch. 1980. Effects of sewage effluent application on litter fall decomposition in cypress swamps. Journal of Applied Ecology **17**: 397-408.

Denslow, J.S. 1985. Disturbance-mediated coexistence of species. In: Pickett, S.T.A., White, P.S. (Eds.), The Ecology of Natural Disturbance and Patch Dynamics. Academic Press, New York, pp. 307–323.

Dhondt, A. A. 1988. Carrying capacity: a confusing concept. Acta Ecologica (Ecol. Gener.) **9**: 337-346.

Dias, P. C. 1995. Source and sinks in population biology. TREE **11**: 326-330.

Dias, P.C. 1996. Sources and sinks in population biology. Trends in Ecology and Evolution **11**: 326-330.

Dickson, R. E. 1989. Carbon and nitrogen allocation in trees. Annales des sciences forestières **46:** 631s-647s.

Dineshram, R., K.K.W. Wong, S. Xiao, Z. Yu, P.Y. Qian, V. Thiyagarajan. 2012. Analysis of pacific oyster larval proteome and its response to high-CO2. Marine Pollution Bulletin **64**: 2160-2167.

Donahue, M.J., M. Holyoak, C. Feng. 2003. Patterns of dispersal and dynamics among habitat patches varying in quality. The American Naturalist **162**: 302-317.

Dray, F. A. Jr. 2003. Ecological genetics of *Melaleuca quinquenervia* (Myrtaceae): population variation in Florida and its influence on performance of the biocontrol Agent *Oxyops vitiosa* (Coleoptera: Curculionidae). Ph.D. dissertation, Florida International University, Miami, FL.

Dray, F. A. Jr., B. C. Bennett, T. D. Center. 2006. Invasion history of *Melaleuca quinquenervia* (Cav.) S. T. Blake in Florida. Southern Appalachian Botanical Society **71**: 210-225.

Elliott-Graves A (2016) The problem of prediction in invasion biology. Biol Phil 31:373-393.

Erbilgin, N., d. a. Galvez, B. Zhang, A. Najar. 2014. Resource availability and repeated defoliation mediate compensatory growth in trembling aspen (Populus tremuloides) seedlings. Peer J **2**: e491.

Ericsson, A., J. Hellkvist, K. Hillerdal-Hagstromer, S. Larsson, E. Mattson-Djos, O. Tenow. 1980. Consumption and pine growth – hypotheses on effects on growth processes by needle-eating insects. Ecology Bulletin (Stockholm) **32**:537-545.

Ewel, K. C. 1990. Multiple demands on Wetlands. Bioscience **40**: 660-666.

Friend, A. L., M. D. Coleman, J. G. Isebrands. 1994. Carbon allocation to root and shoot systems of woody plants. Biology of Adventitious Root Formation **62**: 245-273.

Goolsby, J. A., R. Zonneveld, A. Bourne. 2004. Prerelease assessment of impact on biomass production of an invasive Weed, Lygodium microphyllum (Lygodiaceae: Pteridophyta), by a potential biological control agent, Floracarus perrepae (Acariformes: Eriophyidae). Environmental Entomology **33**: 997-1002.

Goss-Custard, J.D., R.A. Stillman, R.W.G. Caldow, A.D. West, M. Cuillemain. 2003. Carrying capacity in overwintering birds: when are spatial models needed? Journal of Applied Ecology **40**: 176-187.

Greenway, M. 1994. Litter accession and accumulation in a *Melaleuca quinquenervia* (Cav.) S. T. Blake wetland in Southeastern Queensland. Australian Journal of Marine and Freshwater Research **45**:1509-1519.

Grimm, V., U. Berger, F. Bastiansen, S. Eliassen, V. Ginot, J. Giske, J. Goss-Custard, T. Grand, S. Heinz, G. Huse, A. Huth, J.U. Jepsen, C. Jørgensen, W.M. Mooij, B. Müller, G. Pe'er, C. Piou, S.F. Railsback, A.M. Robbins, M.M. Robbins, E. Rossmanith, N. Rüger, E. Strand, S. Souissi, R.A. Stillman, R. Vabø, U. Visser, and D.L. DeAngelis. 2006. A standard protocol for describing individual-based and agent-based models. Ecological Modelling **198**: 115-126.

Grimm, V., U. Berger, D. DeAngelis, J. G. Polhill, J. Giske, and S. F. Railsback. 2010. The ODD protocol: a review and first update. Ecological Modelling **221**: 2760–2768.

Haegeman, B., and M. Loreau. 2014. General relationship between consumer dispersal, resource dispersal, and metacommunity theory. Ecology Letters **17**: 175-184.

Hara, T. 1993. Effects of variation in individual growth on plant species coexistence. Journal of Vegetation Science **4**: 409-416.

Hayward, M.W., J. O'Brien, G.I.H. Kerley. 2007. Carrying capacity of large African predators: Predictions and tests. Biological Conservation **139**: 319-229.

Herbener, K. W., S.J. Tavener, N.T. Hobbs. 2012. The distinct effects of habitat fragmentation on population size. Theoretical Ecology **5**: 73-82.

Hermans, Ch., J. P. Hammond, P. J. White, N. Verbruggen. How do plants respond to nutrient shortage by biomass allocation. Trends in Plant Science **11**: 610-617, 2006.

He, X., and W. Ni. 2013. The effects of diffusion and spatial variation in Lotka-Volterra competition-diffusion system I: heterogeneity vs. homogeneity. Journal of Differential Equations **254**: 528-546.

He, X., and W. Ni. 2013. The effects of diffusion and spatial variation in Lotka-Volterra competition-diffusion system II: heterogeneity vs. homogeneity. Journal of Differential Equations **254**: 4088-4108.

Higgins SI, Richardson DM (1996) A review of models of alien plant spread. Ecological Modelling **87**:249-265.

Howe, R.W., and G.J. Davis. 1991. The demographic significance of "sink" populations. Biological Conservation **57**: 239-255.

Holland, J. N., W. Cheng, J. D. A. Crossley. 1996. Herbivore-induced changes in plant carbon allocation: assessment of below-ground C fluxes using carbon-14. Oecologia **107**: 87-94.

Holt, R.D. 1985. Population dynamics in two-patch environments: Some anomalous consequences of an optimal habitat distribution. Theoretical Population Biology **28**: 181-207.

Holt, R.D. 1997. On the evolutionary stability of sink populations. Evolutionary Ecology **11**: 723-731.

Hotl, R. D., T. H. Keitt, M. A. Lewis, B. A. Maurer, M. L. Taper. 2005. Theoretical models of species' borders: single species approaches. OIKOS **108**: 18-27.

Hutchings, M.J., E.A. John, D.K. Wijesinghe. 2003. Toward understanding the consequences of soil heterogeneity for plant populations and communities. Ecology **84**: 2322-2334.

Ingestad, T. and I. A. Goran. 1991. The influence of plant nutrition on biomass allocation. Ecological Applications **1**:168-174.

Ju, S, and D. L. DeAngelis. 2009. The R* rule and energy flux in a plant-nutrient ecosystem. Journal of Theoretical Biology **256**: 326-332.

Ju, S, and D. L. DeAngelis. 2010. Nutrient fluxes at the landscape level and the R* rule. Ecological Modelling **221**: 141-146.

Kareiva, P. 1983. Local movements in herbivorous insects: applying a passive diffusion model to mark-recapture field experiments. Oecologia **57**: 322-327.

Kaufman, S. R., and P. E. Smouse. 2001. Comparing indigenous and introduced populations of *Melaleuca quinquenervia* (Cav.) Blake: response of seedlings to water and pH levels. Oecologia **127**:487-494.

Keddy, P.A. 1981. Experimental demography of the sand-dune annual, Cakile Edentula, growing along an environmental gradient in Nova Scotia. Journal of Ecology **69**: 615-630.

Keddy, P.A. 1982. Population ecology on an environmental Gradient: Cakile edentula on a sand dune. Oecologia **52**: 348-355.

Koivula, M. J. and H.J.W. Vermeulen. 2005. Highways and forest fragmentation – effects on carabid beetles (Coleoptera, Carabidae). Landscape Ecology **20**: 911-926.

Krug, R. M., and D. M. Richardson. 2014. Modelling the effect of two biocontrol agents on the invasive alien tree Acacia cyclops—Flowering, seed production and agent survival. Ecological Modelling **278**:100-113.

Kulman, H. M. 1971. Effects of insect defoliation on growth and mortality of trees. Annual Review of Entomology **16**: 289-324.

Kuno, E. 1991. Some strange properties of the logistic equation defined with ***r*** and *K*: Inherent defects or artifacts? Researches on population ecology **33**: 33-39.

Latore, J., P. Gould, A.M. Mortimer. 1999. Effects of habitat heterogeneity and dispersal strategies on population persistence in annual plants. Ecological Modelling **123**: 127–139.

Lemke, T. and R. Salguero-Go´mez. 2016. Land use heterogeneity causes variation in demographic viability of a bioindicator of species-richness in protected fen grasslands. Population Ecology **58**: 165-178.

Loreau, M. and D.L. DeAngelis. 1997. Source-sink dynamics and the coexistence of species on a single resource. Theoretical Population Biology **51**: 79-93.

Lou, Y. 2006. On the effects of migration and spatial heterogeneity on single and multiple species. Journal of Differential Equations **223**: 400-426.

Lutscher, F., E. McCauley, M.A. Lewis. 2007. Spatial patterns and coexistence mechanisms in systems with unidirectional flow. Theoretical Population Biology **71**: 267-277.

Maines, A., D. Knochel, T. Seastedt. 2013. Biological control and precipitation effects on spotted knapweed (Centaurea stoebe): empirical and modeling results. Ecosphere **4**:1-14.

Martin, M. R., P. W. Tipping, and J. O. Sickman. 2009. Invasion by an exotic tree alters above and belowground ecosystem components. Biological Invasions **11**: 1883-1894.

Martin, M. R., P. W. Tipping, K. R. Reddy, S. H. Daroub, and K. M. Roberts. 2010. Interactions of biological and herbicidal management of *Melaleuca quinquenervia* with fire: Consequences for ecosystem services. Biological Control **54**: 307-315.

Martin, M. R., P. W. Tipping, K. R. Reddy, P. T. Madiera, and D. Fitzgerald. 2011. An evaluation of the impact of *Melaleuca quinquenervia* invasion and management on plant community structure after fire. Aquatic Botany **95**:287-291.

Mallet, J. 2012. The struggle for existence: how the notion of carrying capacity, K, obscures the links between demography, Darwinian evolution, and speciation. Evolutionary Ecology Research **14**: 627-665.

Matthiessen, B., E. Mielke, U. Sommer. 2010. Dispersal decreases diversity in heterogeneous matacommunities by enhancing regional competition. Ecology **91**: 2022-2033.

Mattiessen, B., and H. Hillebrand. 2006. Dispersal frequency affects local biomass production by controlling local diversity. Ecology Letters **9**: 652–662.

McNaughton, S. J. 1983. Compensatory plant growth as a response to herbivory. OIKOS **40**: 329-336.

Meskimen, G. F. 1962. A silvicultural study of the melaleuca tree in south Florida. Master's thesis, University of Florida, Gainesville, FL.

Mitsch, W. and K. C. Ewel. 1979. Comparative biomass and growth of cypress in Florida wetlands. The American Midland Naturalist **101**: 417-426.

Mitsch, W. J., C. L. Dorage, and J. R. Wiemhoff. 1979. Ecosystem dynamics and a phosphorus budget of an alluvial cypress swamp in southern Illinois. Ecology **60**: 1116-1124.

Monk, C. D. 1966. An ecological study of hardwood swamps in north-central Florida. Ecology **47**:649-654.

Monk, C. D. 1968. Successional and environmental relationships pf the forest vegetation of north central Florida. American Midland Naturalist **79**: 441-457.

Morath, S. U., P. D. Pratt, C. S. Silvers, T. D. Center. 2006. Herbivory by Boreioglycaspis melaleucae (Hemiptera: Psyllidae) Accelerates Foliar Senescence and Abscission in the Invasive Tree Melaleuca quinquenervia. Environmental Entomology **35**: 1372-1378.

Müller, M. J. I., B. I. Neugeboren, D. R. Nelson, A. W. Murray. 2014. Genetic drift opposes mutualism during spatial population expansion. Proceedings of the National Academy of Sciences **111:** 1037-1042.

Muko, S., and Y. Iwasa. 2000. Species Coexistence by permanent spatial heterogeneity in a Lottery Model. Theoretical Population Biology **57**: 273-284.

Myers, R. L. 1983. Site susceptibility to invasion by the exotic tree *Melaleuca quinquenervia* in southern Florida. Journal of Applied Ecology **20**:645-658.

Myers, J. H., and D. R. Bazely. 2003. Ecology and Control of Introduced Plants. Cambridge University Press.

Ngugi, M. R. and D. B. Botkin. 2011. Validation of a multispecies forest dynamics model using 50-year growth from *Eucalyptus* forests in eastern Australia. Ecological Modelling **222**: 3261- 3270.

Ngugi, M. R., D. B. Botkin, D. Doley, M. Cant, and J. Kelley. 2013. Restoration and management of callitris forest ecosystems in Eastern Australia: Simulation of attributes of growth dynamics, growth increment and biomass accumulation. Ecological Modelling **263**: 152-161.

Oesterheld, M., Sala, O.E. and S.J. McNaughton. 1992. Effect of animal husbandry on herbivore-carrying capacity at a regional scale. Nature **356**: 234-236.

Paine, R. T. 1966. Food web complexity and species diversity. American Naturalist **100**: 65-75.

Paine, C.E.T., Marthews, T.R., Vogt, D.R., Purves, D., Rees, M., Hector, A., and Turnbull, L.A. 2012. How to fit nonlinear plant growth models and calculate growth rates: an update for ecologists. Methods in Ecology and Evolution **3**, 245–256.

Pausas, J. G., M. P. Austin, and I. R. Noble. 1997. A forest simulation model for predicting eucalypt dynamics and habitat quality for arboreal marsupials. Ecological Applications **7**: 921-933.

Penfound, W. T. 1952. Southern swamps and marshes. The Botanical Review **18**: 413-445.

Pimm, S. and P. Raven. 2000. Extinction by numbers. Nature **403**: 843–845.

Pimm, S., P. Raven, A. Peterson, C. Sekercioglu, P. Ehrlich. 2006. Human impacts on the rates of recent, present, and future bird extinctions. Proceedings of the National Academy of Sciences **103**: 10941–10946.

Pratt, P.D., M. B. Rayamajhi, T. K. Van, T. D. Center. 2004 Modeling the influence of resource availability on population densities of Oxyops vitiosa. Biocontrol Science and Technology **14:** 51–61.

Pratt, P. D., M. B. Rayamajhi, T. K. Van, T. D. Center, P. W. Tipping. 2005. Herbivory alters resource allocation and compensation in the invasive tree Melaleuca quinquenervia. Ecological Entomology **20**: 316-326.

Pulliam, H.R., B.J. Danielson. 1991. Sources, sinks, and habitat selection: a landscape perspective on population dynamics. The American Naturalist **137**: 50-66.

Pulliam, H.R. 1988. Sources, sinks, and population regulation. The American Naturalist **132**: 652-661.

Rai, P. K. 2015a. Paradigm of plant invasion: multifaceted review on sustainable management. Environmental Monitoring and Assessment **187**:1-30.

Rai, P. K. 2015b. What makes the plant invasion possible? Paradigm of mechanisms, theories and attributes. Environmental Skeptics and Critics 4.

Rayachhetry, M. B., T. K. Van, and T. D. Center. 1998. Regeneration potential of the canopy-held seeds of *Melaleuca quinquenervia* in south Florida. International Journal of Plant Science 159:648-654.

Rayachhetry, M. B., T. K. Van, T. D. Center, and F. Laroche. 2001. Dry weight estimation of the aboveground components of *Melaleuca quinquenervia* trees in southern Florida. Forest Ecology and Management **142**:281-290.

Rayamajhi, M. B., T. K. Van, P. D. Pratt, T. D. Center, and P. W. Tipping. 2007. *Melaleuca quinquenervia* dominated forests in Florida: analyses of natural-enemy impacts on stand dynamics. Plant Ecology **192**:119-132.

Rayamajhi, M. B., P. D. Pratt, T. D. Center, P. W. Tipping, T. K. Van. 2008. Aoverground biomass of an invasive tree Melaleuca (*Melaleuca quinquenervia)* before and after herbivory by adventive and introduced natural enemies: A temporal case study in Florida. Weed Science **56**: 451-456.

Rayamajhi, M. B., P. D. Pratt, T. D. Center, T. K. Van. 2010. Insects and a pathogen suppress melaleucaquinquenervia cut-stump regrowth in Florida. Biological Control **53**: 1-8.

Ritchie, M.E. 1997. Populations in a landscape context: sources, sinks, and metapopulations, Wildlife and Landscape Ecology, Springer, New York. Reference to a chapter in an edited book: 160-184.

Serbesoff-King, K. 2003. Melaleuca in Florida: A literature review on the taxonomy, distribution, biology, ecology, economic importance, and control measures. Journal of Aquatic Plant Management **41**:98-112.

Sevillano, L., C. C. Horvitz, P. D. Pratt. 2010. Natural enemy density and soil type influence growth and survival of *Melaleuca quinquenervia* seedlings. Biological Control **53**: 168-177.

Sevillano, L. 2010. The Effects of Biological Control Agents on Population Growth and Spread of Melaleuca quinquenervia. Ph.D. dissertation, Florida International University, Miami, FL.

Shriver, W.G., and P.D. Vickery. 1999. Aerial assessment of potential Florida grasshopper sparrow habitat: conservation in a fragmented landscape. Florida Ornithological Society **27**: 1-36.

Smith, T. M., and D. L. Urban. 1988. Scale and resolution of forest structural pattern. Vegetation **74**: 143-150.

Snyder, R.E., and P. Chesson. 2003. Local dispersal can facilitate coexistence in the presence of permanent spatial heterogeneity. Ecology Letters **6**: 301-309.

Snyder, R.E., and P. Chesson. 2004. How the spatial scales of dispersal, competition, and environmental heterogeneity interact to affect coexistence, The American Naturalist **164**: 633-650.

Silvertown, J., and R. Law. 1987. Do plants need niches? Some recent developments in plant community ecology. Trends in Ecology and Evolution **1**: 24-26.

Sommer, S., R. Piscia, M. M. Manca, D. Fontaneto, A. Ozgul. 2016. Demographic cost and mechanisms of adaptation to environmental stress in resurrected Daphnia. Journal of Limnology **75**: 30-35.

Southwood, T. R. E., and G. A. Norton. 1973. Economic aspects of pest management strategies and decisions. In: Insects: Studies in Pest Management. Ecological Society of Australia, Canberra pages 168-184.

Stevens, M. T., E. L. Kruger, R. L. Lindroth. 2008. Variation in tolerance to herbivory is mediated by differences in biomass allocation in aspen. Functional Ecology **22:** 40-47.

Thornley, J. H. M. 1995. Shoot: root allocation with respect to C, N, and P: An investigation and comparison of resistance and teleonomic models. Annals of Botany (London) **75**:391-405.

Tilman, D. 1994. Competition and biodiversity in spatially structures habitats. Ecology **75**: 2-16.

Tipping, P. W., M. R. Martin, P. D. Pratt, T. D. Center, M. B. Rayamajhi. 2008. Suppression of growth and reproduction of an exotic invasive tree by two introduced insects. Biological Control **44**:235-241.

Tipping, P. W., M. R. Martin, K. R. Nimmo, R. M. Pierce, M. D. Smart, E. White, P. T. Madeira, T. D. Center.2009. Invasion of a West Everglades wetland by *Melaleucaquinquenervia* countered by classical biological control. Biological Control **48**:73-78.

Tipping, P. W., M. R. Martin, R. Pierce, T. D. Center, P. R. Pratt, and M. B. Rayamajhi. 2012. Post-biocontrol invasion trajectory for *Melaleuca quinquenervia* in a seasonally inundated wetland. Biocontrol **60**:163-168.

Tipping, P. W., M. R. Martin, P. D. Pratt, M. B. Rayamajhi, and T. D. Center. 2013. An abundant biocontrol agent does not provide a significant predator subsidy. Biocontrol **67**:212-219.

Trumble, J. 1993. Plant compensation for arthropod herbivory. Annual Reviews entomology **38**: 93-119.

Turner, C. E., T. D. Center, D. W. Burrows, and G. R. Buckingham. 1998. Ecology and management of *Melaleuca quinquenervia*, an invader of wetlands in Florida, U.S.A. Wetlands Ecology and Management **5**: 165-178.

Van Gils, J.A., P. Edelaar, G. Escudero, T. Piersma. 2004. Carrying capacity models should not use fixed prey density thresholds: a plea for using more tools of behavioural ecology. OIKOS **104**: 197-204.

Van Ha, C., M. A. Leyva-Gonzalez, Y. Osakabe et al. 2013. Positive regulatory role of strigolactone in plant responses to drought and salt stress. Proceedings of the National Academy of Sciences **111**: 851-856.

Van, T. K., M. B. Rayachhetry, and T. D. Center. 2000. Estimating above-ground biomass of *Melaleuca quinquenervia* in Florida, USA. Journal of Aquatic Plant Management **38**:62-67.

Van, T. K., M. B. Rayachhetry, T. D. Center, and P. D. Pratt. 2002. Litter dynamics and phenology of *Melaleuca quinquenervia* in South Florida. Journal of Aquatic Plant Management **40**:22-27.

Vasconcellos, M. and M. A. Gasalla. 2001. Fisheries catches and the carrying capacity of marine ecosystems in southern Brazil. Fisheries Research **50**: 279-295.

Watkinson, A. R., and W.J. Sutherland. 1995. Sources, sinks and pseudo-sinks, Journal of Animal Ecology **64**: 126-130.

Williamson M. 1999. Invasions. Ecography **22**:5-12.

Wilson, H.B. 2001. The evolution of dispersal from source to sink populations. Evolutionary Ecology Research **3**: 27-35.

Wilson., J. B. 1988. A review of evidence on the control of shoot:root ratio in relation to models. Annals of Botany (London) **61**:433-449.

Yu, D.W., H.B. Wilson, N.E. Pierce. 2001 An empirical model of species coexistence in a spatially structured environment. Ecology **82**: 1761-1771.

Zhang, B. X. Liu, D.L. DeAngelis, W. Ni, G. Geoff Wang. 2015. Effects of dispersal on total biomass in a patchy, heterogeneous system: Analysis and experiment, Mathematical Biosciences **264**: 54-62.

Zhao, J., and J. Chen. 2012. Interspecific variation in compensatory regrowth to herbivory associated with soil nutrients in three Ficus (Moracear) saplings. Plos One 7: 1-9.

Appendices

Appendix 1. Spatially discrete environment with parameters r_i and K_i for Chapter 2

Use of two parameters, r and K, rather than the single parameter, g, differs from the mathematical model (1), but can still produce the results found by Lou (2006) if r_i and K_i scale in proportion. To show that, we can write the equilibrium equation for one compartment in a general n-compartment model with terms

$$\frac{D}{2}(X_{i-1} - 2X_i + X_{i+1}) + r_i\left(1 - \frac{X_i}{K_i}\right)X_i = 0 \quad (i = 1, n) \tag{A1.1}$$

and with periodic boundary conditions; $X_{n+1} = X_1$.

Dividing by X_i and summing over n, we obtain

$$\frac{D}{2}\sum_{i=1,n}\frac{K_i}{r_i X_i}\left(X_{i-1} - 2X_i + X_{i+1}\right) + \sum_{i=1,n} r_i - \sum_{i=1,n}\frac{r_i}{K_i}X_i = 0 \tag{A1.2}$$

or

$$\frac{D}{2}\sum_{i=1,n}\frac{1}{X_i}\left(X_{i-1} - 2X_i + X_{i+1}\right) = \sum_{i=1,n}\frac{r_i}{K_i}(X_i - K_i) \tag{A1.3}$$

We can manipulate the left hand side of (A1.3) as follows

$$\frac{D}{2}\sum_{i=1}^{n}\left[\frac{X_{i-1} - X_i}{X_i} + \frac{X_{i+1} - X_i}{X_i}\right]$$

$$= \frac{D}{2}\sum_{i=1}^{n}\left[\frac{X_{i-1} - X_i}{X_i}\right] + \frac{D}{2}\sum_{i=2}^{n+1}\left[\frac{X_i - X_{i-1}}{X_{i-1}}\right]$$

$$= \frac{D}{2}\left(\frac{X_0 - X_1}{X_1}\right) + \frac{D}{2}\sum_{i=2}^{n}\left[\frac{X_{i-1} - X_i}{X_i}\right] + \frac{D}{2}\sum_{i=2}^{n}\left[\frac{X_{i+1} - X_i}{X_i}\right] + \frac{D}{2}\left(\frac{X_{n+1} - X_n}{X_n}\right),$$

or, using $X_0 = X_n$ and $X_{n+1} = X_1$,

$$= \frac{D}{2}\left(\frac{X_0 - X_1}{X_1}\right) + \frac{D}{2}\left(\frac{X_1 - X_0}{X_0}\right) + \frac{D}{2}\sum_{i=2}^{n}\left[\frac{X_{i-1} - X_i}{X_i}\right] + \frac{D}{2}\sum_{i=2}^{n}\left[\frac{X_{i+1} - X_i}{X_i}\right]$$

$$= \frac{D}{2}\sum_{i=1}^{n}\left[\frac{X_{i-1} - X_i}{X_i} + \frac{X_i - X_{i-1}}{X_{i-1}}\right] = \frac{D}{2}\sum_{i=1}^{n}\left[\frac{(X_i - X_{i-1})^2}{X_i X_{i-1}}\right]. \quad \text{(A1.4)}$$

From using (A1.4) in (A1.3) we find that

$$\sum_{i=1}^{n}\frac{r_i}{K_i}(X_i - K_i) = \frac{D}{2}\sum_{i=1}^{n}\left[\frac{(X_i - X_{i-1})^2}{X_i X_{i-1}}\right] \quad \text{(A1.5)}$$

from which it follows that

$$\sum_{i=1,n}\frac{r_i}{K_i}(X_i - K_i) > 0\,. \quad \text{(A1.6)}$$

Our goal is to determine the conditions under which X_i increases from its equilibrium value of K_i as D increases. Note that (A1.6) does not imply that $\sum_{i=1,n}(X_i - K_i) > 0$. However, if r_i and K_i scale in proportion (that is, if the growth rate is proportional to the carrying capacity at a fixed constant, say r/K), then it follows that

$$\sum_{i=1,n}\frac{r_i}{K_i}(X_i - K_i) = \frac{r}{K}\sum_{i=1,n}(X_i - K_i) > 0 \quad \text{and} \quad \sum_{i=1,n}(X_i - K_i) > 0\,. \quad \text{(A1.7)}$$

In this case, r_i/K_i is equivalent to a single parameter g_i .We can further deduce that $X_{total} = \sum_{i=1,n} X_i$ will always increase initially as D increases from zero, by taking the derivative of equation (A1.7) with respect to D:

$$\frac{d}{dD}\left(\sum_{i=1,n}(X_i - K_i)\right) = \frac{d}{dD}\left(\sum_{i=1,n} X_i\right) = \frac{d}{dD}\left(\frac{D}{2}\sum_{i=1,n}\frac{(X_i - X_{i-1})^2}{X_i X_{i-1}}\right)$$
$$= \frac{1}{2}\sum_{i=1,n}\frac{(X_i - X_{i-1})^2}{X_i X_{i-1}} + D\frac{d}{dD}\left(\sum_{i=1,n}\frac{(X_i - X_{i-1})^2}{X_i X_{i-1}}\right) \quad \text{(A1.8)}$$

The right hand side of (A1.8) is positive for $D = 0$, which implies that X_{total} will initially increase. It must also eventually decrease, because it can be shown that as $D \rightarrow \infty$, $X_i \rightarrow X_{mean}$ (for all i), where $X_{mean} = \frac{1}{n}\sum_{i=1,n} X_i$.

It is shown in Appendix 2 that more general criteria can be found for X_{total} increasing with increasing values of D.

Appendix 2: Criterion for X_{total} to increase as D increases from zero for Chapter 2

The objective is to show that

$$\sum_{i=1,n}\left(\frac{(r_i - r_{i-1})(K_i - K_{i-1})}{r_i r_{i-1}}\right) > 0 \tag{A2.1}$$

(Criterion 7 in text) is a sufficient condition for x_{total} to increase as D increases from zero. It is straightforward to demonstrate that this holds for any n.

To show that, we again write the equilibrium equation for one compartment in a general n-compartment model with terms

$$\frac{D}{2}(X_{i-1} - 2X_i + X_{i+1}) + r_i\left(1 - \frac{X_i}{K_i}\right)X_i = 0 \tag{A2.2}$$

Multiplying both sides by $K_i / r_i X_i$ and summing over n, we obtain

$$\frac{D}{2}\sum_{i=1,n}\frac{K_i}{r_i X_i}(X_{i-1} - 2X_i + X_{i+1}) + \sum_{i=1,n}K_i - \sum_{i=1,n}X_i = 0 \tag{A2.3}$$

or

$$\frac{D}{2}\sum_{i=1,n}\frac{K_i}{r_i X_i}(X_{i-1} - 2X_i + X_{i+1}) = \sum_{i=1,n}(X_i - K_i) \tag{A2.4}$$

Our goal is to determine the conditions under which X_i increases from its equilibrium value of K_i as D increases. To determine this, we differentiate both sides of (A1.3) to obtain

$$\frac{1}{2}\sum_{i=1}^{n}\frac{K_i}{r_i X_i}(X_{i-1} - 2X_i + X_{i+1}) + \frac{D}{2}\frac{d}{dD}\left[\sum_{i=1}^{n}\frac{K_i}{r_i X_i}(X_{i-1} - 2X_i + X_{i+1})\right] = \frac{d}{dD}\left[\sum_{i=1}^{n}(X_i - K_i)\right]$$

Setting $D = 0$, and $X_i = K_i$ $(i = 1,n)$, we obtain

$$\frac{1}{2}\sum_{i=1}^{n}\frac{K_i}{r_i K_i}(K_{i-1}-2K_i+K_{i+1})=\frac{d}{dD}\left(\sum_{i=1}^{n}X_i\right)=\frac{dX_{total}}{dD}$$

or

$$\frac{dX_{total}}{dD}=\frac{1}{2}\sum_{i=1}^{n}\frac{1}{r_i}(K_{i-1}-2K_i+K_{i+1})=\frac{1}{2}\sum_{i=1}^{n}\frac{1}{r_i}[(K_{i+1}-K_i)-(K_i-K_{i-1})] \quad \text{(A2.5)}$$

Now we use a general formula for integration by parts

$$\sum_{i=1}^{n}(a_{i+1}-a_i)b_i=\sum_{i=1}^{n}a_{i+1}b_i-\sum_{i=1}^{n}a_i b_i$$

$$=\sum_{i=2}^{n+1}a_i b_{i-1}-\sum_{i=1}^{n}a_i b_i$$

$$=a_{n+1}b_n-a_1b_0+\sum_{i=1}^{n}a_i b_{i-1}-\sum_{i=1}^{n}a_i b_i$$

$$=a_{n+1}b_n-a_1b_0+\sum_{i=1}^{n}a_i(b_{i-1}-b_i)$$

Because $a_{n+1} = a_1$ and $b_0 = b_n$, the first two terms in the last line cancel and we have

$$\sum_{i=1}^{n}(a_{i+1}-a_i)b_i=\sum_{i=1}^{n}a_i(b_{i-1}-b_i) \quad \text{(A2.6)}$$

Let $a_i = K_i - K_{i-1}$, and $b_i = 1/r_i$, and use (A1.5) in (A1.4) to determine that

$$\frac{dX_{total}}{dD}=\frac{1}{2}\sum_{i=1}^{n}\left(\frac{1}{r_i}-\frac{1}{r_{i-1}}\right)(K_i-K_{i-1}) \quad \text{(A2.7)}$$

or

$$\sum_{i=1,n}\left(\frac{(r_i-r_{i-1})(K_i-K_{i-1})}{r_i r_{i-1}}\right)>0$$

Equation (A1.6) implies that if the relationship between the r_i s and K_i s is such that the right hand side of (A1.6) is greater than zero, then X_{total} will increase with an increase in D, at least in the vicinity of the equilibrium point $X_i = K_i$ (i=1,n).This suggests a general criterion for x_{total} to increase with D for any value of n.

Appendix 3. Outline of proof of Criterion 9 for Chapter 2

A criterion parallel to (7) can be found for the spatially continuous one-dimensional form with *r(s)* and *K(s)*; that is, for

$$\frac{\partial X(s)}{\partial t} = D\frac{\partial^2 X(s)}{\partial s^2} + r(s)\left[1 - \frac{X(s)}{K(s)}\right]X(s), \tag{A3.1}$$

where $r(s) > 0$ and $K(s) > 0$ and both are continuous and non-constant in a bounded domain Ω. Neumann (zero flux) boundary conditions are assumed. Denoting the solution at equilibrium still by X(s), i.e;

$$d\Delta X + r(s)X\left(1 - \frac{X}{K(x)}\right) = 0 \quad \text{in space } \Omega, \tag{A3.2}$$

in a paper in preparation, the criterion for X_{total}, $X_{total} = \int_{\Omega} X(s)$, to increase for small increases in *D* from zero is now,

$$\int_{\Omega} \frac{\partial K}{\partial s}\frac{\partial}{\partial s}\left(\frac{1}{r}\right) < 0 \tag{A3.3}$$

or, more generally

$$\int_{\Omega} \nabla K \cdot \nabla \frac{1}{r} < 0 \tag{A3.4}$$

A full proof for this result will be given in the paper in preparation. However, we note here that at equilibrium it is shown that the solution, *X(s)*, approaches *K(s)* at all points in the domain Ω as $D \rightarrow 0$. Dividing both sides of (2) by *r(s)X(s)/K(s)*, and integrating over Ω, we obtain,

$$0 = \int_{\Omega}\left[d\Delta X \cdot \frac{K(s)}{r(s)X} + (K(s) - X)\right] = -d\int_{\Omega} \nabla X \cdot \nabla\left(\frac{K(s)}{r(s)X}\right) + \int_{\Omega}(K(s) - X).$$

From

$$\int_{\Omega} \left| \nabla X(s) \cdot \nabla \left(\frac{1}{\xi X(s)} \right) - \nabla K \cdot \nabla \frac{1}{r} \right| \to 0 \quad \text{as} \quad d \to 0,$$

where ξ is equal to r/K (proof in paper in preparations), it follows that

$$\int_{\Omega} X = \int_{\Omega} K - d\left[\int_{\Omega} \nabla K \cdot \nabla \frac{1}{r} + o(1) \right]$$

So that the criterion for $X_{total} = \int_{\Omega} X(s)$ to increase when $\int_{\Omega} \nabla K \cdot \nabla \frac{1}{r} < 0$ or, for the one-dimensional case, when $\int_{\Omega} \frac{\partial K}{\partial s} \frac{\partial}{\partial s} \left(\frac{1}{r} \right) < 0$, follows.

Appendix 4: for Chapter 3

We used a Monod curve to describe the relationship between Trp concentrations and corresponding growth rate (*r)* when there was no Cyh added in the growth curve measurement, using MATLAB R2015a. The Monod function is: $r = r_{max}*[Trp]/(k+[Trp])$, where r_{max} is the asymptotic growth rate under infinite resources, [*Trp*] is the initial Trp concentration, and *k* is the half-saturation coefficient, defined as the value of [Trp] where $r = r_{max}/2$. A Monod curve for the yeast growth rate as a function of Trp was fit, as shown in Fig.S1, indicating that Trp was the limiting amino acid nutrient for the strain, especially when Trp concentration, *Trp,* was lower than 73.4 mg/L. Therefore, we set 73.4 mg/L as the optimal growth concentration.

Figures

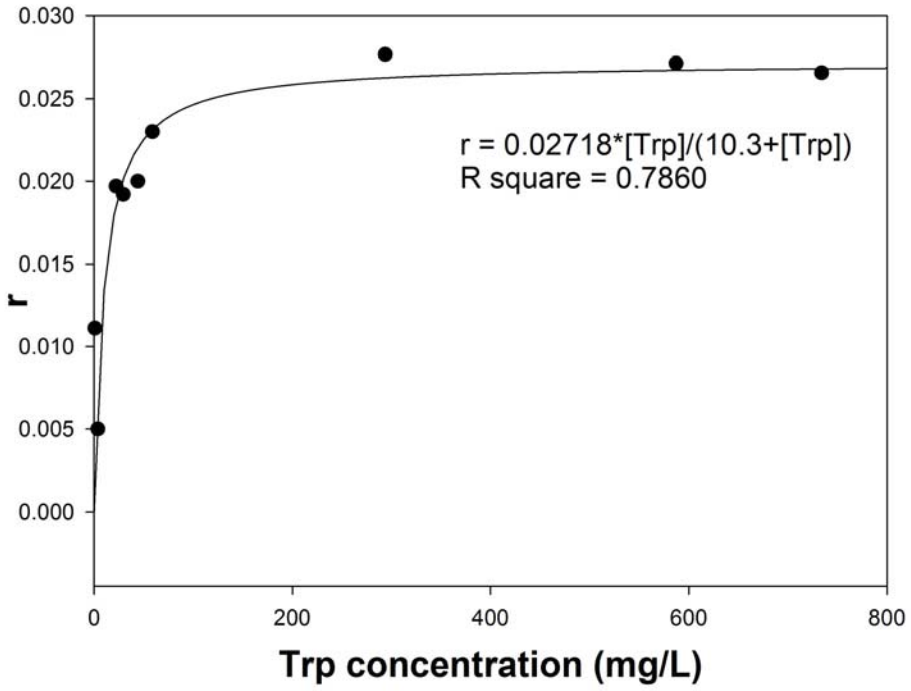

Figure S4.1 The monod fit of the corresponding essential amino acid tryptophan (Trp) concentrations and corresponding growth rate (*r)*. r = 0.02718*[Trp]/(10.3+[Trp]), R^2 = 0.7860.

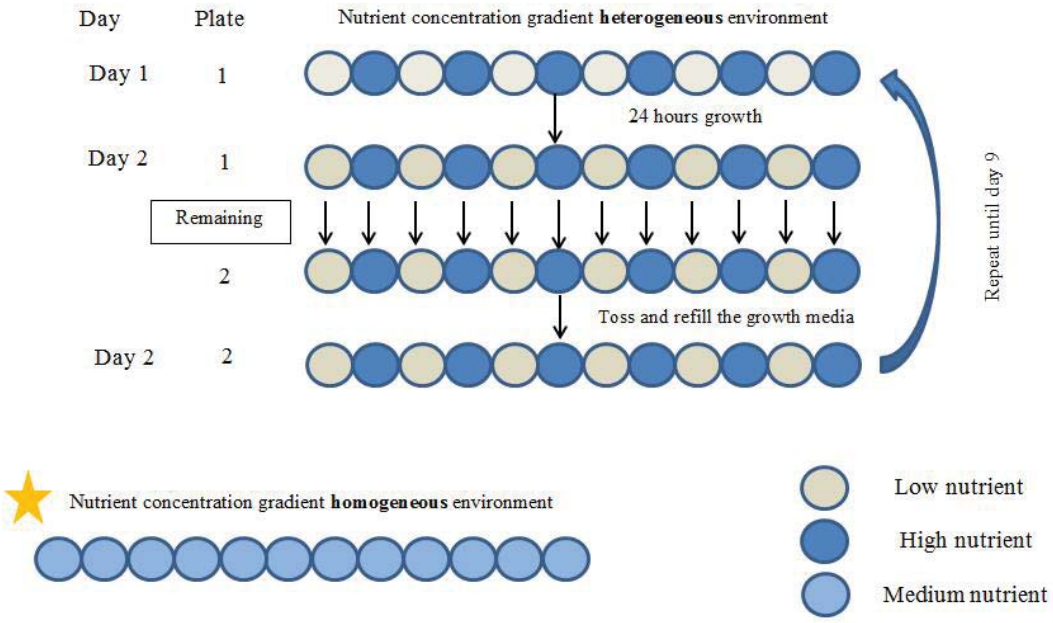

Figure S4.2 Schematic of experimental non-diffusion protocol. Represented is a single spatially distributed "population" composed of one row of 12 wells in a 96-well microtitre plate. Each circle is a single well. Color of a well represents nutrient (Trp) concentration. Alternating white/blue wells represents the heterogeneous environment treatment, while the population on the bottom of figure with all light blue wells represents the homogenous nutrient treatment. The initial yeast population had 24 hours growth at 30 ^{o}C, followed a transfer event that all the yeast with media was moved to the same well from original plate (plate 1) to the new empty plate (plate 2). After the transfer, plate 2 was centrifuged to create a yeast pellet at the bottom in each well, old media was removed and fresh media was added. The yeast population underwent another 24 hours growth, then the previous processes was repeated, until Day 9.

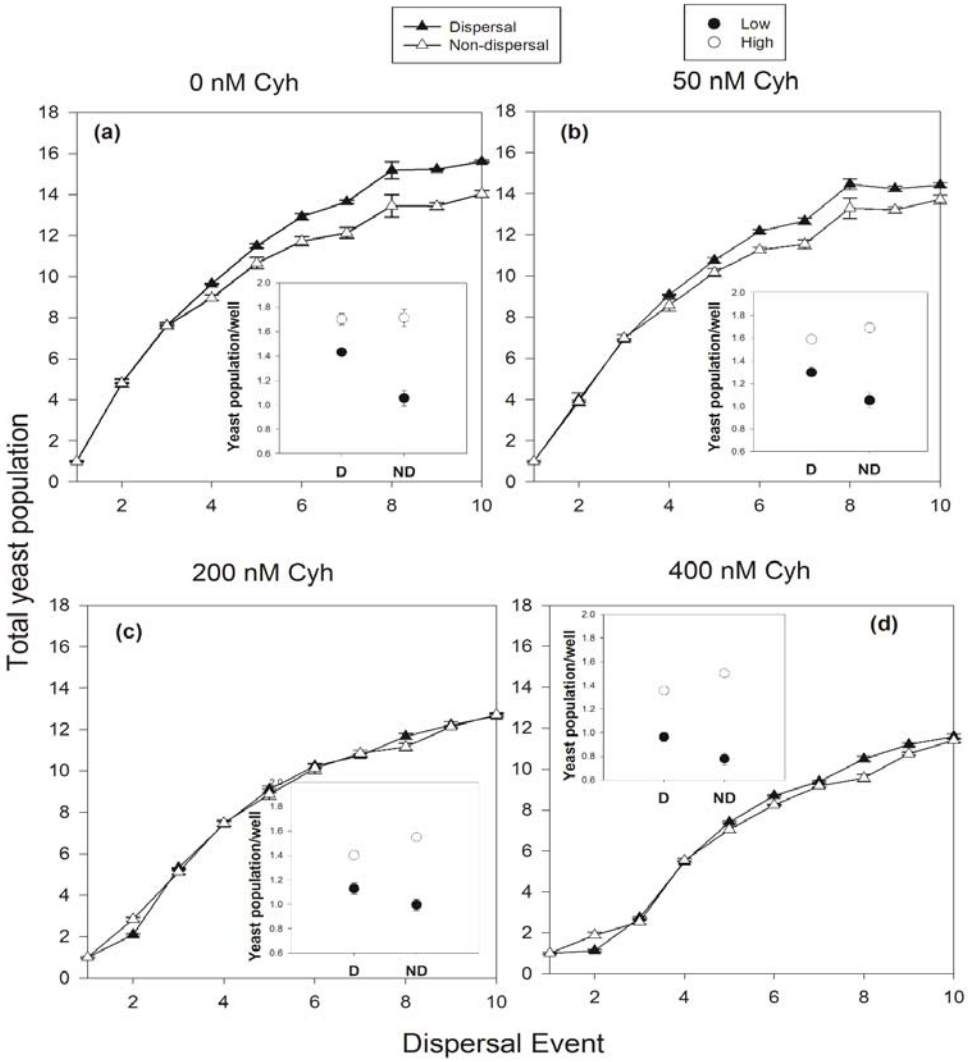

Figure S4.3 The total yeast population measured every 24 hours (1 day) with (filled triangles) and without dispersal (unfilled triangles), with four levels of cycloheximide (Cyh) in the heterogeneous condition: (a) 0 nM; (b) 50 nM; (c) 200 nM and (d) 400 nM. The dispersal rate is 0.06. Insets (a), (b), (c) and (d): the averaged final yeast subpopulation in the low nutrient wells (1.468 mg/L of Trp) (filled dots) and in the high nutrient wells (44.04 mg/L of Trp) (unfilled dots), with dispersal (D) and without dispersal (ND), with four levels of cycloheximide (Cyh) in the heterogeneous scenario (0 nM, 50 nM, 200 nM and 400 nM). Cyh: cycloheximide, Trp: tryptophan. OD 600: optical density.

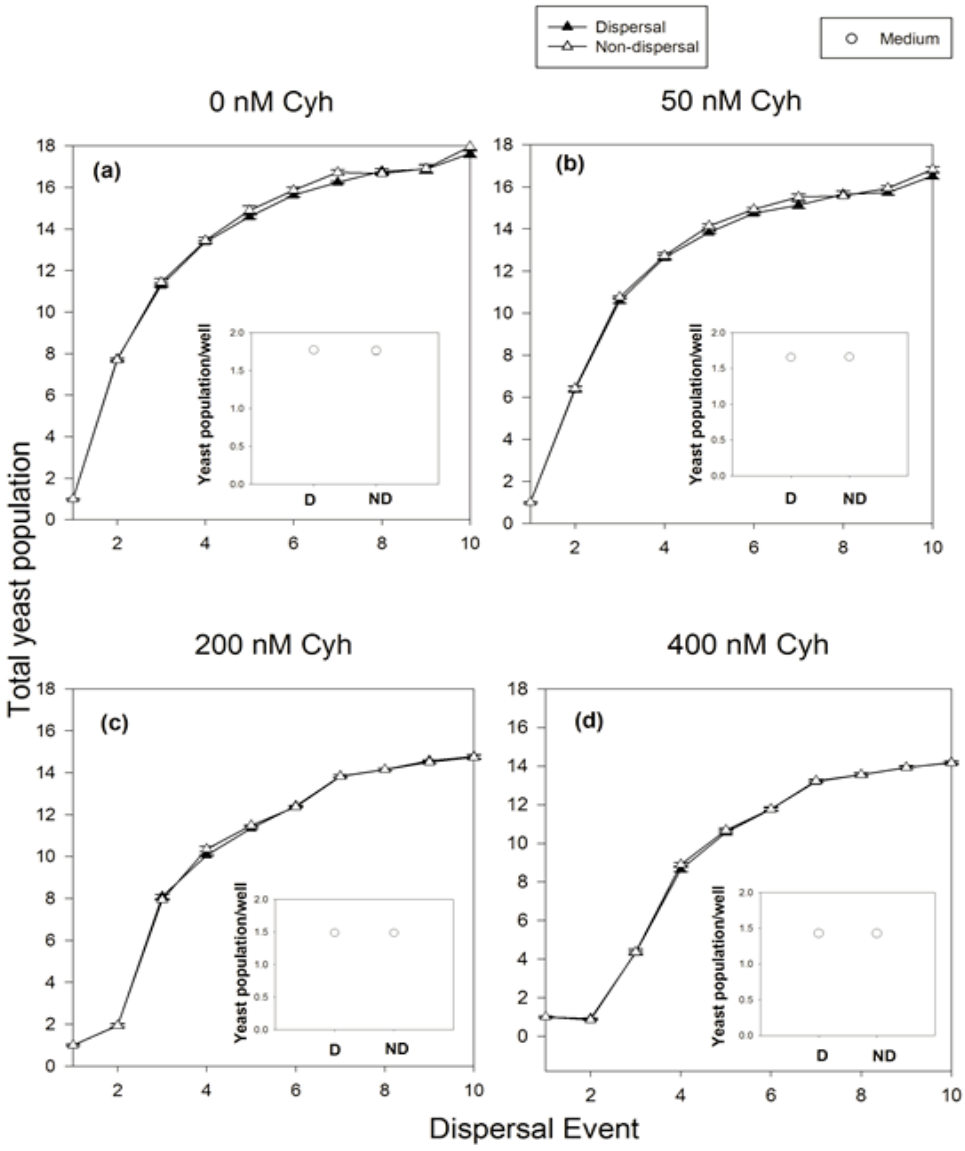

Figure S4.4 The total yeast population measured every 24 hours (1 day) with (filled triangles) and without dispersal (unfilled triangles), with four levels of cycloheximide (Cyh) in homogeneous condition: (a) 0 nM; (b) 50 nM; (c) 200 nM and (d) 400 nM. The dispersal rate is 0.06. Insets (a), (b), (c) and (d): the averaged final yeast subpopulation in medium nutrient well (22.2 mg/L of Trp) with dispersal (D) and without dispersal (ND) (unfilled dots), with four levels of cycloheximide (Cyh) in homogeneous scenario (0 nM, 50 nM, 200 nM and 400 nM). Cyh: cycloheximide, Trp: tryptophan. OD 600: optical density.

Appendix 5: Mathematical models and analysis for diffusion $D \to \infty$.for Chapter 3

A general pair of equations for a consumer-resource system with external resource input is, for consumer, *u(x,t)*, nutrient, *n(x,t)* ;

$$\frac{\partial u(x,t)}{\partial t} = D\frac{\partial^2 u(x,t)}{\partial x^2} + \frac{r\,n(x,t)u(x,t)}{k+n(x,t)} - m(x)u(x,t) - g(x)u(x,t)^2$$

$$\text{(B1a)}\quad \frac{dn(x,t)}{dt} = N_{input}(x) - \eta n(x,t) - \frac{rn(x,t)u(x,t)}{\gamma(k+n(x,t))},$$

(B1b)

where *u(x,t)* is the consumer biomass, *n(x,t)* is the nutrient, $N_{input}(x)$ is the nutrient input, η is the loss rate of nutrient from the system, *r* is the maximum growth rate, *k* is the half-saturation coefficient, γ is the yield, or fraction of nutrient per unit biomass, and *D* is the diffusion rate.

We use a spatially discrete, or patch version of this model in the following, so the equations for each patch are;

$$\frac{dU_i}{dt} = \frac{rN_iU_i}{k+N_i} - m_iU_i - g_iU_i^2 - D(U_i - \frac{1}{2}U_{i-1} - \frac{1}{2}U_{i+1}) \quad (i=1,n)$$

(B2a)

$$\frac{dN_i}{dt} = N_{input,i} - \eta N_i - \frac{rN_iU_i}{\gamma(k+N_i)} \qquad (i=1,n)\ .$$

(B2b)

Wraparound conditions joining patches $i=1$ and $i=n$ are not assumed in order to be consistent with the experment.

Two special cases of this model were analyzed:

Model 1: $\eta = 1$, $m_i > 0$, $g_i = 0$ for all i Model 2: $\eta = 0$, $m_i = 0$, $g_i > 0$ for all i.

Model 1 is a chemostat type model. In Model 2 it is assumed that nearly all of the nutrients are taken up by the yeast and that dead yeast cells are assumed to accumulate at a rate $g_i(U_i^*)^2$. The yeast cells are not physically lost, but they stop reproducing, with no recycling of nutrients. These models are intended only to provide possible qualitative pictures of the nutrient-yeast dynamics.

Our objective is to test mathematically Hypotheses 1, 2, and 3 of the main text. Using realistic models of a consumer and an exploitable resource in a spatial environment, we text whether a diffusing population in an environment with heterogeneously distributed resources can be greater than a non-diffusing population (Hypothesis 1), and whether this occurs when the consumer's growth rate is positively related to the effective carrying capacity (Hypothesis 2). The we test whether the total population dispersing in the heterogeneous system can be greater than the total population when the nutrient inputs are spread homogeneously in space (Hypothesis 3). To determine these, it is easiest to analyze this model mathematically for conditions in which the consumer is well-mixed across identical patches or spatial cells; that is, for $D \to \infty$. This can be shown from numerical evaluations to be a good approximation for the case of smaller diffusion rates, D (see under Model 2 below).

Consider the patch model, equations (B2a, b), where patches have biomasses represented by the variables $U_1, U_2, \ldots, U_n$ (for example, number of yeast cells per patch) and the nutrients $N_1, N_2, \ldots, N_n$ (for example, milligrams nutrient per liter in each patch). Let D approach very large values ($D \to \infty$) in (B2a); that is, $D >> rN_i/(k+N_i) - m_i - g_iU_i$. When the system is at equilibrium, in this limit, it holds that $U_i^* - U_{i-1}^* \to 0$ for all i. This must be true, because $rN_i/(k+N_i) - m_i - g_iU_i$ is bounded to finite values for all values

of U_i when only non-negative values are considered. To determine the total biomass at equilibrium in this limit, we can write a set of equilibrium conditions as follows.

$U_1^* \approx U_2^* \approx ... \approx U_n^* \approx Z$ to obtain at steady state,

$$[rN_i^*/(k+N_i^*) - m_i - g_i Z]Z = (1/2)D(U_{i+1}^* - U_i^*) - (1/2)D(U_i^* - U_{i-1}^*) \quad (i = 2, \ldots, n\text{-}1),$$

(B3)

plus the two end patches, which connect by diffusion only to one adjacent patch. When the *n* equations (B3a) are added together, all of the terms on the right-hand side cancel, and we obtain the equation

$$\sum_{i=1}^{n}\left[\frac{rN_i^*}{k+N_i^*} - m_i - g_i Z\right]Z = 0,$$

(B4)

which can be solved for the non-zero value of *Z*. Then the total population of the *n*-patch system is equal to *nZ*. However, unlike the case studied by DeAngelis et al. (2016), in which there was only one differential equation, in this case there is also the equation for the nutrients, equation (b3b). If (B4) is true, it must also be true that

$$\sum_{i=1}^{n}\left[N_{input,i} - \eta N_i^* - \frac{rN_i^* Z}{\gamma(k+N_i^*)}\right] = 0$$

(B5)

This means that the equilibrium values of N_i , or N_i^* , will be affected by $D \rightarrow \infty$. However, in such cases it is frequently possible to solve for *Z* and $\sum_{i=1}^{n}\left[\frac{rN_i^*}{k+N_i^*}\right]$ simultaneously, using (B4) and (B5) (see Model 2 below). We consider two possible models of the experimental system.

Model 1.

Model analysis: Consider the model with $\eta = 1$, $m_i > 0$, g_i ;

$$\frac{dU_i}{dt} = \frac{rN_iU_i}{k+N_i} - m_iU_i - D(U_i - \frac{1}{2}U_{i-1} - \frac{1}{2}U_{i+1}) \quad (i=1,n)$$

(B6a)

$$\frac{dN_i}{dt} = N_{input,i} - N_i - \frac{rN_iU_i}{\gamma(k+N_i)} \qquad (i=1,n),$$

(B6b)

(wraparound conditions not assumed). First, we solve for equilibria of this model for each patch when there is no dispersal; i.e., $D = 0$. There is one non-trivial equilibrium

$$N_i^* = \frac{km_i}{r-m_i} \qquad U_i^* = \frac{\gamma(N_{input,i} - N_i^*)(k+N_i^*)}{rN_i^*} = \frac{\gamma(N_{input,i} - N_i^{*)}}{m_i}$$

(B7a, b)

We refer to the calculated equilibrium size, or patch carrying capacity, for each patch, as U_i^*, and thus the total summation, $U_{total}^* = \sum_{i=1}^{n} U_i^*$. The value U_{total}^* is the total population size in the absence of dispersal, which can be referred to as 'total carrying capacity in the absence of dispersal' (called $TPop_{hetero,no\ diff}$ in the text);

$$U_{total}^* = \sum_{i=1}^{n} U_i^* = \sum_{i=1}^{n} \frac{\gamma(N_{input,i} - N_i^*)}{m_i} \quad \text{where} \quad N_i^* = \frac{km_i}{r-m_i}.$$

(B8a,b)

The total equilibrium population when dispersal is allowed is the number of patches, n, multiplied by the population on each patch, which in the well-mixed case of $D \to \infty$, is Z; this is found from (B6b) when $U_1^* \approx U_2^* \approx ... \approx U_n^* \approx Z$;

$$nZ = n\frac{\gamma\sum_{i=1}^{n}(N_{input,i} - N_i^*)}{r\sum_{i=1}^{n}\frac{N_i^*}{k+N_i^*}} = \frac{n\gamma\sum_{i=1}^{n}(N_{input,i} - N_i^*)}{\sum_{i=1}^{n}m_i} \qquad \text{where} \quad N_i^* = \frac{km_i}{r-m_i}$$

(B9a,b)

The value nZ (called $TPop_{hetero,diff}$ in the text) is the total population size in the presence of dispersal. (Note that it is important that in summing over (A6b) we sum over the $N_{input,i} - N_i^*$ and $\frac{rN_i^*}{\gamma(k+N_i^*)}$ separately to solve for Z, because the individual consumers are assumed to move rapidly across all patches in the domain such that they are exposed to averages of $N_{input,i} - N_i^*$ and $\frac{rN_i^*Z}{\gamma(k+N_i^*)}$).

Model results:

Using expressions (A8a) and (A9a) we can plot the values of total carrying capacity in the absence of dispersal, U_{total}^*, and total population size with high dispersal, nZ, as functions of parameters. Here we first examine the effects of the values of m_i, which we assume could be different for the low nutrient than from the high nutrient input wells, where $N_{input,i} = 0.6$ in the high input wells (even-numbered in the yeast experiment), and $N_{input,i} = 0.02$ in the low input wells (odd-numbered in the experiment). We refer to the mortality rate in the high nutrient wells as $m_{highnutrient}$ and set that to 0.006. The mortality rate in the low nutrient wells, $m_{lownutrient}$, is allowed to vary. In Figure B1, $U_{total}^* \equiv TPop_{hetero,no\ dif}$ and $nZ \equiv TPop_{hetero,diff}$ are plotted as functions of $m_{lownutrient}$ (odd-numbered wells).

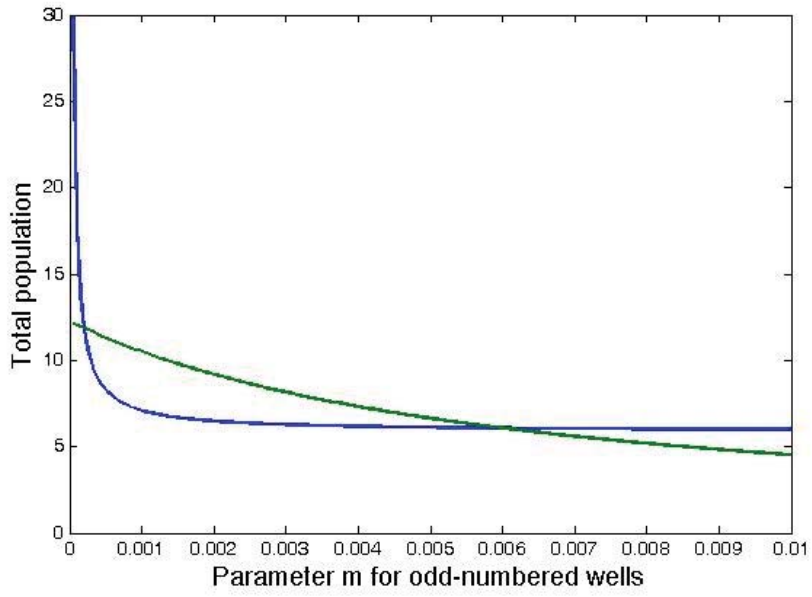

Figure S5.1. Total carrying capacity in the absence of dispersal, $TPop_{hetero,no\ diff}$ (blue curve) and total population size with dispersal, $TPop_{hetero,diff}$ (green curve) as functions of the m_i value for the low nutrient input wells, $m_{lownutrient}$ (odd-numbered wells in experiment), for fixed value of $m_i = 0.006$ for the high nutrient input wells, $m_{highnutrient}$ (even-numbered wells). For simplicity, the other parameters have been set to $r = 0.1$, $k = 0.1$, and $\gamma = 0.01$. The nutrient inputs are distributed heterogeneously; $N_{input,i}$ = (0.02, 0.6, 0.02, 0.6, 0.02, 0.6, 0.02, 0.6, 0.02, 0.6, 0.02, 0.6).

Figure S5.1 shows that the region where $TPop_{hetero,diff} > TPop_{hetero,no\ diff}$ is bounded from the regions where $TPop_{hetero,diff} < TPop_{hetero,no\ diff}$ by the lower value of about $m_{lownutrient} = 0.0002$ and the upper value $m_{lownutrient} = 0.006$. We can ask whether this can be predicted from the expressions for total carrying capacity (population size in the heterogeneous environment without dispersal), $TPop_{hetero,no\ diff}$, and the total population size with dispersal, $TPop_{hetero,diff}$. This would be consistent with the local growth rate and carrying capacities being positively correlated with growth rate. These have the values

Carrying capacity = $U_i^* = \dfrac{\gamma(N_{input,i} - N_i^{*})}{m_i}$

Growth rate = $\dfrac{rN_i}{k + N_i} = m_i$

It can be shown numerically that when $m_{lownutrient}$ crosses a threshold of about 0.0002, the sign of the slope of m_i / U_i^* changes from negative to positive, and when $m_{lownutrient}$ crosses the threshold of 0.006, the sign of the slope of m_i / U_i^* changes from positive to negative, so the sign of the slope of the ratio of local growth rate to local carrying capacity is related to whether total population is greater than total carrying capacity or not.

It is clear then that under certain conditions, when local carrying capacities and growth rates are heterogeneous and positively correlated, it is advantageous to disperse to achieve a higher total population size than total carrying capacity; i.e., to achieve $TPop_{hetero,diff} > TPop_{hetero,no\ diff}$. This answers the first question, related to Hypothesis 1, in the affirmative. It is also consistent with Hypothesis 2, as the growth rate and carrying capacity are positively related over the region in which $TPop_{hetero,diff} > TPop_{hetero,no\ diff}$. These can be proven formally in the same way as in the appendices in DeAngelis et al. (2016). However, our third question was whether, when the nutrient input rates, $N_{input,i}$, are heterogeneously distributed, the total population size, $TPop_{homo}$ can exceed the total population size when the inputs are homogeneously distributed (Hypothesis 3). It is easy to show that the answer to that question is complex. Consider (B8a) and (B9a) again and assume that the values of $N_{input,i}$ are homogeneously distributed. The two forms of $TPop_{homo}$, with diffusion ($TPop_{homo,\ diff}$) and without ($TPop_{homo,\ no\ diff}$) are different. $TPop_{homo,\ diff}$, is the same as expression (B9a), because

$\sum_{i=1}^{n}(N_{input,i} - N_i^*) = \sum_{i=1}^{n}(N_{input,mean} - N_i^*)$, so $TPop_{homo,\ diff}$ coincides with $TPop_{hetero,diff}$ (green curve in Figure B1). But in the case of no diffusion,

$$TPop_{\mathrm{hom}o,no\ diff} = \sum_{i=1}^{n} \frac{\gamma(N_{input,mean} - N_i^*)}{m_i} \quad \text{where} \quad N_i^* = \frac{km_i}{r - m_i}.$$

It can be shown formally that $TPop_{hetero,diff} < TPop_{homo,no\ diff}$ for any parameter values m_i (see Appendix C for a formal proof of a similar statement for Model 2). Here we show this numerically by evaluating this case of homogeneous nutrient input for the same case that was shown in Figure S5.1. For the homogeneous case we obtain the red curve shown in Figure B2, which is always above the curve for the population diffusing in the heterogeneous environment.

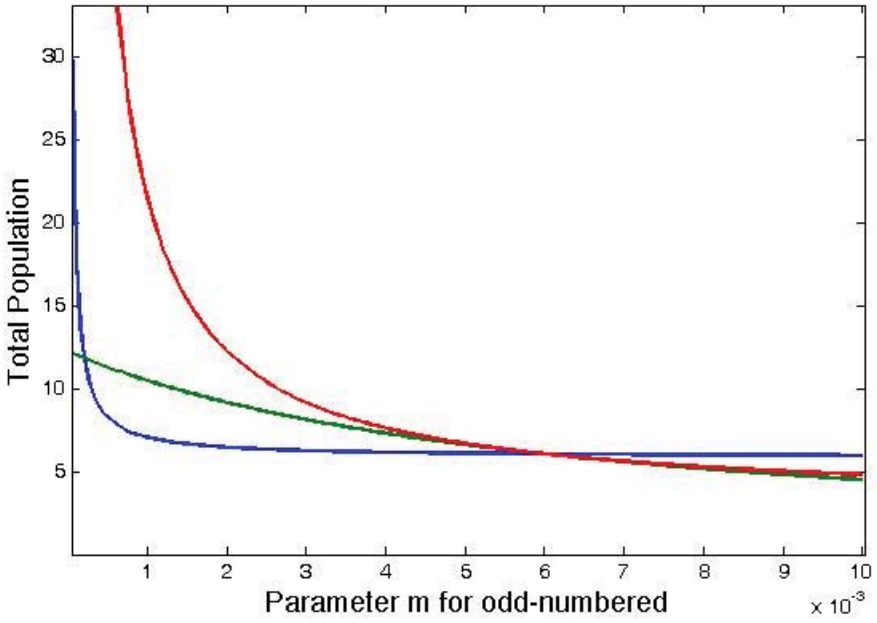

Figure S5.2. This is the same as Figure B1, but with the additional evaluation of total population for the case that the nutrient inputs are uniformly distributed, $TPop_{homo,no\ diff}$, with values of $N_{input,I}$ such that $N_{input,i}$ = (0.31, 0.31, 0.31, 0.31, 0.31, 0.31, 0.31, 0.31, 0.31, 0.31, 0.31, 0.31). This is shown with the added red curve. The blue and green curves are the same as in Figure B1. $TPop_{homo,\ diff}$ coincides with $TPop_{hetero,diff}$. Note, however, that it is possible, if values of $m_{lownutrient}$ exceed 0.006, then $TPop_{homo} < TPop_{hetero,no\ diff}$. Whether this condition on $m_{lownutrient}$ can occur is not known.

Model 2

Consider next Model 2, with $\eta = 0$, $m_i = 0$, $g_i > 0$.

$$\frac{dU_i}{dt} = \frac{rN_iU_i}{k+N_i} - g_iU_i^2 - D(U_i - \frac{1}{2}U_{i-1} - \frac{1}{2}U_{i+1}) \quad (i=1,n)$$

(B10a)

$$\frac{dN_i}{dt} = N_{input,i} - \frac{rN_iU_i}{\gamma(k+N_i)} \qquad (i=1,n)\ .$$

(B10b)

First, we solve for equilibria of this model when there is no dispersal; i.e., $D = 0$. There is a single non-trivial equilibrium;

$$U_i^* = \frac{rN_i^*}{g_i(k+N_i^*)} = \left(\frac{\gamma N_{input,i}}{g_i}\right)^{1/2} \quad \text{where} \quad N_i^* = \frac{k\left(\frac{\gamma g_i N_{input.i}}{r^2}\right)^{1/2}}{1-\left(\frac{\gamma g_i N_{input,i}}{r^2}\right)^{1/2}}\ .$$

(B11a,b)

Then the total population size at equilibrium without dispersal is

$$TPop_{hetero,no\ disp} \equiv U_{total}^* = \sum_{i=1}^{n} U_i^* = \sum_{i=1}^{n}\left(\frac{\gamma N_{input,i}}{g_i}\right)^{1/2}\ .$$

(B12)

The total equilibrium population when diffusion is allowed is the number of patches, n, multiplied by the population on each patch, which in the well-mixed case of $D \to \infty$, is Z. If we use (B10a) and use the same methods as in Model 1, we obtain

$$Z = \frac{\sum_{i=1}^{n} \frac{rN_i^*}{k + N_i^*}}{\sum_{i=1}^{n} g_i}$$

(B13)

However, we could also use (B10b) to obtain

$$Z = \frac{\sum_{i=1}^{n} N_{input,i}}{\sum_{i=1}^{n} \frac{rN_i^*}{\gamma(k + N_i^*)}}$$

(B14)

Therefore, we have to solve these for Z and $\sum_{i=1}^{n}\left[\frac{rN_i^*}{k + N_i^*}\right]$ simultaneously to obtain

$$Z = \left(\frac{\gamma \sum_{i=1}^{n} N_{input,i}}{\sum_{i=1}^{n} g_i} \right)^{1/2} \quad \text{and} \quad \sum_{i=1}^{n}\left[\frac{rN_i^*}{k + N_i^*}\right] = \left(\gamma \left(\sum_{i=1}^{n} g_i \right) \left(\sum_{i=1}^{n} N_{input,i} \right) \right)^{1/2}$$

(B15a,b)

Using expressions (B12) and (B15a) we can plot the values of total carrying capacity without dispersal, $TPop_{hetero,no\ diff}$, and total population size $nZ \equiv TPop_{hetero,diff}$ as a function of parameters. Here we first examine the effects of the values of g_i, which may differ between high and low nutrient wells. In Figure 5 (main text) and Figure B3 below $TPop_{hetero,no\ diff}$ and $TPop_{hetero,\ diff}$ are plotted as functions of the g_i (or $g_{lownutrient}$), the value for the low nutrient input wells (odd wells), while the value of g_i (or $g_{highnutrient}$) = 0.001 for the high nutrient input wells (even wells).

In Figure S5.3 the region where $TPop_{hetero,\ diff} > TPop_{hetero,no\ diff}$ can be seen to be bounded from the regions where $TPop_{hetero,\ diff} < TPop_{hetero,no\ diff}$ by a value of roughly the

lower value $g_{lownutrient} = 0.000038$ and the higher value $g_{lownutrient} = 0.0023$. We can ask the question of whether these regions can be predicted from the expressions for total carrying capacity (population size in heterogeneous environment without dispersal), $TPop_{hetero,no\ disp}$, and total population size in heterogeneous environment with dispersal, $TPop_{hetero,disp}$;

$$TPop_{hetero,nodiff} \equiv \sum_{i=1}^{n} U_i^* = \sum_{i=1}^{n} \left(\frac{\gamma N_{input,i}}{g_i} \right)^{1/2} \quad \text{and} \quad TPop_{hetero,diff} \equiv nZ = n \left(\frac{\gamma \sum_{i=1}^{n} N_{input,i}}{\sum_{i=1}^{n} g_i} \right)^{1/2} .$$

(B16a,b)

As in Model 1, this shows that under certain conditions, when local carrying capacities and growth rates are heterogeneous and positively correlated, a larger population size can result when the population disperses than when it does not, confirming Hypotheses 1 and 2. These can be proven formally in the same way as in appendices of DeAngelis et al. (2017).

However, also as in Model 1, when the nutrient input rates, $N_{input,i}$, are heterogeneously distributed, the population, when dispersing, cannot exceed the total population size when the same inputs are homogeneously distributed. There are two different expressions for $TPop_{homo}$; with diffusion $TPop_{homo,\ diff}$ and without diffusion $TPop_{homo,no\ \ diff}$. $TPop_{homo,\ diff} = TPop_{hetero,\ diff}$ because $\sum_{i=1}^{n} N_{input,i} = \sum_{i=1}^{n} N_{input,mean}$. Therefore. $TPop_{homo,\ diff}$ coincides with $TPop_{hetero,\ diff}$. However, this is true only for $D \rightarrow \infty$. When D is close to zero, it can be shown (Appendix C) that $TPop_{homo,\ diff} > TPop_{hetero,\ diff}$ when

$g_{lownutrient} < g_{highnutrient}$, but $TPop_{homo,\ diff} < TPop_{hetero,\ diff}$ when $g_{lownutrient} < g_{highnutrient}$. Equality holds only when $g_{lownutrient} = g_{highnutrient}$. The expression for $TPop_{homo,no\ diff}$ is

$$TPop_{\mathrm{hom}o,no\ diff} = \sum_{i=1}^{n} U^{*}_{\mathrm{hom}ogeneous,i} = \sum_{i=1}^{n} \left(\frac{\gamma N_{input,mean}}{g_i} \right)^{1/2} . \quad \text{(B17)}$$

If (B16b) and (B17) are compared, it can be shown that in this case that it is always true that $TPop_{hetero,\ disp} < TPop_{homo}$. This is also demonstrated numerically Figure B3, with a curve (red) added corresponding to U^{*}_{total} calculated for the case that the inputs $N_{input,i}$ are distributed uniformly among the patches, and there is no diffusion but adding up to the same total input as in the case in the heterogeneous case, , i.e., $TPop_{homo,no\ diff}$.

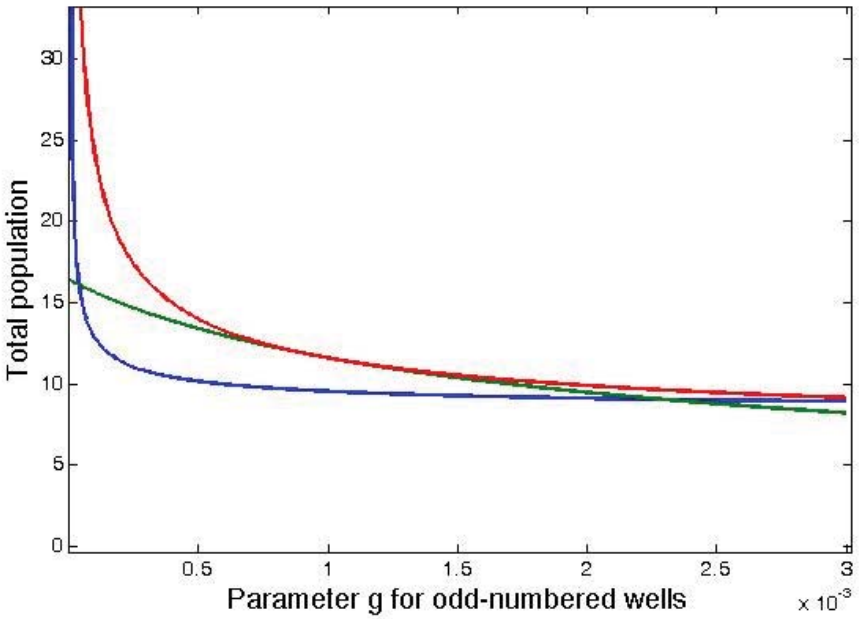

Figure S5.3. Total carrying capacity $TPop_{hetero,no\ diff}$ (blue curve), total population size $TPop_{hetero,diff}$ (green curve), and total population for homogeneously distributed inputs (red curve), $TPop_{homo,\ diff}$, as functions of the g_i value for the low nutrient input wells, $g_{lownutrient}$, (odd wells) for fixed value of the $g_i = 0.001$ for the high nutrient input wells, $g_{highnutrient}$ (even wells). $TPop_{homo,\ diff}$ coincides with $TPop_{hetero,\ diff}$ for $D \to \infty$. For simplicity, the other parameters have been set to $r = 0.1$, $k = 0.1$, and $\gamma = 1.0$. The nutrient inputs are distributed heterogeneously; $N_{input,i}$ = (0.02, 0.6, 0.02, 0.6, 0.02, 0.6,

0.02, 0.6, 0.02, 0.6, 0.02, 0.6). For the red curve the nutrients are distributed homogeneously now; $N_{input,i}$ = (0.31, 0.31, 0.31, 0.31, 0.31, 0.31, 0.31, 0.31, 0.31, 0.31, 0.31, 0.31)

Box 1

Model 1

$$\textit{Total population, heterogeneous diffusion} = \sum_{i=1}^{n} U^{*}_{\textit{no diffusion},i} = \sum_{i=1}^{n} \frac{\gamma(N_{input,i} - N_i^{*})}{m_i}$$

(B18a)

$$\text{Total population, heterogeneous with diffusion} = \sum_{i=1}^{n} U^{*}_{diffusion,i} = \frac{n\sum_{i=1}^{n} \gamma(N_{input,i} - N_i^{*})}{\sum_{i=1}^{n} m_i}$$

(B18b)

$$\text{Total population, homogeneous no diffusion} = \sum_{i=1}^{n} U^{*}_{\text{hom}\,ogeneous,i} = \sum_{i=1}^{n} \frac{\gamma(N_{input,mean} - N_i^{*})}{m_i}$$

(B18c)

where $N_i^{*} = \dfrac{km_i}{r - m_i}$ and $N_{input,mean} = \sum_{i=1}^{n} N_{input,i} / n$

(B18d,e)

Model 2

$$\textit{Total population, heterogeneous no diffusion} = \sum_{i=1}^{n} U^{*}_{\textit{no diffusion},i} = \sum_{i=1}^{n} \left(\frac{\gamma N_{input,i}}{g_i} \right)^{1/2} \quad \text{(B19a)}$$

$$Total\ \ population, heterogeneous\ \ with\ diffusion = \sum_{i=1}^{n} U^{*}_{diffusion,i} = \left(\frac{\sum_{i=1}^{n} \gamma N_{input,i}}{\sum_{i=1}^{n} g_i} \right)^{1/2}$$

(B19b)

$$Total\ population,\ homogeneous\ no\ diffusion = \sum_{i=1}^{n} U^{*}_{\mathrm{hom}ogeneous,i} = \sum_{i=1}^{n} \left(\frac{\gamma N_{input,mean}}{g_i} \right)^{1/2}$$

(B19c)

$$\text{where} \quad N_i^{*} = \frac{k\left(\frac{\gamma g_i N_{input.i}}{r^2} \right)^{1/2}}{1 - \left(\frac{\gamma g_i N_{input,i}}{r^2} \right)^{1/2}} \quad \text{and} \quad N_{input,mean} = \sum_{i=1}^{n} N_{input,i} / n \qquad \text{(B19d,e)}$$

Appendix 6: Mathematical models and analysis for diffusion *D* small. for Chapter 3

In Appendix 5 we found expressions for $TPop_{hetero,disp}$, $TPop_{hetero,no\ disp}$ and $TPop_{homo}$ in the limit that the diffusion rate, D, is very large, showing that there are parameter ranges where $TPop_{hetero,disp} > TPop_{hetero,no\ disp}$ in a heterogeneous environment, but where $TPop_{hetero,disp} < TPop_{homo}$ is always true. Here we consider the opposite limit, where D is very small and show that in this case $TPop_{hetero,disp} < TPop_{homo}$ is always true.

The continuous form of the equations is;

$$\frac{\partial u(x,t)}{\partial t} = D\Delta u(x,t) + \frac{r\, n(x,t)u(x,t)}{k + n(x,t)} - m(x)u(x,t) - g(x)u(x,t)^2$$

$$\text{(C1a)}\ \frac{dn(x,t)}{dt} = N_{input}(x) - \eta n(x,t) - \frac{rn(x,t)u(x,t)}{\gamma(k + n(x,t))},$$

(C1b)

We consider only Model 2, so $\eta = 0$, $m(x) = 0$, and $g(x) > 0$ and continuous. The steady state is

$$N_{input}(x) = \frac{r_{\max} N^*(x)}{k + N^*(x)} \qquad \text{(C2a)}$$

$$D\Delta u^*(x) + u^*(x)\left(\frac{\gamma r_{\max} N^*(x)}{k + N^*(x)} - g(x)u^*(x)\right) = 0 \quad \text{in } \Omega \text{ (with } \partial_\nu u = 0 \quad \text{on } \partial\Omega\,. \qquad \text{(C2b)}$$

We show that if $\gamma N_{input}(x)$ and $g(x)$ are positively related, then $TPop_{homo,diff} > TPop_{hetero,\ diff}$ for D small.

Substituting (C2a) into (C2b), and omitting the steady state symbols * henceforth, we have

$$D\Delta u(x) + \gamma N_{input}(x) - g(x)|u|^2 = 0 \qquad \text{(C3a)}$$

$$\partial_\nu u(x) = 0 \quad \text{on} \quad \partial\Omega . \tag{C3b}$$

For simplicity, we denote $R(x) \equiv \gamma N_{input}(x)$; i.e, (C3.a.b) becomes

$$D\Delta u(x) + R(x) - g(x)|u|^2 = 0 \quad [R(x),\ g(x) \text{ both} > 0 \text{ on } \overline{\Omega}\,] \tag{C3a}$$

$$\partial_\nu u(x) = 0 \quad \text{on} \quad \partial\Omega . \tag{C3b}$$

It can be shown by standard arguments that (C3a,b) has a unique positive solution, denoted by u_D. Now we are interested in the behavion of u_D for $D > 0$ small.

Proposition 1. As $D \to 0$, $u_D \to K$ uniformly, where $K(x) = \sqrt{R(x)/g(x)}$: more precisely,

for any $\varepsilon > 0$, $\exists\ D_\varepsilon > 0$ small, such that $\|u_D - K\|_{L^\infty(\Omega)} < \varepsilon$ for all $0 < D < D_\varepsilon$.

(Pf.) For $\varepsilon > 0$ given, choose a function $\overline{K}_\varepsilon$ such that $\partial_\nu \overline{K}_\varepsilon = 0$ on $\partial\Omega$, and

$\frac{\varepsilon}{2} + K < \overline{K}_\varepsilon < K + \varepsilon$ in Ω. Then

$$D\Delta\overline{K}_\varepsilon + R - g\overline{K}_\varepsilon^2 < D\Delta\overline{K}_\varepsilon + R - g\left(K + \frac{\varepsilon}{2}\right)^2$$

$$= D\Delta\overline{K}_\varepsilon + R - g\left(K^2 + \varepsilon K + \frac{\varepsilon^2}{4}\right) = D\Delta\overline{K}_\varepsilon - \varepsilon K g - \frac{1}{4} g\varepsilon^2 < 0$$

if $D > 0$ is sufficiently small. ($\varepsilon > 0$ is fixed). Thus $\overline{K}_\varepsilon$ is an upper solution.

Similarly, choosing $\hat{K}_\varepsilon$ such that $\partial_\nu \hat{K}_\varepsilon = 0$ on $\partial\Omega$ and

$$(0 <)\ K - \varepsilon < \hat{K}_\varepsilon < K - \frac{\varepsilon}{2} \quad \text{on } \partial\Omega$$

Then we have

$$D\Delta\hat{K}_\varepsilon + R - g\hat{K}_\varepsilon^2 \geq D\Delta\hat{K}_\varepsilon + R - g\left(K - \frac{\varepsilon}{2}\right)^2$$

$$= D\Delta\hat{K}_\varepsilon + R - g\left(K^2 - \varepsilon K + \frac{\varepsilon^2}{4}\right) = D\Delta\hat{K}_\varepsilon + \varepsilon Kg - \frac{1}{4}g\varepsilon^2$$

$$= D\Delta\hat{K}_\varepsilon + \varepsilon g\left(K - \frac{\varepsilon}{4}\right) > 0$$

for D sufficiently small; i.e., $\hat{K}_\varepsilon$ is a lower solution. By the uniqueness of u_D we conclude

$\hat{K}_\varepsilon < u_D < \overline{K}_\varepsilon$, and our assertion is established.

Next we compare u_D to the solution of v_D of the following model:

$$D\Delta v(x) + \overline{R} - g(x)(v)^2 = 0 \qquad \text{in } \Omega \tag{C4a}$$

$$\partial_\nu v(x) = 0 \quad \text{on } \partial\Omega, \tag{C4b}$$

where $\overline{R} = \frac{1}{|\Omega|}\int_\Omega R(x)dx$ is the average of R. Our main result is the following.

Proposition 2. For D small, $\int_\Omega u_D < \int_\Omega v_D$ provided that R and g are positively correlated.

To prove this, we first prove the corresponding result for $D \to 0$; i.e., the following:

Lemma. $\int_\Omega \sqrt{\frac{R}{g}} \leq \int_\Omega \sqrt{\frac{\overline{R}}{g}}$ if R and g are positively correlated; furthermore, the strict inequality

holds if either R or g is not a constant.

(Pf.) If R and g are positively correlated $\Rightarrow R$ and $\frac{1}{g}$ are negatively correlated

$$\Rightarrow \int_{\Omega} \sqrt{\frac{R}{g}} = \int_{\Omega} \sqrt{R}\,\frac{1}{\sqrt{g}} \le \int_{\Omega} \sqrt{R} \int_{\Omega} \sqrt{\frac{1}{g}}$$ (inequality by Prop. A.3(ii), p. 451, DeAngelis et al. 2016a)

$$= \sqrt{\overline{R}}\,|\Omega| \int_{\Omega} \frac{1}{\sqrt{g}} = \int_{\Omega} \sqrt{\frac{\overline{R}}{g}}$$ since $\overline{R}$ is a constant.

Now, Proposition 2 follows readily from the lemma above and Proposition 1.

Remarks. (1) Similarly, the discrete versions of Propositions 1 and 3, as well as the lelmma above, also hold for any number of "wells/compartments".

(2) Comparing the above proof for Proposition1 to previous arguments (DeAngelis et al. 2016b), the proof here allows a more general *K(x)*, but produces less precise estimates. (In DeAngelis et al. 2016, it is actually required that $\partial_{\nu} K = 0$ on $\partial\Omega$, which was inadvertently omitted.)

(3) If R and g are negatively correlated, then the inequality in Proposition 2 is reversed.

References

DeAngelis, D. L., Wei-Ming Ni, and Bo Zhang. 2016. Effects of diffusion on total biomass in heterogeneous continuous and discrete-patch systems. *Theoretical Ecology* 9.4 (2016): 443-453.

DeAngelis, D. L., Wei-Ming Ni, and Bo Zhang. 2016. Dispersal and heterogeneity: Single species. *Journal of Mathematical Biology* 72:239-254.

Appendix 7 Descriptions of scenarios, for chapter 4

Scenario 1. Simulations of both cypress swamp and bay swamp natural communities, without melaleuca, were run over long periods of time (300 years) to reach its stable state (a stochastic equivalent of steady state, meaning that the forest variables vary over time, but within a finite and non-zero range). The purpose of these scenarios was to calibrate the simulated density ratio and size distributions of native species in the two swamps with Casey and Ewel (2006), to establish that JABOWA-II was accurately modeling the natural communities.

Results of scenario 1. In simulations of densities and basal areas of five woody plant species grown together without melaleuca in cypress swamp, pond cypress was the dominant species over the long term. Simulation results showed that pond cypress increased in stem density to a maximum range of 80 - 90 trees/100m^2 (Figure S7.1a, density is log scale), and its basal area reached about 60 cm^2/m^2 (Figure S7.1b, basal area is log scale). The simulations also showed slash pine reaching the second highest density of about 40 trees/100m^2. The other simulated species reached only low densities, with dahoon holly being nonexistent. The percentage stem numbers of pond cypress, slash pine, sweet bay and loblolly bay in cypress swamp were 54%, 43%, 1% and 1%, respectively, when the simulated community reached its stable state (Figure S7.1a). The simulated basal areas of pond cypress agreed with Ewel and Wickenheiser's (1988) empirical measurements of 40-66 cm^2/m^2 in basal area, while the simulated maximum values of stem density were greater than their empirical values of 8.8 – 26.4 trees/100m^2.

It is likely that the pond cypress measured in the field included larger individuals than the simulated ones. The simulated density of slash pine coincided with what Jokela and Martin (2000) found, which was a maximum of 40 trees/100m^2. The empirical stem number percentages of pond cypress, slash pine, sweet bay and loblolly bay in cypress swamp based on Casey and Ewel (2006) were 33%, 15%, 6% and 3%.

When the simulated community had reached stable status in bay swamp, loblolly bay had the highest density (110 trees/100m^2 maximum), and sweet bay had the second highest density (55 trees/100m^2 in maximum) (Figure S7.1c, density is log scale). However, sweet bay had a higher basal area (15 cm^2/m^2 maximum) than loblolly bay, which was about 10 cm^2/m^2 (maximum), as the individual loblolly bay were generally smaller (Figure S7.1d, basal area is log scale). Pond cypress, slash pine and dahoon holly occurred at lower stem and basal area densities in the simulations of this habitat. The simulated stem number percentages of pond cypress, slash pine, dahoon holly, sweet bay and loblolly bay in bay swamp were 2.5%, 2.5%, 5%, 40% and 50%, respectively (Figure S7.1c). An empirically measured basal area of sweet bay was close to 6 cm^2/m^2 (Clewell et al. 2000) and an empirical basal area of loblolly bay with close to 4.64 cm^2/m^2 (Gresham and Lipscomb 1985). The empirical stem number percentages of pond cypress, slash pine, dahoon holly, sweet bay and loblolly bay in bay swamp based on Casey and Ewel (2006) were 8%, 6%, 0%, 21% and 23%.

References

Cao QV, Dean TJ, Baldwin VC Jr (2000) Modeling the size–density relationship in direct-seeded slash pine stands. Forest Sci 46: 317-321.

Ernst KA, Brooks JR (2003) Prolonged flooding decreased stem density, tree size and shifted composition towards clonal species in a central Florida hardwood swamp. Forest Ecol Manage 173: 261-279.

Ewel KC, Wickenheiser LP (1988) Effects of swamp size on growth rates of Cypress trees. Ame Midl Naturt 120: 362-370.

Grelen HE (1990) Silvics of North America: hardwoods. United States department of agriculture.

Gresham CA, Lipscomb DJ (1985). Selected ecological characteristics of *Gordonia lasianthus* in coastal South Carolina. Torrey Bot Soc 112: 53-58

Gower S T, Gholz HL, Nakane K, Baldwin VC (1994) Production and carbon allocation patterns of pine forests. Ecol Bull 43: 115-135.

Jokela EJ, Martin TA (2000) Effects of ontogeny and soil nutrient supply on production, allocation, and leaf area efficiency in loblolly and slash pine stands. Can J Forest Res 30: 1511-1524.

Landman GB, Menges ES (1999) Dynamics of woody bayhead invasion into seasonal ponds in southcentral Florida. Southern Appalachian Bot Soc 64: 130-137.

Kurz H, Wagner KA (1953) Factors in Cypress dome development. Ecology 34: 157-164.

Mitsch W, Ewel KC (1979) Comparative biomass and growth of cypress in Florida wetlands. Amer Midl Natur 101: 417-426.

Rayachhetry MB, Van TK, Center TD, Laroche F (2001) Dry weight estimation of the aboveground components of *Melaleuca quinquenervia* trees in southern Florida. Forest Ecol Manage 142:281-290.

Serbesoff-King K (2003) Melaleuca in Florida: A literature review on the taxonomy, distribution, biology, ecology, economic importance, and control measures. J Aquat Plant Manage 41:98-112.

Teskey RO, Gholz HL, Cropper WP Jr (1994) Influence of climate and fertilization on net photosysthesis of mature slash pine. Tree Physiol 14: 1215-1227.

Tipping PW, Martin MR, Pratt PD, Rayamajhi MB, Center TD (2013) An abundant biocontrol agent does not provide a significant predator subsidy. Biocontrol 67:212-219.

U.S. Department of Agriculture, Forest Service (1965) Silvics of forest trees of the United States. H. A. Fowells, comp. U.S. Dept Agric, Agriculture Handbook 271. Washington, DC. 762p.

Table S7. 1: differences in the initial conditions of cypress swamps and bay swamps in the model (only included are the environmental variables that were used in the model)

	Cypress swamps	Bay swamps
Site environmental condition(Casey and Ewel, 2006)		
Soil depth (organic matter depth)	54 cm	232 cm
Standing water depth	20 cm	8 cm

Table S7. 2. Estimates of key parameters for a list of selected species. These input parameters for the model were estimated using the methods described by Botkin (1993).

Species name	S	N	dbh_{max}	Ht_{max}	A_{max}	G	SAP (cypress swamps)	SAP (bay swamps)	b_2	b_3
Melaleuca quinquenervia	1	1	90	2540	200	400	5000	10000	53.4	0.300
Fagus grandifolia Ehrh	2	3	150	4000	100	240.7	50	5	38.2	0.13
Taxodium distichum (L.) Rich.	2	2	365	4600	162	140.4	50	5	24.55	0.03
I.cassine	3	2	62	1200	144	120.0	0	5	34.29	0.28
M. virginiana	2	2	128	1066	100	100	2	50	14.51	0.06
G. lasianthus	3	3	64	2000	100	100	2	94	58.2	0.454

In Table S7. 2 the symbols are: S, shade tolerance; N, nitrogen tolerance; dbh_{max}, maximum diameter at breast height (cm) and Ht_{max}, maximum height (cm); Amax,

maximum age (years); G, growth rate scaling coefficient determining how rapidly a tree growing under optimum conditions reaches one-half its maximum size or inflection point($G= 5Ht_{max}(\delta dbh_{max}/dbh_{max})$; SAP, maximum number of saplings of species that can be added in any one year to the 0.1 hectare plot, which have different values in cypress and bay swamps; b_2 and b_3, are derived parameters relating height to dbh.

Table S7. 3: Table of all parameters values for each species needed in JABOWA-II

Common name	Scientific name	S	N	SAP (cypress swamps)	SAP (bay swamps)	R	C
Paper-bark tree	*Melaleucaquinquenervia*	1	1	5000	10000	400	0.1
Slash pine	*Pinuselliottii*	2	3	30	5	240	0.1
Pond Cypress	*Taxodiumdistichum*	2	2	40	5	142	0.1
Dahoon holly	*Ilex cassine*	3	2	0	5	120	0.1
Sweet bay	*Magnoliavirginiana*	2	2	2	50	40	0.2
Loblolly bay	*Gordonialasianthus*	3	3	2	94	100	0.01

Common name	D_{MAX}	H_{MAX}	A_{MAX}	A_{INC}	DD_{MIN}	DD_{MAX}	D_T	WLT_{MAX}	LT_{MIN}
Paper-bark tree	110	2540	200	0.01	2000	55300	0.2	0.5	0.1
Slash pine	150	3000	100	0.01	2000	55300	0.5	0.1	0.5
Pond Cypress	365	4600	162	0.01	2000	55300	0.4	0.9	0.5
Dahoon holly	62	1200	144	0.01	2000	55300	0.6	0.5	0.1
Sweet bay	128	1066	100	0.01	2000	55300	0.5	0.274	0.5
Lobloll y bay	64	2000	100	0.01	2000	55300	0.5	0.247	0.1

Common name	References
Paper-bark tree	Rayachhetry et al. 2001; Serbesoff-King et al, 2003; Tipping et al, 2013; Tipping, personal communication
Slash pine	Gower et al. 1994; Teskey et al. 1994; Jokela and Martin 2000; Cao et al. 2000; Plant Guide USDA;
Pond Cypress	Kurz and Wagner 1953; Mitsch and Ewel, 1979; Ewel and Wickenhezsr, 1988; Casey and Ewel, 2006; USDA NRCS plant data
Dahoon holly	Grelen 1990; Ernst and Brooks 2003
Sweet bay	Grelen 1990; Casey and Ewel 2006; Missouri Vitanical Garden (http://www.missouribotanicalgarden.org/)
Loblolly bay	Landman et al, 1999; Grelen 1990; Casey and Ewel, 2006; http://www.nativetreesociety.org

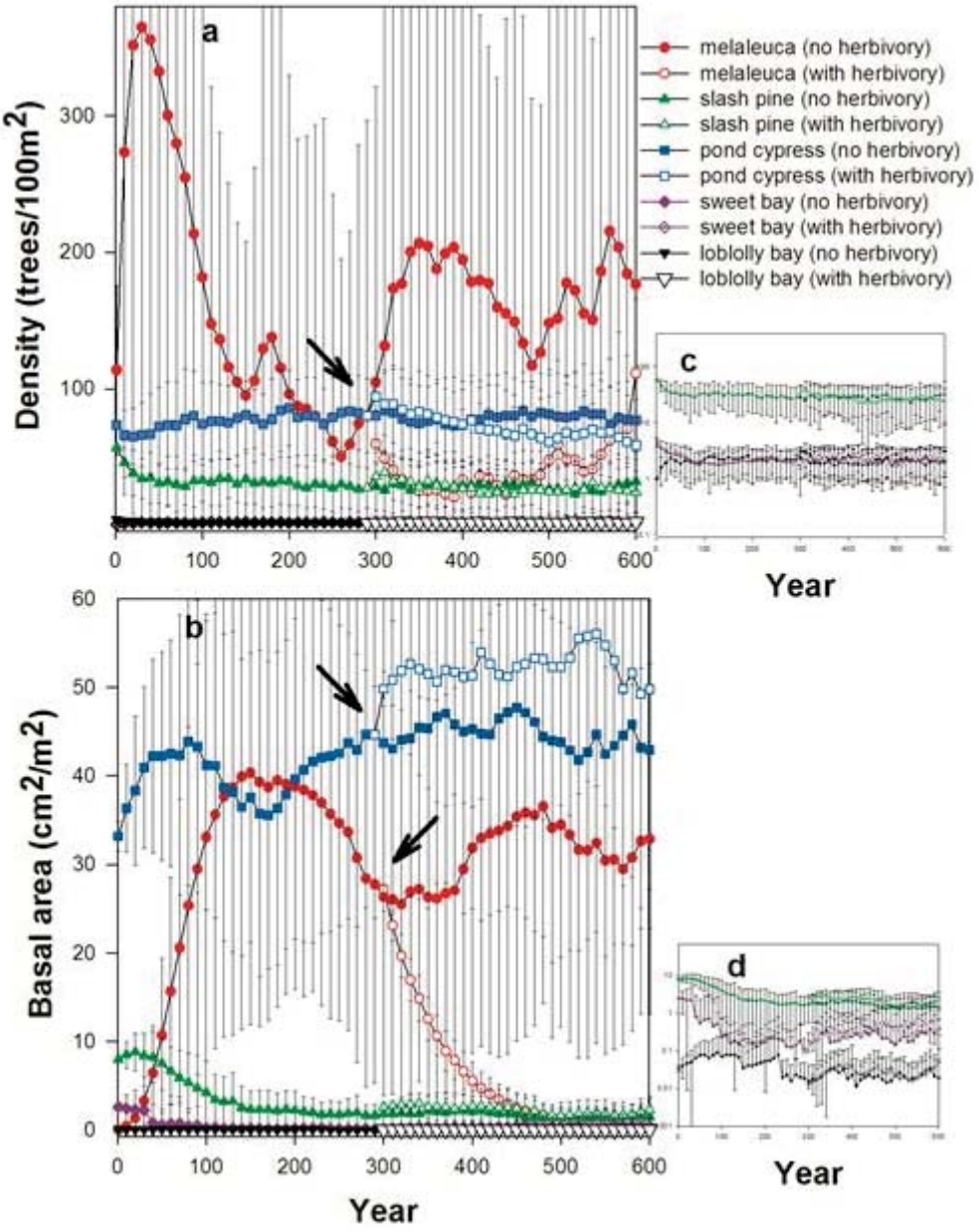

Figure. S7. 1. Results of scenario 2 with error bars for 50 replicate simulations. **a**. Projected densities of woody plant species at different stages of stand development in melaleuca invaded cypress swamps of Florida with and without biocontrol. **b**. Projected basal area of woody plant species at different stages of stand development in melaleuca-invaded cypress swamps of Florida with and without biocontrol. **c** Projected woody plant species which had low basal area for better view. Red circles: melaleuca; green trianglesup: slash pine; blue squares: pond cypress; purple diamonds: sweet bay; black trianglesdown: loblolly bay; filled color: no biocontrol is applied for 600 years; unfilled color: biocontrol is applied at year 300. Arrows show when biocontrol starts to be applied.

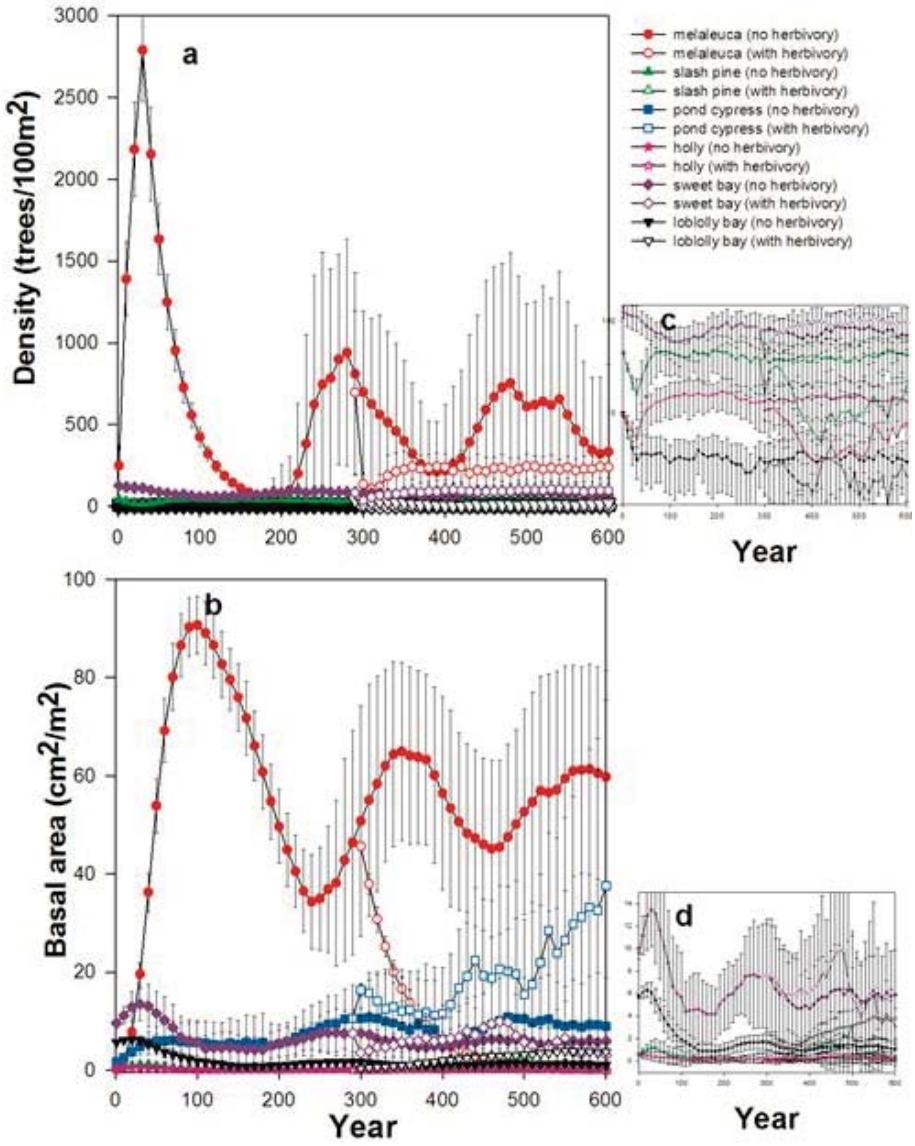

Figure. S7. 2. Results of scenario 4 with error bars for 50 replicate simulations. **a**. Projected densities of woody plant species at different stages of stand development in melaleuca invaded bay swamps of Florida with and without biocontrol. **b**.Projected woody plant species which had low densities level than melaleuca for better view. **c**. Projected basal area of woody plant species at different stages of stand development in melaleuca-invaded bay swamps of Florida with and without biocontrol. Red circles: melaleuca; pink trianglesdown: slash pine; blue squares: pond cypress; black diamonds: dahoon holly; green trianglesup: sweet bay; purple hexagons: loblolly bay; filled color: no biocontrol is applied for 600 years; unfilled color: biocontrol is applied at year 300. Arrows show when biocontrol starts to be applied.

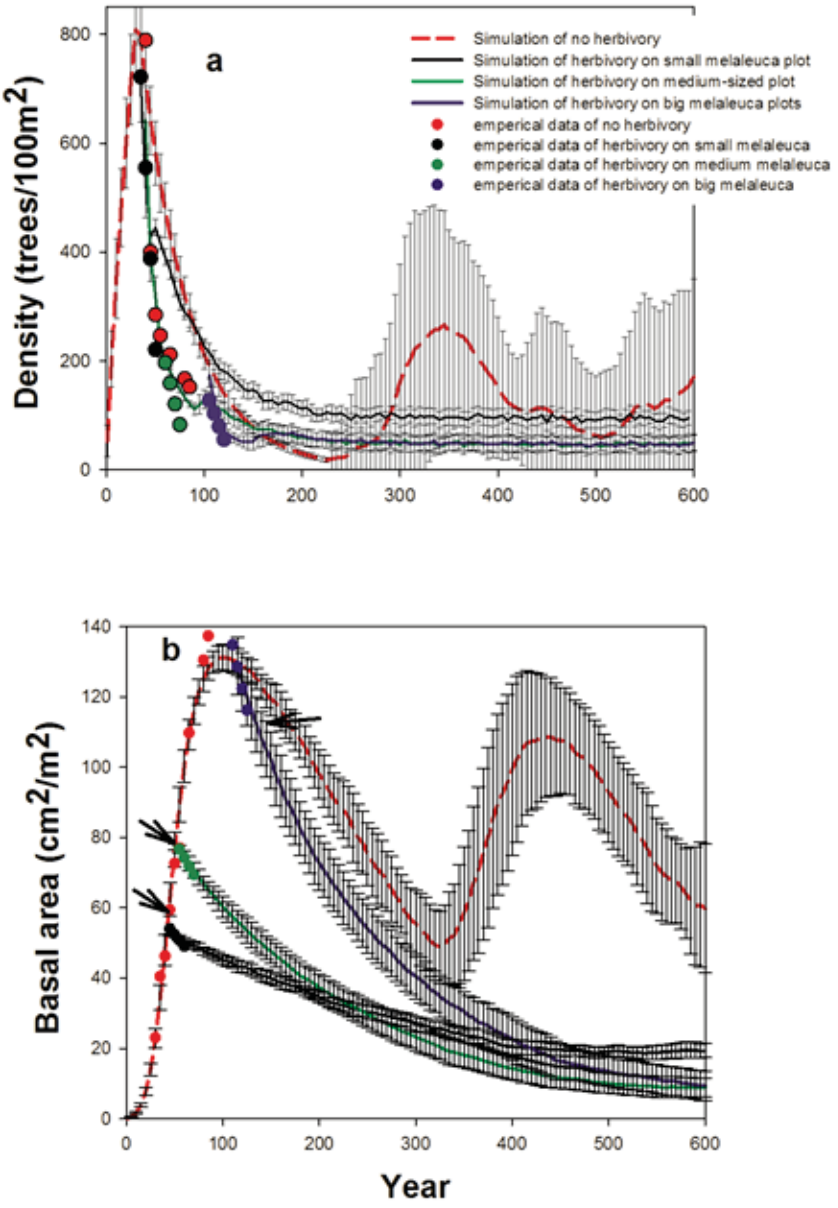

Figure. S7. 3. Result of scenarios 5-6 with error bars included for 50 replicate simulations. **a**. Projected densities of pure melaleuca stand with and without biocontrol. **b**. Projected basal area of pure melaleuca stand with and without biocontrol. The red dashed represents simulation data without application of biocontrol and the solid lines represent simulation results with biocontrol, starting from different size stages. Black line shows biocontrol applied to a stand of high density but small trees; green line shows biocontrol applied to stand of medium-size trees, and blue line shows biocontrol applied to stand with low density but large trees. Circles represents field data published in Rayamajhi et al, (2007). Arrows show when biocontrol began to be applied.

Appendix 8 deriving an Implicit Equation for the Calculation of equilibrium value of G, for Chapter 5

We follow Ju and DeAngelis (2009) to find the equilibrium value G for a given maximum possible photosynthetic rate, R_0, and nutrient input to the system, N_{input}. Those authors also show that a maximum value of growth rate, *Max(G)*, exists for some combination of the three allocation parameters η_f, η_r and η_w, where $\eta_f + \eta_r + \eta_w = 1$. Because η_w is fixed, only η_f and η_r vary and η_r is a function of η_f.

Assume that the system is at steady state, so that each of the eqns 1a-e, g is set to zero. It was not possible to find an explicit analytic expression for G, from which a maximum of G could be determined analytically, but it was possible to do so numerically from an implicit expression. Our first objective was to find an expression for G. We did this in the following steps. We used eqn 1a, set to zero, we expressed C_f in terms of G, and used eqn 1d to express N_f in terms of G in the right hand side of eqn 2. These substitutions result in the implicit equation for G,

$$G = R_0\left(1 - e^{-k_f b_f \eta_f G/(r_f+\varphi_f)}\right)\left[\frac{v_f}{v_f + v_0}\right]. \tag{A1}$$

where

$$v_f = \left[\left(\frac{g_N N_{pore}}{k_N + N_{pore}}\right)\left(1 - e^{-k_r b_r \eta_r G/\gamma_r}\right) - \eta_w \nu_w G\right]\left(\frac{\eta_f}{\eta_f + \rho\eta_r}\right)\left(\frac{1}{\eta_f G}\right) \tag{A2}$$

where

$\eta_r = 1 - \eta_r - \eta_w$.

This equation still contains N_{pore}, which is a variable, so N_{pore} must next be eliminated in terms of G in order to obtain an equation that contains only the variable G. We did that by using the right hand sides of eqns 1d,e,g along with eqn 1c. These allowed us to eliminate N_f, N_r, and C_w, so that N_{pore} is expressed simply in terms of G in the second order equation.

$$QN_{pore}^2 + \left[g_N(1-\lambda)\left(1-e^{-b_r k_r \eta_r G/\gamma_r}\right) + Q(k_N - N_{input})\right]N_{pore} - QN_{input}k_N = 0 \quad \text{(A3)}$$

Solving this for N_{pore} yields,

$$N_{pore} = \frac{-B \pm (B^2 + 4Q^2 N_{input}k_N)^{1/2}}{2Q} \quad \text{(A4)}$$

where

$$B = g_N(1-\lambda)\left(1-e^{-b_r k_r \eta_r G/\gamma_r}\right) + Q(k_N - N_{input}) \quad \text{(A5)}$$

It can be shown that the only relevant solution of eqn 8a is the one with the positive sign. Then N_{pore} can be plugged into eqn (A2) and (A2) into (A1) to obtain the final implicit equation for G. Equation (A1) is an implicit equation for the equilibrium value G, and can be evaluated numerically.

We calculate now find the way that a tree should allocate its energy (or carbon) resources in a way that maximizes its growth rate, G, in the absence of competition. To do this, η_f is varied until G is maximized as Max(G). There is a strategy η_f in the range (0, 1) that maximizes G. Given *Max(G)*, we can find the tree components, foliage, fine roots, and woody material that correspond to *Max(G)*.

Effect of defoliation on Max(G)and Optimal η_f

We allowed the defoliation rate the constant φ_f to increase from zero and computed the changes in *Max(G)*, *Optimal*(η_f), *Min*(N_{pore}) , *Max*($\eta_r G$), *Max*($\eta_f G$) and the corresponding optimized values of C_r, C_f, N_r, N_f , and N_r:C_f.